Characterisation of air-borne sound sources using surface coupling techniques

Liangfen Du

N°d'ordre NNT : 2016LYSEI028

THESE de DOCTORAT DE L'UNIVERSITE DE LYON
préparée au sein de
l'INSA LYON

Ecole Doctorale N° 162
MECANIQUE, ENERGETIQUE, GENIE CIVIL, ACOUSTIQUE

Spécialité de doctorat : Acoustique

Soutenue publiquement le 31/03/2016, par :
Liangfen DU

Characterisation of Air-borne Sound Sources using Surface Coupling Techniques

---

Devant le jury composé de :

GARCIA, Alexandre	Prof.	Conservatoire National des Arts et Métiers	Président
DESMET, Wim	Prof.	Katholieke Universiteit Leuven	Rapporteur
FENG, Leping	Assoc. Prof.	KTH Royal Institute of Technology	Rapporteur
MOORHOUSE, Andy	Prof.	University of Salford	Examinateur
MARTIN, Vincent	Directeur de Recherche	Université Pierre et Marie Curie	Examinateur
PAVIC, Goran	Prof. Emer.	INSA-LYON	Directeur de Thèse

Characterisation of Air-borne Sound Sources using Surface Coupling Techniques

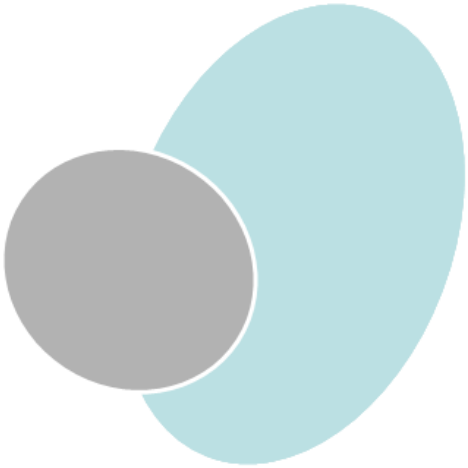

Liangfen DU

Laboratoire Vibrations Acoustique
INSA-Lyon

This dissertation is submitted for the degree of
Doctor of Philosophy

Université de Lyon February 2016

I would like to dedicate this thesis to my loving parents and my dear husband Lilei.

路漫漫其修远兮，吾将上下而求索。

— 屈原《离骚》

"The road ahead will be long, and our climb will be steep."

— Qu Yuan (340-278 BC), *Li Sao*

Acknowledgements

First of all, I would like to acknowledge the China Scholarship Council (CSC) and Laboratoire Vibrations Acoustique (LVA) to support my thesis.

All my respect and thanks to my supervisor, Goran Pavić. I feel very fortunate to have such a supervisor whose broad scientific view and enthusiasm to research always inspires me. Thank you for guiding my study smoothly in the past four years. Your patience and kindness helped me pass through the difficult times. I also express my gratitude to Patrick Blachier, Thomas Monnier, François Girardin. Without you, I could not finish my experimental work in my thesis.

I would like to thank Corinne and Anders. Corinne, thank you and your mother Mrs Lotto for inviting my husband and me to celebrate new years with you from the first year I was in France. During the past four years, you helped me a looooot. Because of you, I did not feel alone. I know you are always there when I need you, as you always said to me. My scientist brother, Anders, you are really special and nice for me. Once I had any scientific problems, you were always the first person that came to my mind. I am so lucky that you were always there. Your hard and solid work encouraged me to be a Ph.D student like you. I also appreciate your greeting and invitation from Bretagne during my thesis redaction.

I would like to thank my friends in Lyon, Liang Yu, Jin Cui, Yao Zhu, Antonio, Ha, Magda and Clotilde. We passed so much wonderful time together. I would also like to thank my colleges in the lab, Loïc, Fulbert, Min Yao, Ge Xin, Sandra,...

At last, I would like to appreciate the support and unconditional love from my parents. Their optimism and open-minded attitude towards the life always encourage me when I feel depressed. My darling Lilei, thank you for always being beside me, for sharing my happiness and sadness, for wiping my tears and fears, for everything.

J'aime Lyon!

Abstract

The thesis investigates possibilities of air-borne sound characterisation of arbitrary sound sources. To this end a particular approach is studied where the source characterisation is done via an interface surface which fully or partially envelopes the physical source. Two frequency-dependent descriptors are defined across such a surface: the blocked sound pressure and the source impedance. The former represents the sound pressure created by the operating source which acts on the enveloping surface when this is made immobile. The latter represents the ratio of pressure response amplitudes and normal velocity excitation amplitudes across the surface. The enveloping surface defines an air volume containing the physical source, called the source space.

The two source descriptors defined on the source space, the blocked pressure and the source impedance, are shown to be intrinsic to the source, i.e. independent of the surrounding acoustical space. Once defined, these descriptors allow one to find the sound pressure and normal particle velocity at the interface surface when the source space is coupled to an arbitrary receiver space, i.e. a room. This in turn allows for sound prediction in the receiver space. The coupling conditions require that the receiver space is characterised using the same enveloping surface as the source space.

Bearing the measurement simplicity in mind, the enveloping surface has been conceived as consisting of one or several rectangular plane surfaces. The research challenge was then to obtain meaningful surface impedance across a (continuous) rectangular plane surface as well as the blocked pressure compatible with impedance formulation. This has led to a spatial decomposition of sound pressure and particle velocity into finite number of components, each defined by a complex amplitude and a particular spatial distribution. In this way the blocked pressure reduces to a vector of complex pressure amplitudes while the impedance becomes a matrix of pressure and velocity complex amplitude ratios. Two decomposition methods have been investigated in detail: the surface harmonic method and the patch method. The former approximates the surface pressure and normal velocity by combinations of 2D trigonometric surface functions while the latter splits the surface into small patches and treats each patch in a discrete way, using patch-averaged values.

Following an introduction to the subject and a literature review, the principles of the enveloping surface approach are outlined. The feasibility of the approach is then demonstrated by a simple measurement, using straight tubes as source and receiver spaces and a loudspeaker driver as the physical source. The need for careful transducer matching was observed. A 3D study of the approach by analytical and FEM modelling is then carried out for both surface harmonic and patch methods. The criteria are established regarding the selection of parameters of each method which allow a straightforward comparison of the two from a measurement point of view. The patch method, considered as more suitable, is then employed to perform an experimental 3D validation. Two cavities are used to this end, acting as source and receiver spaces. The validation is done by comparing the sound pressure spectra in the receiver cavity, once using the coupling procedure based on the developed characterisation approach and then using direct measurements. Reasonably good matching between coupling and direct measurements was obtained; the observed discrepancies could be attributed to the identified measurement imperfections. The experiment has shown that a major effort is needed to design and produce the coupling surface as well as driving and receiving patches required to carry out the measurement of blocked pressure and surface impedances.

The principle of coupling by an envelope surface, used for source characterisation, is further extended towards numerical modelling of multiple-connected spaces. An assessment of this technique is done via case studies of 3-room and 4-room assemblies, modelled by both surface harmonics and patch approaches.

Table of contents

List of figures

List of tables

Chapter 1

Introduction

1.1 Context

'Quieter', as an ever increasingly important feature of many industrial products such as vehicles, machines or domestic appliances, is frequently required by both manufacturers and users. For users, 'quieter' means healthier life and more comfortable user experience. Hence for manufactures, 'quieter' makes products more competitive in gaining a large market share. The requirement of quieter products promotes the research on noise reduction.

In practice, noise reduction of a product can be performed at two different production stages, i.e., before or after the final assembly. Traditional methods evaluate noise levels on assembled products. The NVH (Noise, vibration, and harshness) engineers are left the choice to reduce noise at the source, on the transmission paths, or changing the characteristics of the receiver, i.e., the acoustical environment. Take as an example the noise reduction in the cabin of an excavator. The engineers should decide which engine is less noisy, which absorption material should be used to reduce noise, and which earmuff is preferred for a driver. Using a basic trial and error approach, the excavator should be assembled with different engines respectively, and tested with all combinations of absorption materials and earmuffs. The advantage of this traditional method is that once the measurement is performed, we know the effects of various solutions on the noise reduction. However, the disadvantage is also obvious that for all possible solutions, assembling and testing require high cost and are time-consuming. Especially, repetitive reconstruction of acoustical spaces is always nontrivial.

To avoid costly and time-consuming experiments, the emphasis is growing on predicting sound radiation before the final operation of assembly, i.e., during the design stage of a product. Continuing with the excavator example, if we can obtain the intrinsic characteristics of noise emitted by different engines as well as the characteristics of the cabin equipped with

different absorption materials and earmuffs, we may be able to predict operator's noise for all possible engine/absorption/earmuff combinations on a virtual assembly platform. Even though the prediction may be only a rough estimation of the actual noise, it provides valuable information about different product solutions and thus helps us to save time and cost. A few feasible solutions can be then realized in the real environment and be tested by measurement. The combination of virtual simulation and real experimentation provides an efficient way of figuring out an optimal solution of noise reduction.

A usual way to predict the sound level emitted by a source in a large space is to measure the sound power radiated by the source into a standardised environment. The sound power measurement can be done in different ways, e.g., in a room of known absorption area, in a free or semi-free space or by using sound intensity measurements. The methods are standardised, the most commonly used one being the open-space method based on measurement of sound pressure levels, ISO 3744. However, it turns out that the sound power is not a convenient quantity to intrinsically characterise an acoustical source especially where small spaces are concerned. Not only the sound power depends on the environment into which the source outputs its sound, and thus is not an independent source descriptor, but also the power cannot account for the interaction of the source with its surrounding space which decisively affects the transmitted sound.

Alternatively, researchers have made efforts on the study of sound prediction or sound field reconstruction, aiming at finding an economic way to replace a sound source and reconstruct its sound radiation in a specific space. Equivalent source method (ESM) is one of the commonly used methods of source modelling; its main idea is to replace an original noise source by several simple sources, i.e., monopoles or dipoles. The objective is to find a composition of simple sources, which are parameterized by different amplitudes and phases, to reproduce the sound pressure by the original source. Generally, the ESM is a straightforward replacement solution and can provide reliable sound equivalence by carefully turning the acoustic parameters, i.e., amplitude and phase of each simple substitute source. However, as the sound radiation of the original source is dependent on the receiving acoustical space, for each acoustical space, we still have to seek an equivalent substitute solution: the ESM is not intrinsic.

Numerical characterisation methods, such as finite element method (FEM), carry out sound prediction in a completely virtual way. Specifically, computer-aided design (CAD) is used to design shape and structure of a certain sound source, and FEM helps to simulate sound vibration and predict the sound radiation in an acoustical receiver. These methods shorten the period of developing a product and thus are much more economic compared with the traditional approaches. However, current acoustic simulations are restricted to ideal

cases because many practical parameters are empirically determined. For example, damping factors, a property of mechanical joints, are usually dealt with as known parameters but are actually a rough estimate of real values. As a result, predicted sound radiation by these methods may produce large discrepancies in comparison validation.

In addition, neither Equivalent source method nor characterisation methods can take all the parameters of a complex sound source into account, which is another disadvantage of these two kinds of methods.

1.2 Focus and Contribution

A noise source may radiate noise through structure-borne and/or fluid-borne paths, but most probably, the sound will be emitted into air and reach one's ears. While many characterisation methods have dealt with structure-borne and in-duct sources fairly extensively, the air-borne characterisation has received less attention, probably because the measurement of air-borne sound is considered as a simple, self-evident task. However, the problem of independently characterising air-borne sound sources is far from obvious, so this thesis will focus on the characterisation of air-borne sound sources.

It is known that sound radiation of a physical source depends on its surrounding acoustical receiver. Sound radiation due to the same source in different acoustical receivers varies. If we could characterise a given source in a given surrounding space by two independent models – a source model and a receiver model, the sound radiation due to the same source in any acoustical receiver could be reconstructed by coupling the established source model to the corresponding receiver model. Obviously, the source model should be intrinsic, i.e., independent of surrounding spaces. Such an intrinsic model can then provide sound prediction.

An independent source characterisation method named *source characterisation via enveloping surface* can provide such an independent source model. The core idea of this source characterisation method is to split an entire acoustical system by determining an enveloping surface to carry out the characterisation. Imagine that a given sound source will be installed in a target acoustical space, as shown in Fig. 1.1. A virtual enveloping surface is applied to both the source and the acoustical space. The enveloping surface can *fully or partially* envelop the source and divide the entire acoustical system into two independent spaces: one space with the source and the other one without the source. The space with the source will be called 'Source space' while the other one will be called 'Receiver space'. The source space and the receiver space are coupled through the enveloping surface and together compose the entire acoustical system.

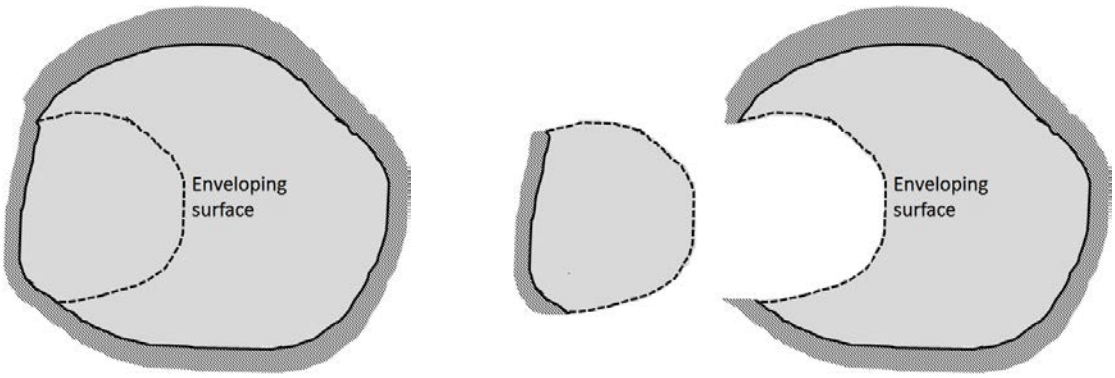

Fig. 1.1 Principle of source characterisation. (a) Acoustical system, (b) Source space, (c) Receiver space

As the source and receiver spaces are independent of each other, the two spaces can be characterised through the same enveloping surface separately. The objective is to find suitable descriptors for the source and the receiver. In this thesis, the descriptors will be the blocked pressure and the impedance.

In the source space, when the enveloping surface is blocked, the pressure across the enveloping surface due to the operating source is *Blocked pressure*. When the source is switched off, the impedance of the surface is *Source impedance*. The two source descriptors – Blocked pressure and Source impedance – represent the source model which intrinsically characterise the acoustical properties of the source space at the enveloping surface.

In the receiver space, the impedance of the enveloping surface is *Receiver impedance*. It is a receiver descriptor which intrinsically characterises the acoustical properties of the receiver space at the enveloping surface. Under the continuity conditions of pressure and normal particle velocity across the enveloping surface, the coupling velocity across the enveloping surface can be obtained using the identified source and receiver descriptors. The enveloping surface with the prescribed normal velocity acts as an equivalent source driving the receiver space taken on its own. Then the sound radiation due to the original source can be predicted.

As the enveloping surface plays an important role in the source characterisation, the attention should be paid to the selection of enveloping surface. A surface consisting of one or several plane rectangular surface is preferred because it is easier to carry out the measurement on a plane surface than on an uneven one.

The current challenge is how to identify the blocked pressure, source and receiver impedances via the enveloping surface. The thesis focuses on developing two surface coupling techniques – 'Continuous surface coupling technique' and 'Patch surface coupling technique' – to compute and measure these descriptors, either for source characterisation via

enveloping surface, or for sound reconstruction of a given source in an arbitrary acoustical receiver.

- **Continuous surface coupling technique:** by expanding the sound field into surface harmonics, the pressure and the impedance of the surface are expressed by a number of continuous spatial functions, called surface harmonics. Using the prescribed plane surface harmonics, the pressure across a surface is expressed by the complex amplitudes of these harmonics while the surface impedance is expressed by a corresponding matrix. Hereby the Continuous surface coupling technique is named 'Harmonic technique'.

- **Patch surface coupling technique:** it is an alternative way to obtain the descriptors. It consists dividing the surface into a number of patches. The pressure and the impedance of the surface are defined on the basis of the patch concept. The surface is divided into a number of patches. The pressure across the surface is expressed by the pressure amplitude averaged across each patch while the surface impedance is expressed by patch-averaged pressure and velocity amplitudes. Hereby the Patch surface coupling technique is also named 'Patch technique' for short.

The main contribution of this thesis is that we provide a comprehensive study of the above two techniques. We apply both analytical and numerical modelling to demonstrate the use of the two techniques for sound prediction. Moreover, we apply the Patch technique by measurement to characterise laboratory sound sources such as compression driver and audio speaker. A few challenging practical problems in measurement are addressed to complete the study.

1.3 Outline

The work carried out during this thesis is divided into eight chapters:

Chapter 1 is the introduction. The context of this thesis is introduced to explain: the motivation of characterising sound sources via enveloping surface, the challenge we will meet during the study on the characterisation of sound sources.

Chapter 2 will survey relevant literature prior to the discussion of the two proposed surface coupling techniques. Research work on sound reconstruction will be summarized and commented. The advantages and disadvantages of the surface coupling techniques will be indicated by comparing with the related work.

Chapter 3 will first introduce the principle of source characterisation via enveloping surface and present the concepts of blocked pressure, source and receiver impedances. To

illustrate and validate the approach, the characterisation of a compression driver will be carried out via a virtual enveloping surface, and then its sound radiation in a tube will be predicted with the measured blocked pressure, source and receiver impedances.

Chapter 4 and Chapter 5 will successively investigate the two techniques – 'Continuous surface coupling technique' and 'Patch surface coupling technique'. Analytical and numerical modelling are applied on a few cases to validate and compare the two techniques. The limitation of the techniques will be also analysed.

In Chapter 6, the characterisation of a laboratory source in a 3D acoustical space will be experimentally validated using the Patch technique. A few practical problems will be presented and addressed for accomplishing the sound prediction of the source in the acoustical space.

Chapter 7 will show an application of two surface coupling techniques alternative to source characterisation – the sound prediction in multiple connected spaces.

The final chapter, Chapter 8, will conclude the thesis and show the perspectives of future work.

Chapter 2

Literature Review

Before going into details of the proposed two surface coupling techniques, we first review the related literature on methods of source characterisation. Specifically, all these methods focus on developing a representative source model to obtain the characteristic of an original sound source. The source model could either be an equivalent source replacing the original source or be just a set of descriptors completely characterising the acoustical properties of the source. In practice, designing a good source model depends on the size of the original source and the frequency of its sound.

If the sound wavelength λ is much larger than the typical dimension L of the original source, $\lambda \gg L$, the original source can be simply considered as being condensed at a point, like monopole, dipole, quadrupole, etc, or a combination of them. At the other end of sound frequency range with the sound wavelength λ being much smaller than the typical source dimension L, i.e., $\lambda \ll L$, the source is often characterised by a single descriptor – the total radiated sound power [1]. The sound power can be measured in a diffuse field with the known absorption area [2]. However, as the sound power depends on the surrounding acoustical space of the source, it does not act as an intrinsic descriptor and can not explain the interaction between the source and its surrounding space.

Besides, the case of middle frequencies, i.e., when the sound wavelength λ approximates the source dimension L ($\lambda \approx L$), is the most common situation in practical applications and on which the present work focuses. Since in this case a simple solution, such as modelling the source by the sound power, is no longer suitable, alternative source models have been developed, e.g. [3, 4]. The source methods, classified as the *source reconstruction methods*, mainly aim at reconstructing the vibration velocity over the boundary surface of sound source. In contrast to these methods the *equivalent source methods* work on replacing the actual sound source by a set of adequately located elementary sources such as monopoles and dipoles. However, the equivalent source methods are not specifically oriented towards

independently characterising sound sources with respect to different surrounding spaces. Yet another group of methods exists, the *coupling source characterisation methods* which intrinsically characterise the source by avoiding to reconstruct its surface vibration.

2.1 Source Reconstruction Methods

The source reconstruction methods aim at reconstructing the vibration velocity across the boundary surface of an original source, then sound radiation due to the vibration of the original source in an arbitrary space can be predicted from the reconstructed surface velocity. In other words, the reconstructed velocity on the source surface is a source model sufficient to predict the sound radiation. Two classical source reconstruction methods will be outlined in this section: Near-field acoustical holography (NAH) which is mainly applied to sources of simple geometries and Inverse boundary element method (IBEM) which is more adapted to sources of complex geometries. A recently developed technique, the Dummy source method (DSM), aims at source reconstruction using simplifications applicable in industrial applications.

Before going into details of the three methods, we first show the general schematic view of a sound radiation model. Considering a sound source of finite volume V_s, bounded by a continuous surface S_s, as shown in Fig. 2.1, the source radiates sound in the free field domain V. A surface S_h, called acoustical hologram, is used to divide the volume V into two parts: the volumes V_b and V_f, accordingly $V = V_b \bigcup V_h$. The acoustical hologram S_h is close to the source surface S_s. We first measure the pressure or velocity on the surface S_h. The procedure of the velocity reconstruction on the boundary surface S_s by the measured sound data on the hologram S_h is called 'backward propagation'; the sound radiation in the

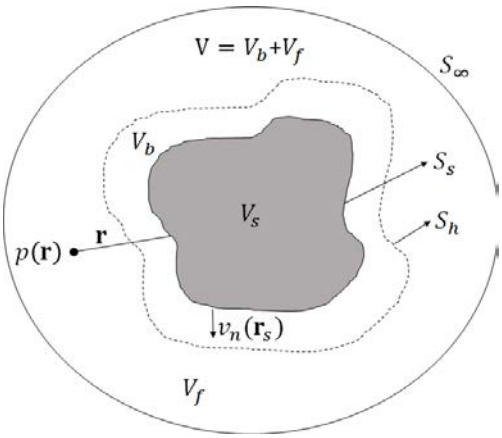

Fig. 2.1 Schematic view for sound radiation

volume V originated from the velocity on the source boundary surface S_s is called 'forward propagation'. Concretely, the backward propagation is first performed to reconstruct the normal velocity on the boundary surface S_s. Once the velocity distribution across the source surface is obtained, we can apply forward propagation to predict the sound radiation in the volume V. The sound pressure $p(\mathbf{r})$ at an arbitrary point $\mathbf{r}$ in the volume V satisfies the Helmholtz equation; all the discussion in this section is on the base of this equation.

$$\nabla^2 p(\mathbf{r}) + k^2 p(\mathbf{r}) = 0 \tag{2.1}$$

where k is the wave number of the sound, ∇^2 denotes the Laplace operator.

2.1.1 Near-field Acoustical Holography

NAH, introduced by Maynard *et al.* [5], is a spatial Fourier transform based method. The procedure of source reconstruction by NAH is:

1. Measuring the pressure responses due to an original source in the frequency domain at sampling points on the acoustical hologram S_h shown in Fig. 2.1;
2. Translating the measured pressures in the frequency domain to that in the wave number domain by the spatial Fourier transform;
3. In the wave number domain, projecting the pressure field to the boundary surface velocity of the source by multiplying specific propagators;
4. Taking the inverse spatial Fourier transform to transfer the surface velocity of the source in the wave number domain to that in the frequency domain, which is the expected final result.

To increase the resolution of the reconstructed surface velocity, the evanescent wave components should be captured, which can be carried out if the acoustical hologram S_h is fairly close to the boundary surface S_s of the source. Specifically, the procedure of the source reconstruction in the frequency domain by NAH is indicated by the following equation,

$$\hat{v}(S_s) = \mathscr{F}_s^{-1}\{\mathscr{F}_s[p(S_h)]G_s\} \tag{2.2}$$

where $\hat{v}(S_s)$ is the reconstructed vibration velocity on the boundary surface S_s of a vibrating body, $p(S_h)$ is the pressure measured on the acoustical hologram S_h in frequency domain, G_s denotes a propagator in a specific coordinate while $\mathscr{F}_s$ represents the corresponding spatial Fourier transform.

Williams [6] presents a complete review of the principle of NAH including the spatial Fourier transforms in Cartesian, Cylindrical and Spherical coordinates, respectively. Based on NAH, the velocities of planar, cylindrical and spherical sources in an unbounded field can be reconstructed from the measured pressures on the holograms [5, 7, 8]. It should be noted that the pressure measured at sampling points on the hologram generates replicated sources because of the spatial Fourier transform. And the generated replicated sources would introduce artificial wave numbers that actually not exist, which therefore causes wraparound errors to the final reconstruction result. To eliminate the wraparound errors, it is suggested introducing the truncated Green's function or increasing the size of measurement aperture for decreasing the influence of replicated sources [5, 6].

Concerning the difficulty in measuring the relative phase between the acoustic pressure on the hologram and the normal velocity of the source, Loyau *et al.* [9] presented a method, Broadband Acoustic Holography from Intensity Measurements (BAHIM), to overcome this problem. It is shown that the relative phase between those two variables can be obtained from components of sound intensity parallel to the plane of the specific source. The intensity values are measured independently at points on the hologram and do not require a phase reference signal corresponding to the original source. This method is thus applicable to sources emitting a broadband spectrum and, more generally, to industrial sources, for which the excitation is not known.

Generally, source reconstruction by the traditional NAH requires the source surface described by separable coordinates, thus it is only suitable for the simplest cases, such as planar, cylindrical and spherical sources. Several advanced NAH based methods were then proposed for source reconstruction in relatively complex cases. Sarkissian [10] proposed a new formulation of NAH for sources of an axisymmetric geometry. The author suggested that the surface normal velocity is expanded in an orthogonal set of functions related to the eigenvectors of the equivalent Laplace problem. For separable geometries, the acoustic field is decomposed into Laplace polynomials multiplied by weighting coefficients. Their experiments showed that the velocity reconstruction of a cylindrical shell with flat endcaps matches well the reference result.

Villot *et al.* [11] described a technique named 'Phonoscopy' which associates the acoustical holography technique to the image sources method to make possible the source reconstruction by NAH in a bounded sound field. With the help of image sources, the acoustic field is computed as a superposition of contributions from original sources and their images. The sound radiation of plane sources inside an enclosure is studied.

Moreover, some derivative NAH techniques were proposed to resolve specific problems. For example, unlike the traditional NAH scanning the complete hologram surface pressure,

Patch NAH [12] only requires to scan a small area (i.e., a patch) on the surface. Another example, SONAH (Statistically Optimal NAH) [13], avoids the errors caused by the use of spatial DFT/FFT in conventional planar cases. Overall, there is no general NAH method commonly useful for sources of arbitrary geometry because the measurement on the hologram varies due to different geometries. A thorough review about NAH-based source reconstruction methods was presented in [14].

2.1.2 Inverse Boundary Element Method

Since the NAH method relies on analytical modelling of the prescribed hologram near a vibrating body, the measurement differs with respect to sources of different shapes. Therefore the second reconstruction method, Inverse boundary element method (IBEM), was originally proposed to overcome the limits of NAH, i.e., to deal with arbitrarily shaped sources [15–17]. We take the same radiation model in Fig. 2.1 to introduce IBEM that is based on the Kirchhoff-Helmholtz integral equation.

$$\alpha p(\mathbf{r}) = \int_{S_s} [p(\mathbf{r}_s)\frac{\partial G(\mathbf{r},\mathbf{r}_s)}{\partial n} - \frac{\partial p(\mathbf{r}_s)}{\partial n} G(\mathbf{r},\mathbf{r}_s)] dS_s \tag{2.3}$$

where $\mathbf{r}_s$ and $\mathbf{r}$ are, respectively, the source point and the field point; $G(\mathbf{r},\mathbf{r}_s)$ is the free-field Green's function with the distance $|\mathbf{r}-\mathbf{r}_s|$ between the field point $\mathbf{r}$ and the source point $\mathbf{r}_s$; $\partial/\partial n$ means the derivative in the direction normal to the source surface. One can see that this equation relates the acoustic pressure within a sound field (i.e., $p(\mathbf{r})$) to the pressure $p(\mathbf{r}_s)$ on the boundary surface of the source. Theoretically, the boundary surface of an arbitrarily shaped source can be discretized into small sections, thus either forward or backward propagation by Eq. (2.3) is achievable.

The coefficient α in Eq. (2.3) depends on the position of the field point,

$$\alpha = \begin{cases} 1, & \mathbf{r} \in V \\ \frac{1}{2}, & \mathbf{r} \in S_s \\ 0, & \mathbf{r} \in V_s \end{cases} \tag{2.4}$$

Besides, the normal particle velocity on the boundary surface S_s of the source is defined by the Euler's equation,

$$v_n(\mathbf{r}_s) = \frac{1}{j\rho_0\omega}\frac{\partial}{\partial n} p(\mathbf{r}_s) \tag{2.5}$$

By assigning $\alpha = \frac{1}{2}$ in Eq. (2.4) and with the boundary surface discretized into adequate elements, combining Eqs. (2.3) and (2.5) [18] yields ,

$$\{v_n\}_s = ([D_f][D_s]^{-1}[M_s] + [M_f])^{-1}\{p\}_f \tag{2.6}$$

The matrices $[D_s]$ and $[M_s]$ are dipole and monopole matrices of the surface pressure, $[D_f]$ and $[M_f]$ are those corresponding to field pressures, $\{p\}_f$ and $\{v_n\}_s$ represent the field pressure vector and source velocity vector. Eq. (2.6) indicates the principle of source reconstruction by IBEM. Obviously, the source reconstruction by IBEM is an inverse problem, which is generally expressed as [19],

$$\mathbf{q} = \mathbf{H}^{-1}\mathbf{p} \tag{2.7}$$

where $\mathbf{q}$ denotes the source model going to be determined, i.e., the reconstructed velocity across the boundary surface; $\mathbf{H}$ denotes the system model; and $\mathbf{p}$ is the measured value, i.e., the field pressure.

Gardner and Bernhard [15] firstly displayed the principle of IBEM. The author formulated and evaluated a noise source reconstruction procedure based on the inverse Helmholtz integral equation and numerical models. Compared to NAH, the method shown in the paper permits the field point data to be taken at any general location throughout the acoustic space. Besides, the authors demonstrated that once the identification procedure is complete, the identified solution can be used to further identify source interaction with other sources and any external physical system.

In terms of numerical simulation, Bai [17] adopted a pulsating sphere, a cylinder with spherical endcaps and a vibrating piston set in a rigid sphere to verify the algorithm of IBEM. Satisfactory agreement has been achieved between the holographically transformed results and reference analytical solutions. Kim and Ih [20] used IBEM to reconstruct the normal velocity distribution on irregularly shaped cavities. Particularly, based on the minimisation of the mean square error given by the variance of the measurement noise and the deviation introduced in the reconstruction process, they optimize measurement positions, reduce the number of measurement points, as well as improve the resolution of the reconstructed field.

As the traditional IBEM assumes that measurement is done in a free field and can not be used when there are perturbations or exterior sources. Langrenne *et al.* [21, 22] proposed a double layer BEM method for recovering free field conditions from bounded noisy environment, so that the velocity reconstruction on the vibrating surface could be achieved properly. The double layers close to the surface surrounding the source were used for separating the outgoing field of the original source from the ingoing field of all

secondary sources. The free pressure field radiated by the source was the outgoing field with the scattering sound field removed. The satisfactory results obtained on simulation opened possibility of characterisation of real sources in noisy spaces. Besides, Langrenne and Garcia [23] presented another method named 'Data completion method' which can also allow the characterisation of sound sources on the exterior domain or in a confined domain where there exists acoustic perturbation. Different from IBEM, the pressure and normal surface gradient instead of pressure should be measured. And under the condition or assumption of no extra sources between the measurement hologram and structure source, Data completion method could be applied for source characterisation.

From Eq. (2.7) we can see that if the matrix $\mathbf{H}$ is ill-conditioned, the matrix inversion $\mathbf{H}^{-1}$ may yield large error due to small singular values. Veronesi and Maynard [16] solved Eq. (2.7) using Singular Value Decomposition (SVD) and suggested that only using the highest singular values can improve the quality of reconstruction results. The idea appeared in the paper is similar to that of a latter classical technique for regularising ill-posed problems – 'Truncated Singular Value Decomposition' (TSVD). Nowadays, many other regularization techniques are also employed to treat the ill-posed problems and to avoid unstable solutions dominated by errors [24, 25]. A well-known technique to regularize ill-posed problems is Tikhonov regularization [26], whose idea is to include a regularization term $\eta^2\|\mathbf{q}\|^2$ in minimization [27]:

$$\hat{\mathbf{q}}(\eta) = \text{Argmin}\{\|\mathbf{p} - \mathbf{H}\mathbf{q}\|^2 + \eta^2\|\mathbf{q}\|^2\} \tag{2.8}$$

The key is to find a suitable regularization parameter η that produces a solution well fitting the measurement data. Besides, a Generalized Weighted Inverse Beamforming (GWIB) technique proposed by Presezniak *et al.* [28] was proposed to optimize the regularization strategy and increase the quantity of source identification.

In conclusion, compared with NAH, IBEM has the following advantages:

- It is flexible with respect to the source geometry;
- It has no restriction on the location of the field point, whereas NAH requires the hologram to be fairly close to the source;

However, the price to be paid for these advantages is that much more measurement points are required by IBEM. In order to increase the robustness of Eq. (2.7), the number of measurement points should be made much larger than that of the reconstructed quantities, so that the matrix $\mathbf{H}$ gets over-determined. This requirement may pose problems in handling the sources of complex geometry.

2.1.3 Dummy Source Method

IBEM requires large number of measurement points for the velocity reconstruction of a complex source. A similar approach, the Dummy Source Method (DSM) developed by Lindberg and Pavić [29], uses source shape simplification as well as coarse surface vibration discretisation to avoid the drawback. The dummy is a closed cabinet of similar size but much simpler shape than the real source, equipped with a flush-mounted array of loudspeaker drivers, Fig. 2.2. It accounts for both sound radiation and diffraction by the source. In-depth discussion about this method were provided in [30, 31].

The pressure $\hat{p}(\mathbf{r})$ at a point $\mathbf{r}$ in an acoustical space due to the original source is approximated by a superposition of pressures from each driver,

$$\hat{p}(\mathbf{r}) = \sum_{i=1}^{M} Z_i(\mathbf{r}, \mathbf{r}_s) Q_i(\mathbf{r}_s) \tag{2.9}$$

where M is the number of drivers integrated in the dummy surface; $Q_i(\mathbf{r}_s)$, the volume velocity of the i^{th} driver at the position $\mathbf{r}_s$, represents the source model; $Z_i(\mathbf{r}, \mathbf{r}_s)$, the transfer impedance, satisfies the principal acoustical features of the observation space and relates the volume velocity amplitude of the i^{th} driver to the corresponding pressure response $p_i(\mathbf{r})$ at a receiving point $\mathbf{r}$,

$$Z_i(\mathbf{r}, \mathbf{r}_s) = \frac{p_i(\mathbf{r})}{Q_i(\mathbf{r}_s)} \tag{2.10}$$

The source model $Q_i(\mathbf{r}_s)$ can be obtained in this way: install the original source in an laboratory space, such as semi-anechoic room, measure the exact pressure responses $p(\mathbf{r})$ at few receiving points. Then replace the original source by the dummy source, and measure the transfer impedance $Z_i(\mathbf{r}, \mathbf{r}_s)$ between drivers and the same receiving points. Substituting the measured $p(\mathbf{r})$ and $Z_i(\mathbf{r}, \mathbf{r}_s)$ into Eq. (2.9) yields the volume velocity $Q_i(\mathbf{r}_s)$ of each driver. With each driver operating with corresponding volume velocity $Q_i(\mathbf{r}_s)$, the dummy source can be as an equivalent source to predict the sound radiation and diffraction due to the original source. Moreover, the number of required drivers M and the average spacing δ between two adjacent source positions are roughly given by [29]

$$M \approx 4S\frac{f_{max}^2}{c^2}, \quad \delta \approx \frac{c}{2f_{max}} \tag{2.11}$$

where S is the area of the dummy surface and f_{max} is the maximum frequency.

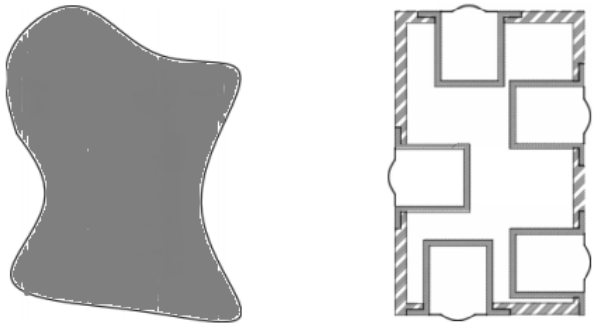

(a) Source (b) Dummy

Fig. 2.2 Schematic view of a vibrating body (left) which can be characterised by a closed cabinet equipped with a driver array (right) [30].

2.2 Equivalent Source Methods

This section will introduce the second group of methods to source modelling – Equivalent source method (ESM), also named in the literature 'wave superposition method' and 'substitute source approach'. The basic idea of this method is that the sound field of the original source can be simulated by a finite number of elementary sources, such as monopoles and dipoles [32–34], located on an inner auxiliary surface. As shown in Fig. 2.3, a vibration source of volume V_s and with normal vibration velocity $v_n(\mathbf{r}_s)$ is replaced by a set of elementary sources. Then the pressure $p(\mathbf{r})$ at a point $\mathbf{r}$ in the volume V due to the original source is approximately reconstructed by N elementary sources, that is

$$\hat{p}(\mathbf{r}) = \sum_{i=1}^{N} c_i q_i(\mathbf{r}, \mathbf{r}_i) \tag{2.12}$$

where $\hat{p}(\mathbf{r})$ is the reconstructed pressure response; $\mathbf{r}_i$ is the position of the i^{th} elementary source; $q_i(\mathbf{r}, \mathbf{r}_i)$, a weighting function; c_i, the coefficient of the weighting function, represents the strength of the i^{th} elementary source. $\hat{p}(\mathbf{r})$ satisfies the Helmholtz equation Eq. (2.1) and the imposed boundary conditions. The parameters c_i and $q_i(\mathbf{r}, \mathbf{r}_e)$ together present the source model, and they are determined by minimizing the error between the reconstructed and exact velocities across the source surface.

The equivalent source can be given by a finite number of multipoles q_i of source strengths c_i located at a single position $\mathbf{r}_i$; the method is then an *one-point multipole method*. If more than one source locations are used, the method becomes a *multi-point multipole method*. Moreover, if the source only consists of monopoles, the method is called *single layer method*; if the source is a hybrid combination of monopoles and dipoles, the method is called *double*

layer method [35]. Specifically, the equivalent source model can be composed of a set of elementary sources that may be placed inside the real source [35] (Fig. 2.3, the usual case), on the surface of the real source [36], or even outside the surface of the real source [37].

Koopmann *et al.* [38] described the acoustic field of arbitrarily shaped sources as a superposition of waves generated by a continuous distribution of monopoles. This single layer method, having an array of monopoles within the volume occupied by the real source, is used to reproduce a velocity prescribed on the surface of the source. The monopoles are assumed to be located over a spherical surface inside the source for convenience. The strengths of the monopoles are determined by imposing a minimal discrepancy between the velocity $\hat{v}_n(\mathbf{r}_s)$ generated by the monopoles and the prescribed velocity $v_n(\mathbf{r}_s)$ on the surface's boundary, i.e., $\min\{\|\hat{v}_n(\mathbf{r}_s) - v_n(\mathbf{r}_s)\|^2\}$. Numerical experiments involving spherical and cube radiators in the paper demonstrated that the method has the uniqueness of solution and nonexistence of singularities.

Jeans and Mathews [39] presented a hybrid combination of single and double layer method to study the numerical stability and robustness of the equivalent source formulation. The velocity reconstruction error is minimized to select the optimal interior nodal positions for multipoles. Numerical results of both the spherical and spheroid surfaces indicate that the optimal solution needs the equivalent source nodal points to be placed at a fixed distance along the normal from the surface boundary of the real source, otherwise a dramatic loss of solution accuracy may occur when the multipoles are placed at any other locations.

Pavić [40] presented a particular 'greedy search' procedure to identify suitable positions of monopoles by an iterative elimination technique. Later, the author [41] found that keeping the same order of complexity (the product of the source number and source order), multipoles may perform better in providing more accurate solution than the monopoles.

Ochmann [42] presented an overview about a few equivalent source methods. It was shown that the number of elementary sources depends on a variety of parameters, e.g.,

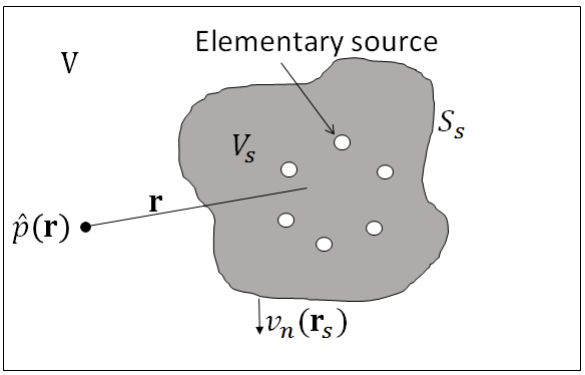

Fig. 2.3 Schematic view of equivalent source model.

the type of poles, the shape of the real source, the desired accuracy of the solution, the minimisation process. Specifically, various minimisation techniques such as the least square minimisation technique, the null-field equations, the Cremer equations are investigated and the corresponding error functions are given.

The methods by Koopmann [38] and Jeans and Mathews [39] work out the acoustic parameters, the type of equivalent sources and the nodal positions, by minimizing the error of the boundary surface velocity. In contrast of this, Wang and Wu [43] proposed to solve the Helmholtz equation directly with the sound field expressed by means of an expansion of spherical harmonics. In other words, solutions to Eq. (2.1) subject to specific boundary conditions can be approximated by Eq. (2.12). The source model $c_i, q_i(\mathbf{r}, \mathbf{r}_s)$ is determined by making the error of the pressure minimized, i.e., $\min\{\|\hat{p}(\mathbf{r}) - p(\mathbf{r})\|^2\}$, through the least-squares method. Thus this method is called Helmoholtz Equation Least-Squares (HELS) by the authors. The method has been applied to reconstruct sound radiation in different cases, such as that of a vibrating body inside a cavity [44] or a complex nonspherical structure [45].

Ochmann [46] then developed the so-called Full-Field Equations (FFE). Two kinds of functions have been tested: spherical Bessel and Hankel functions; whereas the solution of the former lacks uniqueness, the latter always yields unique solution. The full-field equations are solved directly, which leads to low time-consuming singular value decomposition.

Other extended techniques have been proposed to improve the performance of the point multipole method. For instance, a Multiple Multipole Expansion Algorithm (MMEA) [47] employs the truncated multipole expansion (monopole + dipole + quadrupole) to develop a non dimensional convergence criterion in terms of the source spatial extent. The use of the multipole expansion together with an efficient numerical implementation allows a quick and reliable evaluation of the radiated sound power. Another example is the Complex Equivalent Source Method (CESM) [33, 48] that allows the equivalent sources locating at complex source nodal points based on the wave superposition. Johnson *et al* [49] calculate the sound field inside an enclosure containing scattering objects, where the equivalent sources are located outside the enclosure boundary. Moorhouse and Seiffert [50] have found that a line of four monopoles was sufficient to characterise a small motor. Tomilina *et al.* [51] used ESM to model the radiation by elastic bodies the velocity of which is not prescribed but affected by the radiation loading.

The Equivalent Source Method has been widely used to characterise arbitrarily shaped sources. One of the disadvantages of the ESM is that it cannot take into account the diffraction around the source as the point equivalent sources are transparent. Apart from that, it relies on experience to find optimal positions of the equivalent sources since no general rule exists for constructing the source system [42, 52].

2.3 Coupling Source Characterisation Methods

Acoustical holography is applicable to sources of simple shape which produce sound by vibration. IBEM can treat sources of more complex shape but have the limitation on the number of measurement points, and thus on the detail of velocity distribution of the source represents a restriction. The equivalent source methods produce the characterisation of a sound source dependent of the surrounding acoustical space. In other words, the same sound source located at various acoustical receivers requires different source models.

Is there a solution that can use the same set of source parameters applicable to different receivers? Ideally, such a solution should:

- apply to sources of very complex geometry;
- apply also to sources which produce sound by mechanisms other than vibration.

This section will refer to coupling source characterisation methods which fully or partially meet the stated requirements. For the sake of a comprehensive introduction to this subject, some techniques of independent characterisation of structure-borne, fluid-borne and air-borne sound sources will be presented respectively.

2.3.1 Characterisation of Structure-borne Sound Sources

The 'mobility approach' is used a lot to characterise structure-borne sound sources. O'Hara [53] introduced the mechanical mobility concept of a vibrating structure. With a structure excited by the force distribution F, the velocity response can be derived with the mobilities Y, that is $V = YF$, where the mobility Y describes invariant characteristics of the structure. Ideally, the source mobility is independent of the receiver structure.

As shown in Fig. 2.4, using the mobility Y concept, the coupling conditions between the source and a receiver , both supposed to be linear, read

$$v_c = Y_s F_c + v_s^0, \quad \text{(source side)} \tag{2.13a}$$

$$-v_c = Y_r F_c, \quad \text{(receiver side)} \tag{2.13b}$$

which gives

$$F_c = -(Y_s + Y_r)^{-1} v_s^0 \tag{2.14a}$$

$$v_c = Y_r (Y_s + Y_r)^{-1} v_s^0 \tag{2.14b}$$

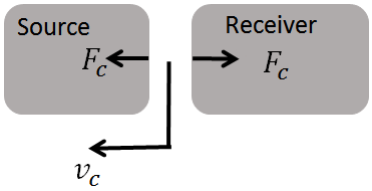

Fig. 2.4 Coupling of source and receiver through a contact point

where v_c, F_c – coupling velocity and coupling force respectively. The subscripts 's' and 'r' refer to source and receiver while v_s^0 denotes source velocity before coupling.

The source is thus characterised by an active descriptor, the free velocity v_s^0, and a passive one, the source mobility Y_s. The receiver is characterised passively by its mobility Y_r. The two source descriptors characterise intrinsically the source, while the receiver descriptor characterises intrinsically the receiver. If the receiver is blocked at the connection, $Y_r \to 0$, the blocked force F_{sb} is generated. It is related to the free velocity of the source via the source mobility by inserting $Y_r = 0$ in to Eq. (2.14a), $F_c = F_{sb} = -Y_s^{-1} v_s^0$. These formulas derived for a single, one Degree-of-Freedom (DoF) contact, fully apply to multi-point, multi DoF contacts. In such a case the forces and velocities become vectors while the mobilities become matrices.

From a measurement point of view the blocked force can be more useful as a descriptor since some sources cannot operate in free (uncoupled) conditions. If the blocked force is used as the active source descriptor, then the most appropriate way to describe the passive descriptor is by using impedance Z rather than mobility concept. This is mostly a formal choice: impedance is difficult to measure directly as it requires full blocking of the contact degrees of freedom and mobility is measured instead. The impedance can be then obtained by inversion since $Z = Y^{-1}$. Using the impedance formulation the relationships equivalent to Eq. (2.14) read:

$$V_c = -(Z_s + Z_r)^{-1} F_{sb} \tag{2.15a}$$

$$F_c = Z_r (Z_s + Z_r)^{-1} F_{sb} \tag{2.15b}$$

Note that $Z_s + Z_r$ represents the impedance of the coupled system (series connection), giving thus $F_{sb} = -Z_c V_c$.

Now the problem is how to obtain the source or receiver descriptors, i.e, the mobilities Y_s, Y_r and the free velocity v_s^0 or the blocked force F_{bl}, by means of measurement. Some sources can not operate if they are decoupled from their receivers, which means it is difficult to measure free velocity under the decoupled source-receiver condition. With respect to the measurement of Y in coupled state, Pavić and Elliott [54] proposed two methods. The

one fulfills the identification of descriptors by introducing coupling connectors of known mechanical properties. Using the known connector mobilities and the measured mobilities of the coupled system on the source side and receiver side give the final result: the mobilities Y_s, Y_r and the free velocity v_s^0. The other simpler method fulfills the measurement of the mobilities Y_s, Y_r also in the coupled-state, but under the assumption that the forces and moments do not vary across the connectors, which is strictly valid only for ideal resilient mounts. The authors examined the feasibility of the two methods in [55].

Measurement of blocked force by literally applying the definition, i.e., blocking the source connection points, is extremely challenging in most cases. To overcome this difficulty, Elliott and Moorhouse [56, 57] demonstrated an in-situ measurement to obtain the blocked force under the coupled source-receiver condition. According to Eq. (2.15), the blocked force can be obtained by $F_{sb} = -(Z_s + Z_r)V_c$ with the coupled impedance $Z_s + Z_r$ and coupling velocity V_c known. The coupled mobility and coupling velocity can be obtained by in-situ measurement. Since no separation of the source and receiver structures is required during the measurement, this method could be used in many practical situations where a source can only be run when it is tightly coupled to a receiver structure. Experimental validation of two beams coupled at two points is shown in [57] to demonstrate the feasibility of this approach. Moreover, Elliott *et al.* [58] presented central difference method and finite element method to measure the force and moment mobilities including the angular velocity due to moment type. It was shown that the mobility matrices of two sub-structures, including force and moment mobilities could be used to predict the coupled mobility of two sub-structures when combined as an assembly.

Lennström *et al.* [59] carried out the characterisation of automotive source in various boundary conditions using the blocked force method from in-situ measurements. Concretely, a vacuum pump in nine degrees of freedom and fixed to a modified bracket in order to achieve different dynamical properties was tested experimentally. The good agreement between the reconstructed and directly measured magnetic tonal harmonics showed that the blocked force obtained from one source-receiver assembly could be used to reconstruct the response when the same source was mounted on a different receiver.

Based on the mechanical mobility concept, Mondot and Petersson [60] introduced the power transmission from the source to the receiver. Using the source mobility Y_s and free velocity v_s^0, the power transition Q for a single point connection can be express by the product of a source description S and a coupling function C_f of the source and receiver mobilities at a contact point, i.e., $Q = SC_f$, where

$$S = (v_s^0)^2 / Y_s^*, C_f = Y_s^* Y_r / \|Y_s + Y_r\|^2 \tag{2.16}$$

Eq. (2.16) can be used as an alternative way to predict the transmitted power from the source to the receiver if the free velocity and the mobilities are identified by measurement.

To facilitate the use of mobility approach to multi-point and multi-DoF connections, the concept of effective mobility is introduced to reduce a multi-point case to an equivalent single-point case [61–63]. For a general mobility matrix formulation of a multi-point connection, it is possible to neglect the influence of some elements in the matrix and rearrange it into several corresponding effective mobilities. Petersson and Plunt tested the accuracy of the effective mobility by estimating the transmitted power [62] and also developed the effective mobility for engineering applications [63].

Additionally, many other methods about the characterisation of structure-borne sound sources were proposed for various application tasks, such as Pseudo-forces methodology [64] and Reception plate method [65, 66].

2.3.2 Characterisation of Fluid-borne Sound Sources

The characterisation of fluid-borne sound sources, such as fans, compressors, pumps, has been in development over a few decades. As we have mentioned, the characterisation aims at providing an independent source model, which does not depend on the properties of the receiver. Such a model, together with the corresponding receiver model, can completely describe the interaction between the source and the receiver.

Many fluid-borne sources can be modelled as linear time-invariant one-port sources, where the source can be characterised by a source strength and a source impedance in analogy with the electric two-pole sources [67, 68]. For instance, an in-duct acoustic source shown in Fig. 2.5 can be represented as an equivalent acoustic circuit shown in Fig. 2.6 and expressed by the following equation [69],

$$p_s Z = pZ_s + pZ \tag{2.17}$$

which is just an alternative form of Eq. (2.15b). Here the source strength p_s can be interpreted as the pressure generated by the source-side in the reference section when the source is blocked; the source impedance Z_s is the normalized impedance at the reference cross section; p is the acoustic pressure at the reference cross section and Z is the receiver impedance, i.e., the normalized acoustic impedance of the rest of the system seen from the source. One should note that the source model described by p_s and Z_s, is the original source plus the medium between the source and the reference cross section (coupling point).

The challenge to identify the source descriptors p_s, Z_s is the source should operate during the identification. With respect to the blocked pressure p_s, it has to be measured when the

source operates to ensure the operating condition. With respect to the source impedance Z_s, as the impedance of the cross section is different with the source turned on or off, the source impedance Z_s should be identified still with the source operating.

Two measurement methods are mostly used to determine the source descriptors p_s, Z_s: the direct method with an external source [70, 71] and the indirect method without external source [72, 73]. The direct method is a two-step method. First, identify the source impedance Z_s. Keep the source running and operate an external source, the source impedance Z_s can be obtained by the two-sensor technique [74]. In the second step, with the identified source impedance Z_s in the first step, the external source is removed and the source strength p_s is determined by measuring the pressure p when a known acoustic load Z is applied to the original source, referring to Eq. (2.17).

For the indirect method, since there are two unknowns p_s and Z_s in Eq. (2.17), the two-load method [72] is used to solve the equations. The two-load method allows characterisation by using two known acoustic loads Z_1, Z_2 and measuring the corresponding pressure responses p_1, p_2. Replacing p and Z in Eq. (2.17) by the known acoustic loads Z_1, Z_2 and the responses p_1, p_2 yields the source descriptors p_s and Z_s.

Compared with the mentioned two methods for linear time-invariant systems, the multiple load method was proposed for determining the source characteristics of linear time-variant systems [75]. Concretely, the three-load [73] and four-load methods [76] were proposed to measure the amplitudes of the pressures instead of complex pressures. The alternative expression of Eq. (2.17) using spectra S_S, S of source strength p_s and pressure response p is

$$S = \frac{|Z_r|^2}{|Z_s + Z_r|^2} S_s = \frac{|Z_r|^2}{|Z_s|^2 + |Z_r|^2 + 2\Re\{Z_s Z_r^*\}} S_s \tag{2.18}$$

with $\Re$ – real part and $[\cdot]^*$ – conjugate transpose of matrix. To obtain three unknowns S_s, real and imaginary parts of Z_s in Eq. (2.18), at least three acoustic load have to be used to solve Eq. (2.18), hereby to get the source descriptors. In addition, the four-load method can be applied to obtain the fourth unknown $|Z_s|^2$.

2.3.3 Characterisation of Air-borne Sound Sources

The independent model of Eq. (2.17) can be applied to characterise air-borne sound sources as described by Bobrovnitskii and Pavić [3]. However, the descriptors – the source strength p_s, the source and receiver impedances Z_s, Z – have obtained new significance. For an air-borne source in a given acoustical space, a surface is created to envelop the source and divide the entire space into an active system, the source space, and a passive system, the

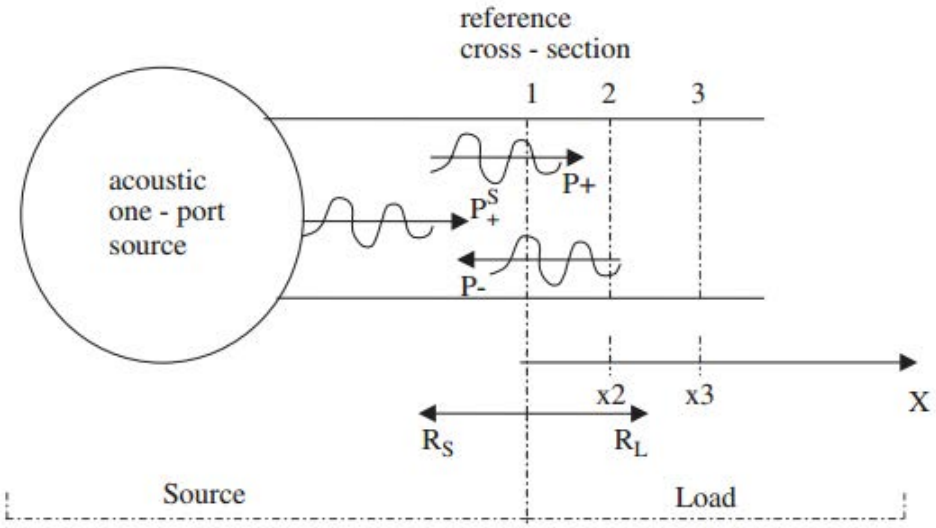

Fig. 2.5 An in-duct source modelled as an acoustic one-port [77].

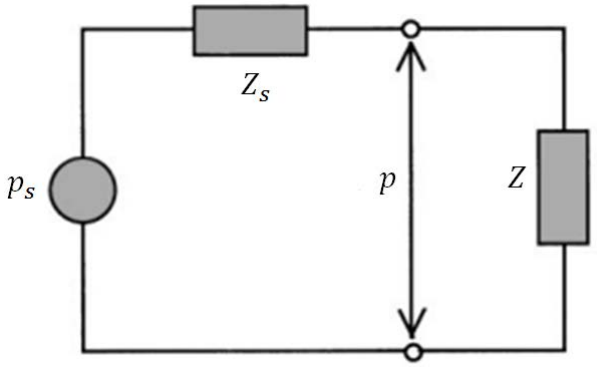

Fig. 2.6 One-port source model for fluid-borne sources [69].

receiver space as described in Section 1.2. The active system includes the source and the medium from the source to the enveloping surface. The passive system is the entire space with the active system removed. The active and passive systems are connected through their common enveloping surface.

For the source space, the 'blocked pressure' p_b denotes the pressure across the enveloping surface due to the operating source when the source space is blocked by the surface. The source impedance Z_s is the impedance of the enveloping surface in the source space when the original source is switched off. Besides, the impedance on the side of the enveloping surface looking to the receiver space is the receiver impedance Z_r. According to Eq. (2.17),

the velocity across the enveloping surface is determined by

$$Q = Z_r^{-1} p_b = (Z_s + Z_r)^{-1} p_b \tag{2.19}$$

Therefore, once the three descriptors are identified and the coupling velocity is computed, by applying the coupling velocity to the enveloping surface, the sound field can be reconstructed in the receiver space.

In the paper of Bobrovnitskii and Pavić [3], the authors demonstrated the computational process of identifying the descriptors by using a spherical interface surface with respect to the known spherical surface harmonics. Nevertheless, from the implementation point of view, a surface consisting of one or several rectangular interfaces demands less effort in practical use. Pavić [78] suggested a technique called Patch impedance to determine the descriptors where the enveloping surface is divided into patches. The blocked pressure is represented by the pressures averaged across each patch while the source and receiver impedances are represented by the coupling impedance between all the patches. An example of reconstructing sound radiation of monopoles in a rectangular cavity is carried out analytically. The good agreement between the predicted and reference results shows the feasibility of the patch concept. Besides, it has been found that 1/3 of minimal wavelength could serve as a good guiding criterion for selecting the patch size [79]. Based on the previous work, this thesis will complete the study by conducting numerical analysis for complex cases as well as experimental validation for laboratory sound sources.

An alternative technique called plane surface harmonics was also proposed to compute the descriptors [80]. The main idea is expanding the sound field into surface harmonics where all the descriptors could be expressed by the amplitudes of corresponding harmonics. Actually, the idea is similar to the wave-based technique proposed by Desmet [81] which approximates the field variable using three types of wave functions [82]. But the difference is the Plane surface harmonics concerns the pressure field on prescribed plane surfaces, thereby it approximates the field variable using 2D trigonometric surface harmonics. Since only basic concepts about the technique were displayed in the paper [80], this thesis will continue the development of Plane surface harmonics in both simple and complex cases and compare it with the patch technique.

2.4 Conclusions

This chapter presented three groups of source modelling methods: Source reconstruction methods, Equivalent source methods and Coupling source characterisation methods, where typical source models were outlined for each group.

In general, the conventional method, NAH, has been fairly studied for many regular shaped noise sources. To overcome the difficulties of the sound prediction of irregular sources, IBEM, DSM and ESM were developed subject to specific boundary conditions of the original source. Concerning the independence on the surrounding acoustical environment and the complexity of sources, the coupling source characterisation methods are presented for structure-borne, fluid-borne and air-borne sources. In order to further expand the implementation of an independent characterisation method for prediction of air-borne noise, we will continue the study of surface coupling and explain the details in the following chapters.

Chapter 3

Source Characterisation via Enveloping Surface

The chapter will present a general principle of source characterisation via enveloping surface. With a surface enveloping a sound source, the source is characterised by two descriptors via the enveloping surface – its blocked pressure and surface impedance. Both descriptors are independent of the surrounding acoustical space, which allows one to predict the sound radiation of the characterised source in an arbitrary acoustical environment. To demonstrate the basic principle, a small loudspeaker will be characterised by its two descriptors, then the sound prediction in a tube will be predicted using the identified descriptors. This 1D case will be studied on the one hand to validate the idea, on the other hand to illustrate the procedure of sound prediction. All the analysis in the following chapters will be done in the frequency domain and the time factor $e^{j\omega t}$ will be suppressed for the sake of brevity.

3.1 Principle

The principle of source characterisation using an enveloping surface has been established in [3]. The key step of source characterisation is to define an appropriate virtual surface *fully or partially* enveloping the source. As shown in Fig. 3.1(a), a virtual surface fully envelops a physical source respectively. The enveloping surface, the physical source and the medium between them compose a source space. When the enveloping surface is blocked, the pressure amplitude acting across the immobile surface due to the operating source will be called *Blocked pressure*, denoted by P_b. When the source is switched off, the impedance of the enveloping surface, denoted by Z_s, will be called *Source impedance*. Blocked pressure P_b

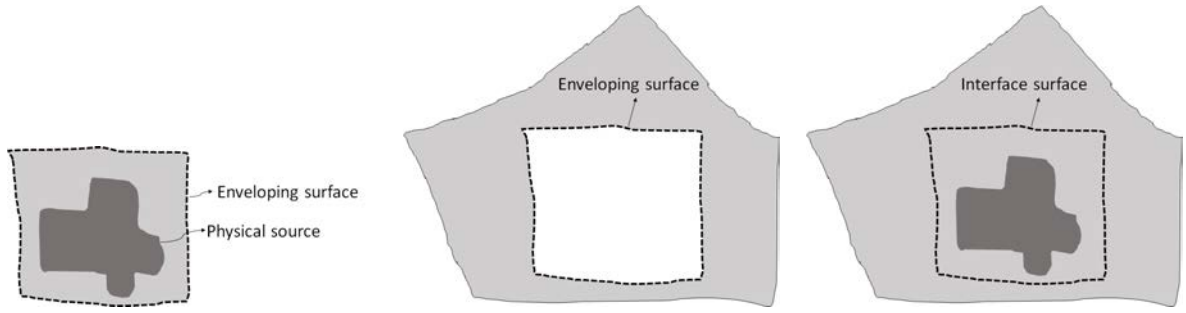

(a) (b) (c)

Fig. 3.1 Source characterisation via enveloping surface: (a) Source space; (b) Receiver space; (c) Sound radiation of a physical source in an acoustical environment.

and source impedance Z_s are two source descriptors characterising the acoustical properties of the source space at the enveloping surface.

To predict the sound radiation due to the source in an arbitrary acoustical environment, such as the acoustical environment shown in Fig. 3.1(c), without installing the source inside, the acoustical environment will be characterised in an analogous way to the source characterisation. A same enveloping surface is inserted in the acoustical environment as shown in Fig. 3.1(b). The acoustical environment with the source space removed represents a receiver space. The impedance of the enveloping surface in the receiver space, denoted by Z_r, will be called *Receiver impedance*. The receiver impedance is a receiver descriptor characterising the acoustical properties of the receiver space at the enveloping surface.

In Fig. 3.1, the source space is fully immersed in the entire acoustical space concerned. However, it should be noted that this is not a necessary condition of the application of the enveloping surface approach. A source may be external to the targeted receiver space and thus only partially coupled to it as shown in Fig. 1.1. Moreover, a source can be coupled to more than one receiver space, as later demonstrated in Chapter 7, in which case driving- and cross- surface impedances should be identified to assure correct coupling conditions.

Since the two enveloping surfaces in the source and receiver spaces (Fig. 3.1 (a) and (b) respectively) are the same, when coupling the two spaces, two enveloping surfaces overlap as a single coupling interface surface in the sound radiation model or between the source and receiver spaces, as the interface surface illustrated in Fig. 3.1(c). For simplicity, either enveloping surfaces with respect to uncoupled source and receiver spaces or the coupling interface surface with respect to two coupled spaces will be named as *interface surface*. Under the condition of the continuity of the velocity and pressure on the interface surface, the coupling velocity on the interface surface can be determined with the respectively identified source and receiver descriptors. Applying the coupling velocity to the interface surface in

the receiver space, the sound radiation due to the physical source can be predicted. The procedure of sound prediction will be explained in the following text.

Regarding the impedance Z of the interface surface in any of the two spaces, it describes the surface sound pressure P_z resulting from the velocity V_z applied to the interface surface,

$$P_z = ZV_z \tag{3.1}$$

The same relationship can be applied to the pressure response at a receiving point of interest in the receiver space. In this case, Z denotes the coupling impedance between the interface surface and the receiving point.

Now we do pressure analysis at the interface surface in the source and receiver spaces respectively. As schematically illustrated in Fig. 3.2, looking from the source space, the pressure $P_{c,s}$ at the interface surface in the source space is contributed by two parts. One part is the pressure response due to the operating source when the interface surface is blocked, it is the blocked pressure P_b. The other part is the pressure response due to the velocity $V_{c,rs}$ applied on the interface surface from the receiver space side. The relationship of $P_{c,s}, P_b$, and $V_{c,rs}$ at this interface surface reads

$$P_{c,s} = P_b + Z_s V_{c,rs} \tag{3.2}$$

In the receiver space, no sound source exists. The pressure $P_{c,r}$ at the interface surface only originates from the velocity $V_{c,sr}$ applied on the interface surface from the source space side,

$$P_{c,r} = Z_r V_{c,sr} \tag{3.3}$$

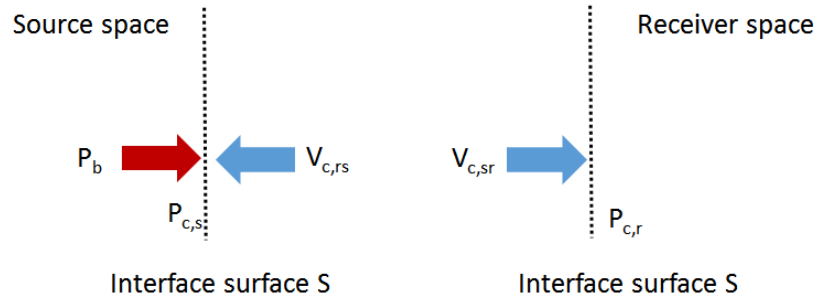

Fig. 3.2 Pressure analysis at the interface surface in the source space (left) and the receiver space (right).

The continuity conditions of both sound pressure and particle velocity at the interface surface when coupling the two spaces provide the coupling relationships,

$$P_c = P_{c,s} = P_{c,r};\;\; V_c = -V_{c,rs} = V_{c,sr} \tag{3.4}$$

where P_c and V_c, named coupling pressure and coupling velocity, are the sound pressure and particle velocity at the interface surface when the source and receiver spaces are coupled. It should be noted that the positive direction of coupling velocity V_c is set towards the receiver space. Combining Eqs. (3.2), (3.3) and (3.4) yields

$$V_c = (Z_s + Z_r)^{-1} P_b \tag{3.5a}$$

$$P_c = Z_r V_c = Z_r (Z_s + Z_r)^{-1} P_b \tag{3.5b}$$

This equation enables one to calculate the coupling velocity with identified source and receiver descriptors, P_b, Z_s and Z_r. Then in the receiver space, sound radiation from the physical source can be predicted by applying the identified coupling velocity V_c to the interface surface. In other words, the vibrating interface surface acts as an equivalent source driving the uncoupled receiver space.

To predict the pressure response(s) at field point(s) of interest in the receiver space, we can either compute or measure the coupling impedance Z_{rp} between a field point and the interface surface, and obtain the pressure response at this point by

$$P_{rp} = Z_{rp} V_c \tag{3.6}$$

For the needs of practical measurements, the blocked pressure P_b has to be represented in terms of auto and cross spectra, denoted by G_b. Using the inter-spectral matrix G_b, the auto and cross spectra of predicted pressures P_{rp} is

$$G_{rp} = T G_b T^*,\;\; T = Z_{rp} (Z_s + Z_r)^{-1} \tag{3.7}$$

with $[\cdot]^*$ – conjugate transpose. The relationship in Eq. (3.7) is applicable to stationary sources.

According to the definitions of the descriptors and the procedure of sound prediction, we can see that:

Firstly, the source descriptors – blocked pressure P_b and source impedance Z_s – are invariants of the source space. Thus once the source descriptors are identified via the defined interface surface, it is possible to make sound predictions in arbitrary receiver spaces. All

what is needed to do is to create the same interface surface in the relevant acoustic receiver and to identify the corresponding receiver impedance Z_r. Then we can obtain the coupling velocity V_c using Eq. (3.5) and establish an equivalent source model.

Secondly, no matter how complex the shape of physical source is or how many radiating components are located in the source space, the interface surface enveloping the source can be used to characterise it. As the interface surface plays an important role in the source characterisation, it should be selected with care. On one hand, the size and the shape of the interface surface should make sure that the surface can envelop the prescribed physical source and also can be adapted to the target receiver space. On the other hand, the shape of the interface surface should allow one to compute or measure the descriptors conveniently. Thus we suggest using one or several plane surfaces as the interface surface. This demands less effort than adopting surfaces of curved geometries.

The identification of source descriptors is the keystone of source characterisation via enveloping surface. The biggest challenge is how to identify these descriptors by means of computation and, in particular, by measurement. The objective of the thesis is to clarify these questions step by step.

3.2 Characterisation of a Compression Driver in a Tube

To make an introductory step on source characterisation via enveloping surface, we will use a small loudspeaker as a source, characterise it by measurement and then predict the sound level by coupling the source to a circular tube. The experimental scheme will be set up at first, explaining how to measure the blocked pressure, source impedance and receiver impedance. Then the measurement and predicted results will be presented to demonstrate the feasibility of sound prediction by the source characterisation method.

Fig. 3.3 shows the schematic view of our measurement setup. The acoustical space is a straight tube making the acoustical field a 1D one. The excitation signal is amplified by an amplifier, transmitted to a source and played in the acoustical space. Microphones in the acoustical space measure pressure responses at points of interest. The FFT analysis system is OROS 4.2 while the microphones are $\frac{1}{4}$ inch PCB 130C10 condenser microphones.

3.2.1 Experimental Scheme

A driver is placed at one end of a tube with an absorption layer mounted at the other end, as shown in Fig. 3.4(a). To characterise the driver, we take a cross section in the tube as the interface surface. The interface surface divides the tube into two coupled spaces: the

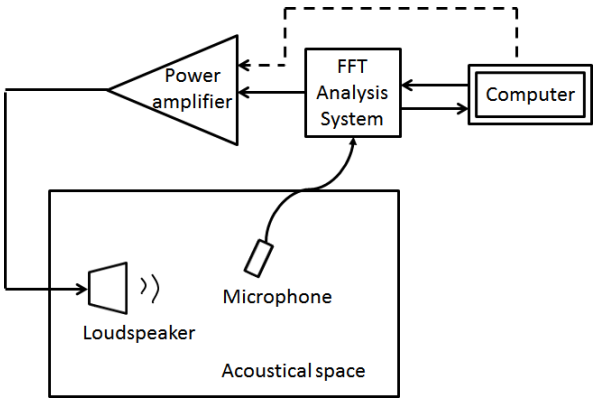

Fig. 3.3 Schematic view of measurement setup

source space with the driver and the receiver space. The identification of source and receiver descriptors will be carried out in the two spaces respectively.

- **Identification of blocked pressure** P_b

The blocked pressure is the pressure response due to the operating source when the interface surface is blocked in the source space. We mount a rigid lid at the position of the interface surface, as shown in Fig. 3.4(b). A microphone fixed on the rigid lid can be used to measure the pressure response due to the operating driver, that is the blocked pressure P_b.

- **Identification of source and receiver impedances** Z_s, Z_r

In the source space, when the source is switched off, the impedance of the interface surface is source impedance. Theoretically, if the velocity excitation applied on the interface surface and pressure response on the interface surface are known, the ratio of the pressure response and the velocity excitation is the source impedance. But these two parameters can not easily obtained. To circumvent the difficulty, we use *two-microphones method* to indirectly measure the surface impedance.

An external tube, represented by the dashed part in Fig. 3.5, is introduced to measure the surface impedances Z_s, Z_r. This tube has the same diameter as the acoustical space. A loudspeaker is placed at one end of this tube and two microphones are mounted between its extremities. First, connect the external tube to the source space, switch off the compression driver, switch on the loudspeaker. The signals from the two microphones can be used to reconstruct the pressure and particle velocity on the interface surface, that is to measure the source impedance Z_s. Similar to the identification of source impedance, by connecting the external tube to the receiver space, we can measure the receiver impedance Z_r. The

measurement procedure of the surface impedance using two-microphones method is presented in Appendix B.

With the identified blocked pressure, source impedance and receiver impedance, the coupling velocity V_c is computed by $V_c = (Z_s + Z_r)^{-1} P_b$ (Eq. (3.5a)). By applying the coupling velocity V_c to the interface surface in the receiver space, the sound radiation in the receiver space can be predicted. In addition, the coupling pressure P_c on the interface surface can be predicted by $P_c = Z_r V_c$ (Eq. (3.5b)).

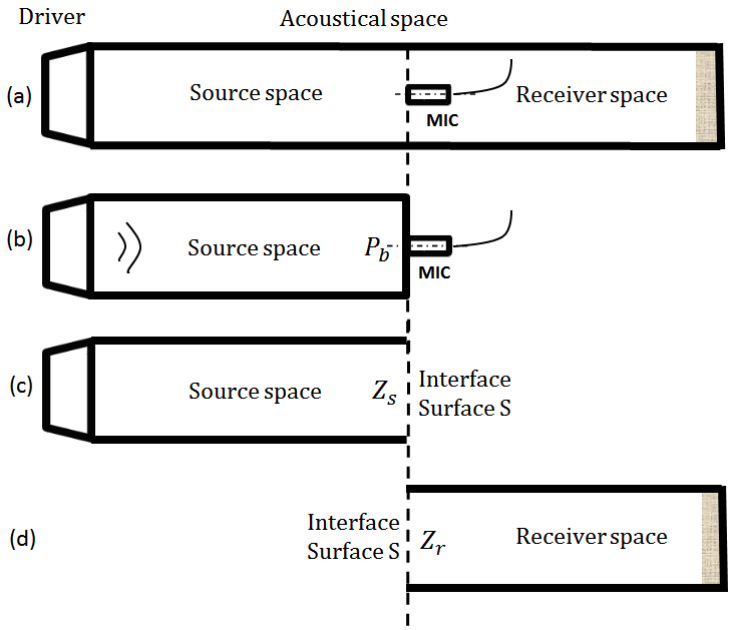

Fig. 3.4 Characterisation of a driver: (a) sound radiation of the driver in a tube; (b) measurement of the blocked pressure P_b; (c) identification of source impedance Z_s; (d) identification of receiver impedance Z_r.

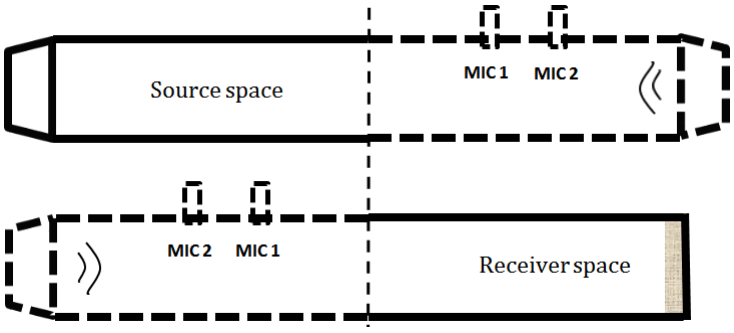

Fig. 3.5 Measurement of source impedance (top) and receiver impedance (bottom) using the two-microphones method.

3.2.2 Calibration of Microphones

Since several $\frac{1}{4}$ inch PCB 130C10 condenser microphones will be used for measuring the descriptors, calibration of microphones is first performed in order to reduce the influence of microphone mismatch. Take the calibration of three microphones as an example. Fig. 3.6 shows three microphones mounted at the rigid end of a tube. As the tube is long enough, when a driver at one end emits sound at frequencies where only plane waves can propagate, the pressure response measured at the same time by the the microphones must be identical. We take one microphone MIC i as the reference and measure the mismatch between other microphones MIC m and MIC n with the reference.

Let H^c_{mi}, H^c_{ni} denote the transfer functions between two microphones MIC m and MIC n and reference MIC i during the calibration procedure. For three microphones PCB130C10-11633 (MIC m), PCB130C10-11644(MIC n), PCB130C10-10123(MIC i), the transfer functions are shown in Fig. 3.7. From the figure, we can see that mismatch exists in both amplitude and phase. The data measured during measurement must be corrected by H^c. The correction of auto- and cross- spectra can be obtained by:

$$\hat{G}_{mm} = \frac{G_{mm}}{\|H^c_{mi}\|^2}, \quad \hat{G}_{nn} = \frac{G_{nn}}{\|H^c_{ni}\|^2}, \quad \hat{G}_{mn} = \frac{G_{mn}}{(H^c_{mi})^* H^c_{ni}}, \quad \hat{H}_{mn} = H_{mn}\frac{H^c_{ni}}{H^c_{mi}} \tag{3.8}$$

here G is the auto or cross spectrum, $\hat{G}$ is the corrected auto or cross spectrum; H is the measured transfer function, $\hat{H}$ is the corrected transfer function. One should use the corrected parameters in computation.

Fig. 3.6 Calibration of three microphones

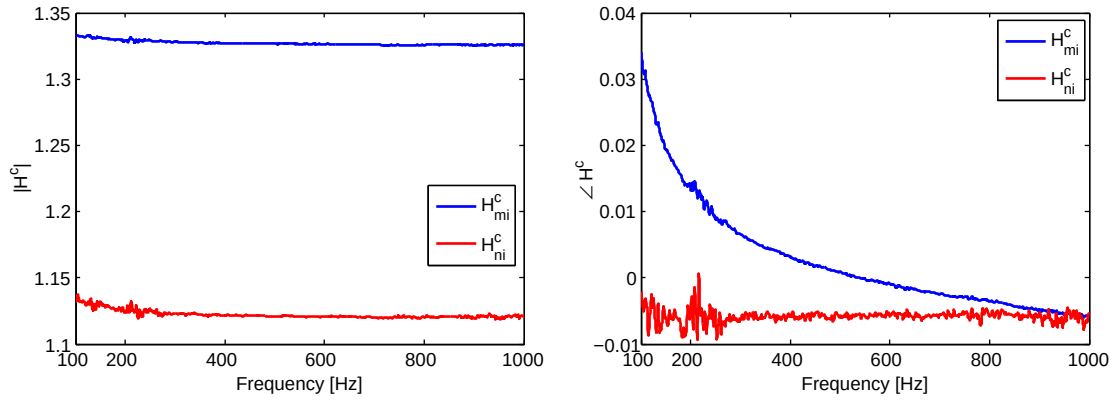

(a) $|H^c|$ (b) $\angle H^c$

Fig. 3.7 Transfer functions of two microphones measured during the calibration procedure.

3.2.3 Measurement and Results

A. Measurement of descriptors

Following the experimental scheme, now we introduce the details of measurement. As shown in Fig. 3.8, a compression driver is located at the left end of a circular tube of length $1.82m$. Two microphones spaced by $0.05m$ are mounted in the tube. Close to the middle of the tube, $1m$ from the driver, an interface surface is set. It divides the tube into a source space and a receiver space. The distance between the interface surface and the closer microphone is $0.16m$. Referring to the configuration shown in Fig. 3.8, a loudspeaker at the right end of the tube is used for the measurement of the source and receiver impedances. Besides, another tube with a rigid lid helps to measure the blocked pressure, as shown in Fig. 3.8(b).

The amplitudes and phases of the two impedances, Z_s and Z_r, are shown in Fig. 3.9 (a) and (b). Fig. 3.9 (c) is the measured blocked pressure due to the white noise generated by the driver. Substituting the identified descriptors into $P_c = Z_r(Z_s + Z_r)^{-1}P_b$ (Eq. (3.5b)) obtains the predicted coupling pressure at the interface surface S, as the solid curve shown in Fig. 3.9(d). One microphone placed at the interface surface directly measures the coupling pressure with the driver operating: this is shown by the dash curve in Fig. 3.9(d). We can see that the two curves match well, which validates the principle of sound prediction by source characterisation using source impedance and blocked pressure descriptors.

B. Discussion

The extreme values of mismatch between the predicted and reference coupling pressure is between -3.5dB and 3.5dB, as shown in Fig. 3.10. This mismatch is attributable to the

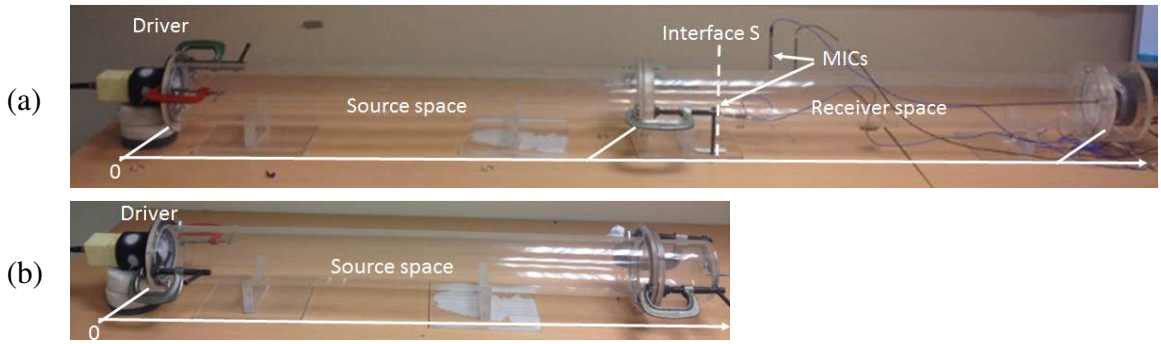

Fig. 3.8 Configuration of measurement. Top: measurement of source and receiver impedances, bottom: measurement of blocked pressure.

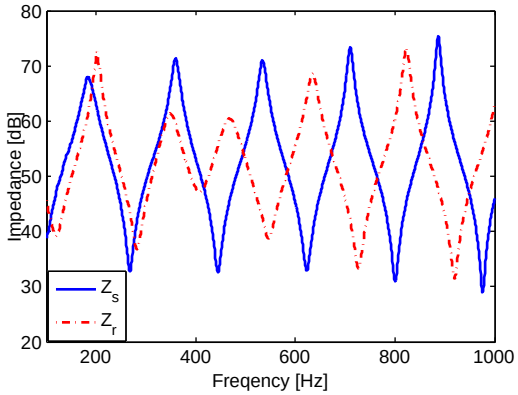

(a) Amplitudes of Z (ref. $1kg \cdot m^{-2} \cdot s^{-1}$)

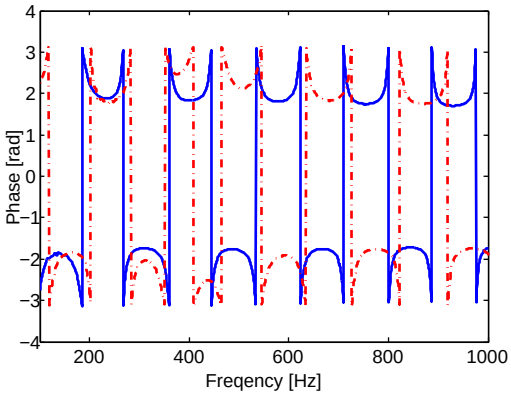

(b) Phases of Z

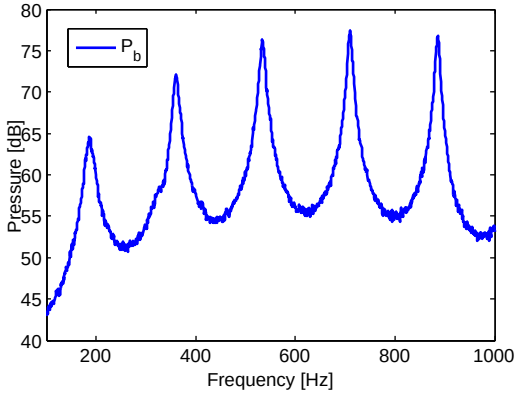

(c) P_b

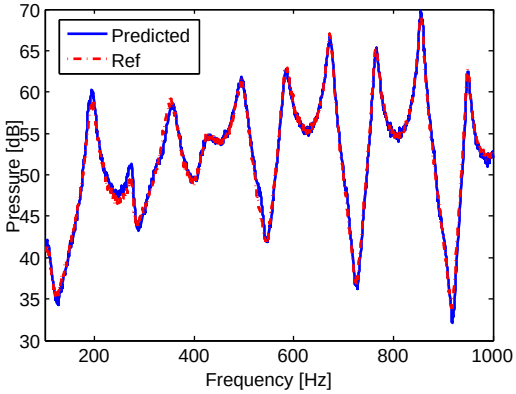

(d) P_c

Fig. 3.9 Measured descriptors and predicted pressure response

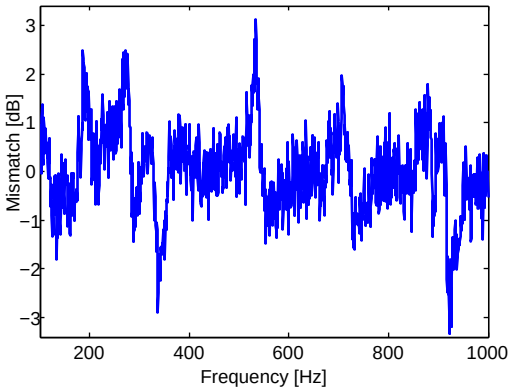

Fig. 3.10 Mismatch between predicted and reference responses

fact that the impedance of the source space changes when the driver is switched on and off. Indeed, the physical source used in this experiment, i.e., the driver, has an electro-mechanical impedance which changes with the driving voltage switched on and off. The impedance of the driver represents the boundary condition of the source space, it therefore influences a lot the prediction close to the resonance frequencies of the blocked source space. Nevertheless, for a typical mechanical source that needs to be characterised by the proposed descriptors, the influence of such an impedance change is negligible since a typical source would normally have an impedance which remains unaffected by its operation.

3.3 Conclusions

This chapter introduced the principle of source characterisation via enveloping surface. With an interface surface enveloping a sound source, the source is characterised by two source descriptors – blocked pressure and source impedance – defined on the interface surface. With the identified source descriptors, invariant with the acoustical receiver, the sound radiation of the operating source in an arbitrary acoustical space can be predicted. To demonstrate the source characterisation method, the sound radiation of a compression driver in a tube was predicted by means of measurement. Good overall matching of the predicted and directly measured sound pressure on the interface surface demonstrates the feasibility of sound prediction by source characterisation via enveloping surface.

Chapter 4

Source Characterisation using Continuous Surface Coupling Technique

The previous chapter introduced the principle of source characterisation via enveloping surface and validated sound prediction of a compression chamber in a tube. With respect to more complex cases, the following two chapters will present two techniques, namely 'Continuous surface coupling technique' and 'Patch surface coupling technique', to identify source and receiver descriptors therefore carrying out the characterisation of sound sources.

This chapter will present source characterisation using Continuous surface coupling technique (hereby called Harmonic technique) to obtain the source and receiver descriptors, i.e., the blocked pressure, the source impedance and the receiver impedance. The main idea of this technique is employing continuous plane-surface functions for describing the source pressure and the source and receiver impedances on the interface surface.

Using H prescribed plane surface harmonic functions, called surface harmonics, pressure and velocity across the entire interface surface can be expressed as a linear superposition of basis harmonics weighted by particular amplitudes. This allows us to establish two harmonic impedance matrices to characterise the concerned source and receiver spaces. Consequently, the blocked pressure will be expressed by a $H \times 1$ harmonic vector and the impedance matrices are of size $H \times H$. Comparing with the patch technique dividing the interface surface into small patches, the harmonic technique always treats the surface as an entirety. At first glance, the vectorisation of the two techniques are alike, however the computation and measurement (especially for the impedances) is quite different.

We will explain the necessary steps to obtain the three descriptors and show the procedure of sound prediction using the Harmonic technique. First, analytical modelling of a simple source-receiver case will illustrate the details of the Harmonic technique. After that, a more realistic source case of a vibrating box within an irregular space will be analysed by numerical

modelling. Finally, the sound transmission in the receiver space will be calculated first by direct computation then by the continuous surface coupling technique. The consistency between the two results will demonstrate the effectiveness of the proposed approach.

4.1 Plane Surface Harmonics

As mentioned in previous chapters an interface surface consisting of one or several rectangular plane surfaces is better adapted to characterisation by measurement than other geometrical shapes. The Harmonic technique is proposed on the base of this kind of interface surface. The sound field across a rectangular plane surface will be expanded into plane surface harmonics.

Imagine, for simplicity, that the source space and the receiver space are coupled by a single rectangular interface surface S of the size $b \times h$ lying the $y-z$ plane. Let the sound field across S be approximated by $H = (2L+1)(2M+1)$ space functions of the form:

$$q_{lm}(y,z) = \phi_y(\frac{l\pi y}{b}) \cdot \phi_z(\frac{m\pi z}{h}), \;\; l = l_1, \cdots, L, \;\; m = m_1, \cdots, M \tag{4.1}$$

For the sake of convenience, ϕ will be taken to be either sine or cosine functions, the integers l_1 and m_1 are equal to 1 for sine and 0 for cosine terms. The function basis q will be called the "surface harmonics". To distinguish between the 4 families of functions, i.e., cos-cos, cos-sin, sin-cos and sin-sin, the harmonics will be denoted by superscripts cc, cs, sc and ss. Each harmonic q is uniquely defined by a pair of integers l, m. Note that $q_{00}^{cc} \equiv 1$.

A given field quantity, sound pressure or particle velocity, will be then represented as a linear superposition of harmonics, each harmonic weighted by its (complex) amplitude. Each l, m combination, $l, m > 0$, yields 4 amplitudes relative to ss, sc, cs and cc terms. The knowledge of harmonic amplitudes allows one to fully reconstruct the entire field across the surface S up to the H^{th} order of approximation. Thus the (complex) amplitude of sound pressure will read:

$$P(y,z) = \Pi_{00} + \Pi_{01}^{cs} q_{01}^{cs} + \Pi_{10}^{sc} q_{10}^{sc} + \sum_{l=1}^{L} \sum_{m=1}^{M} (\Pi_{lm}^{cc} q_{lm}^{cc} + \Pi_{lm}^{cs} q_{lm}^{cs} + \Pi_{lm}^{sc} q_{lm}^{sc} + \Pi_{lm}^{ss} q_{lm}^{ss}) \tag{4.2}$$

the instantaneous sound pressure being $p(y,z,t) = \Re\{P(y,z)\exp(j\omega t)\}$. The decomposition in Eq. (4.2) is in fact a 2D Fourier series representation truncated to H terms. The truncation implies that the series in Eq. (4.2) is an approximation of the field quantity it represents. In order to produce acceptable results, the truncation should stop at the harmonic indices L and M which are sufficiently high. This point will be addressed at a later stage.

The entire set of H harmonic pressure amplitudes will be arranged in an $H \times 1$ column vector $\mathbf{\Pi}$:

$$\mathbf{\Pi} = (\Pi_{00}^{cc}, \cdots, \Pi_{LM}^{cc}, \Pi_{01}^{cs}, \cdots, \Pi_{LM}^{cs}, \Pi_{10}^{sc}, \cdots, \Pi_{LM}^{sc}, \Pi_{11}^{ss}, \cdots, \Pi_{LM}^{ss})^t \tag{4.3}$$

where t - transpose. The distribution of particle velocity amplitudes normal to S, $V(y,z)$, can be represented in an analogous way, in terms of harmonic velocity amplitudes $\Gamma_{lm}^{cc}, \Gamma_{lm}^{cs}, \Gamma_{lm}^{sc}, \Gamma_{lm}^{ss}$. The complete set of these amplitudes will become an $H \times 1$ column vector $\mathbf{\Gamma}$:

$$\mathbf{\Gamma} = (\Gamma_{00}^{cc}, \cdots, \Gamma_{LM}^{cc}, \Gamma_{01}^{cs}, \cdots, \Gamma_{LM}^{cs}, \Gamma_{10}^{sc}, \cdots, \Gamma_{LM}^{sc}, \Gamma_{11}^{ss}, \cdots, \Gamma_{LM}^{ss})^t \tag{4.4}$$

It has been implicitly assumed in the above that both the sound pressure and the particle velocity are expanded using the same ensemble of surface harmonics q, Eq. (4.2). This however is not a necessary condition but it is advantage from a practical point of view.

For the sake of simplicity, the function basis q will be represented as a single row vector consisting of 4 families of functions ordered in cos-cos, cos-sin, sin-cos and sin-sin sequence as done in Eqs. (4.3) and (4.4). The $l-m$ indices will be replaced by single integers ranging from 1 to H. Thus q_{00}^{cc} at the first position will become q_1, q_{LM}^{ss} at the last position will become q_H, etc. For the same reason the amplitudes of different harmonics in vectors $\mathbf{\Pi}$ and $\mathbf{\Gamma}$ will be defined by the same set of indices.

Let now assume that a given acoustical space is driven across S by a continuously distributed normal velocity of unit amplitude which has the spatial pattern of a k^{th} surface harmonic, i.e., $\Gamma_k = 1$. Such an excitation will produce across S a sound pressure which, in a general case, will be a linear superposition of all the surface harmonics, each with a particular amplitude $\Pi_i, i = 1, \cdots, H$. Since the driving velocity amplitude is unity, the column vector containing all of H pressure amplitudes represents in this way the column of impedances relative to the k^{th} excitation. By scanning the driving velocity pattern over all of H velocity surface harmonics and assembling the pressure response into columns, the following relationship between the harmonic pressure vector $\mathbf{\Pi}$ and the harmonic velocity vector $\mathbf{\Gamma}$ can be obtained

$$\mathbf{\Pi} = \mathbf{\Omega\Gamma} \tag{4.5}$$

where $\mathbf{\Omega}$, a $H \times H$ matrix, is named the Harmonic impedance.

In order to assess the coupling between the source space and the receiver space across the interface surface S, the source space and the receiver space, a single pressure harmonic at the interface surface between the two spaces will be considered first. The k^{th} pressure

harmonic, $p_k^S(y,z,t)$, acting on the interface surface on the source space side will be the superposition of the k^{th} pressure harmonic $p_{b,k}(y,z,t)$ produced by the running source across the blocked interface and of the k^{th} pressure harmonic arising from the moving interface S. The latter is the sum of k^{th} pressure harmonics generated by all the surface velocity harmonics $v_i(y,z,t), i = 1,\cdots,H$. Looking from the receiver space side of S the same pressure harmonic, $p_k^R(y,z,t)$, will equal the sum of all the k^{th} pressure harmonics arising from the surface velocity harmonics. By respecting the continuity conditions at S and using the definition of harmonic impedance $\mathbf{\Omega}$ the equality of the k^{th} pressure harmonics at the opposite sides of the interface in terms of harmonic amplitudes reads:

$$\Pi_k = \Pi_{bk} - \sum_{i=1}^{H} \Omega_{ki}^S \Gamma_{i,} = \sum_{i=1}^{H} \Omega_{ki}^R \Gamma i, \tag{4.6}$$

The symbols Ω_{ki}^S and Ω_{ki}^R stand for the $k-i$ elements of the source and receiver impedance matrices respectively. The two sums represent the products of the k^{th} rows of source and receiver impedance matrices with the amplitudes of particles velocities harmonics at the interface. The entire amplitude vector of velocity harmonics $\mathbf{\Gamma}_c$ and pressure harmonics $\mathbf{\Pi}_c$ at the interface surface can then be represented by:

$$\mathbf{\Gamma}_c = (\mathbf{\Omega}_s + \mathbf{\Omega}_r)^{-1} \mathbf{\Pi}_b \tag{4.7a}$$

$$\mathbf{\Pi}_c = \mathbf{\Omega}_r \mathbf{\Gamma}_c = \mathbf{\Omega}_r (\mathbf{\Omega}_s + \mathbf{\Omega}_r)^{-1} \mathbf{\Pi}_b \tag{4.7b}$$

where $\mathbf{\Pi}_b$ - vector of blocked pressure harmonics, $\mathbf{\Omega}_s$ and $\mathbf{\Omega}_r$ - source and receiver harmonic impedance matrices respectively. Eq. (4.7) will also be named the coupling function with new descriptors $\mathbf{\Pi}_b$, $\mathbf{\Omega}_s$ and $\mathbf{\Omega}_r$ corresponding to blocked pressure P_b, source impedance Z_s and receiver impedance Z_r in Eq. (3.5).

Once the harmonic amplitudes of the interface velocity $\mathbf{\Gamma}$ have been identified, the interface velocity $v(y,z,t)$ can be readily obtained using Eq. (4.1). This velocity can be considered as the external driving velocity of the receiver taken on its own, which in turn allows the computation of sound pressure within the receiver space.

4.2 Identification of descriptors using Surface harmonics

Using plane surface harmonics, this section will introduce the relationship between surface harmonics and field variables, concretely, the relationship between descriptors $\mathbf{\Pi}_b, \mathbf{\Omega}_s, \mathbf{\Omega}_r$ and the descriptors $\mathbf{P}_b, \mathbf{Z}_s, \mathbf{Z}_r$. Then the way to identify the descriptors $\mathbf{\Pi}_b, \mathbf{\Omega}_s, \mathbf{\Omega}_r$ and $\mathbf{\Gamma}_c$ will be introduced.

4.2.1 Relationship between surface harmonics and field variables

The instantaneous values of sound pressure and particle velocity across the interface S can be represented by $y-z$ – dependent amplitudes P and V. These amplitudes can be readily linked to the harmonic amplitudes Π and Γ via the surface harmonic function q, Eq. (4.2).

It will now be assumed that the sound pressure $p(y,z,t)$ and the normal component of particle velocity $v(y,z,t)$ are known at I points $(y_i,z_i), i=1,\cdots,I$. The (complex) amplitudes of pressure and velocity at these points will be arranged into column vectors $\boldsymbol{P}$ and $\boldsymbol{V}$:

$$\boldsymbol{P}=(P_1,\cdots,P_I)^t,\ \ \boldsymbol{V}=(V_1,\cdots,V_I)^t \tag{4.8}$$

Using Eq. (4.1) the field amplitudes at I points and the amplitudes of H surface harmonics can be represented by the following relationship:

$$\boldsymbol{P}=\boldsymbol{\Phi}_p\boldsymbol{\Pi},\ \ \boldsymbol{V}=\boldsymbol{\Phi}_v\boldsymbol{\Gamma} \tag{4.9}$$

In the case of the same function basis q of pressure and velocity, the two transfer matrices are equal, $\boldsymbol{\Phi}_p=\boldsymbol{\Phi}_v=\boldsymbol{\Phi}$. The $(i-k)^{th}$ element of the transfer matrix $\boldsymbol{\Phi}$, Φ_{ik}, relating a given field variable, pressure or velocity, at the point (y_i,z_i) with the corresponding amplitude of the k^{th} surface harmonic thus reads:

$$\Phi_{ik}=q_{l=l(k),m=m(k)}(y_i,z_i)=\phi_{y,k}(\frac{l(k)\pi y_i}{b})\cdot\phi_{z,k}(\frac{m(k)\pi z_i}{h}) \tag{4.10}$$

where $\phi_{,k}$ either since or cosine function depending on the index k.

To make the system determined, the number of field points I has to match the number of surface harmonics, i.e., $I=H$. One can alternatively make the system over-determined by using more points than the minimum number required. This should, as a rule, improve the robustness of the method where measurements are concerned.

If the sound field is known at I points, the field point impedance Z can be established such that its $(m-n)^{th}$ element is defined in terms of point pressure and point velocity amplitudes as $Z_{mn}=P_m/V_n$. This results in $\boldsymbol{P}=\boldsymbol{Z}\boldsymbol{V}$. Such an impedance can be measured under a known excitation. In sucha case, Eqs. (4.5)(4.9) allow one to establish the direct relationship between the harmonic impedance $\boldsymbol{\Omega}$ and the field impedance $\boldsymbol{Z}$ defined at field points $i=1,\cdots,I$:

$$\boldsymbol{\Omega}=\boldsymbol{\Phi}^{-1}\boldsymbol{Z}\boldsymbol{\Phi} \tag{4.11}$$

It should be noted that the field impedance is defined here as the relationship between the sound pressure and the normal particle velocity at discrete points. Such an impedance has

thus not the meaning of the ratio response pressure/driving velocity. It simply establishes the links between the dissimilar field quantities – pressure and velocity in a sound field. Thus the field impedance is not intrinsic to the acoustical space concerned, but is case sensitive. This could be quantity conveniently used in measurements under a given known excitation.

4.2.2 Identification of descriptors

Referring to Eq. (4.9), if the sound field across the interface surface is represented at K discrete points, the blocked pressure $\mathbf{P}_b$ can be represented by (complex) amplitudes as an $K \times 1$ vector while the coupling velocity $\mathbf{V}_c$ can be expressed by (complex) velocity amplitudes also as an $K \times 1$ vector. Using plane surface harmonics, the blocked pressure $\mathbf{P}_b$ can be given by the amplitude vector of blocked pressure harmonic $\mathbf{\Pi}_b$ while the coupling velocity $\mathbf{V}_c$ can be represented by the amplitude vector of coupling velocity $\mathbf{\Gamma}_c$,

$$\boldsymbol{P}_b = \mathbf{\Phi}_b \mathbf{\Pi}_b, \;\; \boldsymbol{V}_c = \mathbf{\Phi}_c \mathbf{\Gamma}_c \tag{4.12}$$

The function basis $\mathbf{\Phi}_b, \mathbf{\Phi}_c$ can be mutually different, which allows different numbers of sampling points K_b, K_c and harmonics H_b, H_c. But for simplicity, the function basis $\mathbf{\Phi}_b$ and $\mathbf{\Phi}_c$ will be considered to be identical, i.e., $\mathbf{\Phi}_b = \mathbf{\Phi}_c = \mathbf{\Phi}$ of the size $K \times H$, where K – number of sampling points and H – number of harmonics.

Generally, the source space is characterised by two harmonic descriptors, the harmonic blocked pressure $\mathbf{\Pi}_b$ and the harmonic source impedance $\mathbf{\Omega}_s$; the receiver space is characterised by the harmonic receiver impedance $\mathbf{\Omega}_r$. The three descriptors can be identified as follows:

- **Identification of $\mathbf{\Pi}_b$**

In the source space, pressure responses are measured at K_b sampling points on the interface surface with the physical source switched on to get $\boldsymbol{P}_b$ referring to Eq. (4.8). $\mathbf{\Pi}_b$ is then obtained by Eq. (4.12) via the computed function basis $\mathbf{\Phi}_b$.

- **Identification of $\mathbf{\Omega}_s$ and $\mathbf{\Omega}_r$**

Following the concept of $\mathbf{\Omega}$ presented by Eq. (4.5), the procedure of measuring the source harmonic impedance $\mathbf{\Omega}_s$ is outlined in the following steps.

1. Apply a normal velocity excitation to the interface surface in the source space with the physical source switched off.

2. Measure the pressures and the velocities at K_s sampling points to get pressure and velocity amplitude vectors $\boldsymbol{P}_s$ and $\boldsymbol{V}_s$ of the size $K_s \times 1$.

3. Develop $\boldsymbol{P}_s$ and $\boldsymbol{V}_s$ into amplitude vectors $\boldsymbol{\Pi}_s(H \times 1)$ and $\boldsymbol{\Gamma}_s(H \times 1)$ with the help of Eq. (4.9), $\boldsymbol{\Pi}_s = \boldsymbol{\Omega}_s \boldsymbol{\Gamma}_s$.

4. Repeat Step 2 and Step 3 H times with various independent normal velocity excitations. Assemble the vectors $\boldsymbol{\Pi}_s$ and $\boldsymbol{\Gamma}_s$ of the size $H \times 1$ into the matrices $\boldsymbol{\Pi}_s^{'}$ and $\boldsymbol{\Gamma}_s^{'}$ of the size $H \times H$. The harmonic impedance $\boldsymbol{\Omega}_s$ can be then computed by

$$\boldsymbol{\Omega}_s = \boldsymbol{\Pi}_s^{'}(\boldsymbol{\Gamma}_s^{'})^{-1} \tag{4.13a}$$

$$\boldsymbol{\Pi}_s^{'} = [\cdots, \boldsymbol{\Pi}_s, \cdots] \tag{4.13b}$$

$$\boldsymbol{\Gamma}_s^{'} = [\cdots, \boldsymbol{\Gamma}_s, \cdots] \tag{4.13c}$$

From the computation point of view, the simplest velocity excitations are the copies of H surface harmonics with unit amplitude. This makes $\boldsymbol{\Gamma}_s^{'}$ an identity matrix, thus $\boldsymbol{\Omega}_s = \boldsymbol{\Pi}_s^{'}$. If however the identification of the matrix $\boldsymbol{\Omega}_s$ is done by measurements, it could be difficult to produce the prescribed velocity distribution across the interface surface. In such a case, the full procedure as described by steps 1 to 4 should be applied. The measurement of the receiver harmonic impedance $\boldsymbol{\Omega}_r$ is same to that of $\boldsymbol{\Omega}_s$.

4.2.3 Procedure of sound prediction

The procedure of sound prediction using plane surface harmonics is carried out through the following steps.

1. Define an interface surface to divide the sound radiation model into the source and receiver spaces.

2. With the interface surface blocked and the source operating, measure the pressure responses at K points to get blocked pressure $\boldsymbol{P}_b$.

3. Compute function basis $\boldsymbol{\Phi}$ at K points to get pressure harmonic amplitudes $\boldsymbol{\Pi}_b = \boldsymbol{\Phi}^{-1}\boldsymbol{P}_b$.

4. Get harmonic impedances $\boldsymbol{\Omega}_s$, $\boldsymbol{\Omega}_r$ using the procedure outlined in the previous section.

5. Compute $\boldsymbol{\Gamma}_c$ by Eq. (4.7), and then obtain $\boldsymbol{V}_c$ by Eq. (4.12).

6. Apply the velocity distribution $\boldsymbol{V}_c$ on the interface surface in the receiver space to predict the sound radiation in the receiver space.

From this procedure, it can be seen that the two source descriptors $\boldsymbol{\Pi}_b, \boldsymbol{\Omega}_s$ and the receiver descriptor $\boldsymbol{\Omega}_r$ can be identified separately because of their independence of each other. If the receiver space changes, all to do is to repeat the identification of receiver impedance $\boldsymbol{\Omega}_r$ and compute the new coupling conditions.

4.3 Analytical Modeling

In order to demonstrate the outlined step of sound prediction by source characterisation, an analytical modeling of source-receiver coupling impedance has been made. This section will focus on the computation of sound pressure excited by a vibrating surface and coupling harmonic impedance in a parallelepipedic cavity.

4.3.1 Pressure Response Created by Vibrating Surface using Spatial Harmonics

A parallepipedic cavity, as shown in Fig. 4.1, is of length a, width b, height h. The pressure response $P(x,y,z)$ at a point $\boldsymbol{r} = (x,y,z)$ due to a sinusoidal point source of volume velocity Q_e at $\boldsymbol{r}_e = (x_e, y_e, z_e)$ in the cavity is [83]

$$P(\mathbf{r}) = \frac{j\omega\rho_0 c^2}{U} Q_e(\mathbf{r}_e) \sum_{n=1}^{N} \frac{\phi_n(\mathbf{r})\phi_n(\mathbf{r}_e)}{\omega_n^2 - \omega^2 + 2j\varepsilon\omega} \tag{4.14a}$$

$$\phi(x,y,z) = \zeta(n) cos(\frac{n_x \pi x}{a}) cos(\frac{n_y \pi y}{b}) cos(\frac{n_z \pi z}{h}) \tag{4.14b}$$

$$\zeta(n) = \sqrt{2^{sgn(n_x+n_y+n_z)}} \tag{4.14c}$$

Here ω is the excitation angular frequency, ω_n is the natural angular frequency, ε is damping coefficient, ρ_0 is the air mass density, c is the sound speed of air and U is the volume of the cavity. The integers $n_x = n_x(n), n_y = n_y(n), n_z = n_z(n)$ are room mode indices in x,y,z axis and N is the number of effectively contributing cavity modes.

The excitation is provided by a vibrating surface of width b_0 and height h_0 is located on the $y-z$ plane at $x = 0$ with one corner aligned to (y_0, z_0). The vibration pattern is assumed to be decomposed into surface harmonics. The response to one of these harmonics will be obtained analytically. Take as an example a $cos - sin$ combination of trigonometric functions; the velocity distribution of the surface is $V_l(y_e, z_e) = \Gamma^{cs}_{l_y l_z} q^{cs}_{l_y l_z} = \Gamma^{cs}_{l_y l_z} cos(\frac{l_y \pi}{b_0}(y_e -$

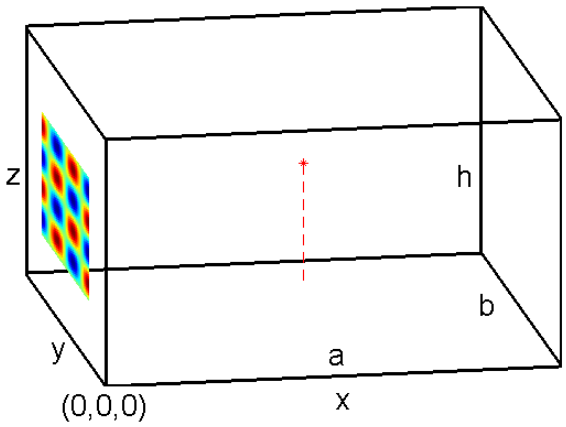

(a)

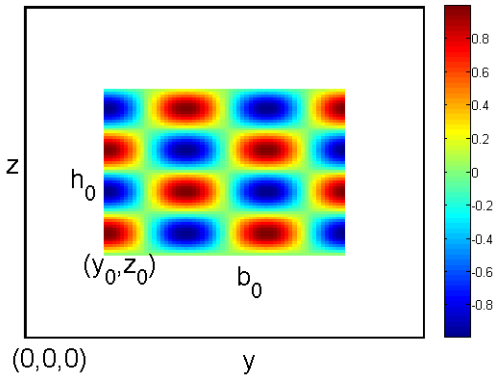

(b)

Fig. 4.1 Top: sound radiation model, bottom: excitation surface at $x = 0$ plane.

$y_0))sin(\frac{l_z\pi}{h_0}(z_e - z_0)$ with $y_e \in [y_0, y_0 + b_0], z_e \in [z_0, z_0 + h_0]$. $\Gamma^{cs}_{l_y l_z}$ is the velocity amplitude of the l_y^{th} cosine and l_z^{th} sine surface harmonic. The integers $l = [l_y, l_z]$ define surface harmonics in y, z directions. The pressure response at a point (x, y, z) due to the vibrating surface is

$$P(x,y,z) = \int_{y_0}^{y_0+b_0} \int_{z_0}^{z_0+h_0} \frac{j\omega\rho_0 c^2}{U} V_l(y_e, z_e) \sum_{n=1}^{N} \frac{\phi_n(x,y,z)\phi_n(x_e = 0, y_e, z_e)}{\omega_n^2 - \omega^2 + 2j\varepsilon\omega} dy_e dz_e \quad (4.15)$$

By substituting V_l and Eq. (4.14b) into Eq. (4.15),

$$P(x,y,z) = \sum_{n=1}^{N} \Gamma^{cs}_{l_y l_z} \frac{j\omega\rho_0 c^2}{U} \frac{\zeta^2(n)}{\omega_n^2 - \omega^2 + 2j\varepsilon\omega} cos(\frac{n_x\pi x}{a}) cos(\frac{n_y\pi y}{b}) cos(\frac{n_z\pi z}{h})$$
$$\int_{y_0}^{y_0+b_0} cos[\frac{l_y\pi}{b_0}(y_e - y_0)] cos(\frac{n_y\pi}{b} y_e) dy_e \int_{z_0}^{z_0+h_0} sin[\frac{l_z\pi}{h_0}(z_e - z_0)] cos(\frac{n_z\pi}{h} z_e) dz_e \quad (4.16)$$

By using abbreviations:

$$A_n = \Gamma^{cs}_{l_y l_z} \frac{j\omega\rho_0 c^2}{U} \frac{\zeta^2(n)}{\omega_n^2 - \omega^2 + 2j\varepsilon\omega} \tag{4.17}$$

$$B_{l,n} = \int_{y_0}^{y_0+b_0} cos[\frac{l_y\pi}{b_0}(y_e - y_0)]cos(\frac{n_y\pi}{b}y_e)dy_e \int_{z_0}^{z_0+h_0} sin[\frac{l_z\pi}{h_0}(z_e - z_0)]cos(\frac{n_z\pi}{h}z_e)dz_e \tag{4.18}$$

Eq. (4.16) becomes

$$P(x,y,z) = \sum_{n=1}^{N} A_n B_{l,n} cos(\frac{n_x\pi x}{a})cos(\frac{n_y\pi y}{b})cos(\frac{n_z\pi z}{h}) \tag{4.19}$$

The term $B_{l,n}$ relative to y_0, b_0, z_0, h_0, n, l is derived in Appendix C.1. Replacing $cos[\frac{l_y\pi}{b_0}(y_e - y_0)]$ and $sin[\frac{l_z\pi}{h_0}(z_e - z_0)]$ of $B_{l,n}$ by other combinations of trigonometric functions provides the pressure response due to the four prescribed types of velocity excitations.

4.3.2 Source and receiver harmonic impedances

Following the identification steps outlined in Section 2.4 with defined basis functions, the computational procedure of the source harmonic impedance $\mathbf{\Omega}_s$ in a parallelepipedic cavity is hereby outlined.

1. Apply the velocity excitation by one surface harmonic of unit velocity amplitude ($\Gamma^{c(s)c(s)}_{l_y,l_z} = 1$) to the interface surface.

2. Compute the pressure responses $P_i, i = 1, \cdots, K_s$ at K_s different points on the interface surface due to the velocity excitation in Step 1 by Eq. (4.19), that is obtain the pressure vector across the interface $\boldsymbol{P}_s$, referring to Eq. (4.8).

3. Compute $\mathbf{\Pi}_s$ by Eq. (4.9) with the defined basis function $\mathbf{\Phi}_s$. $\mathbf{\Pi}_s$ is one column of $\mathbf{\Omega}_s$ corresponding to the excitation surface harmonic of mode pair (l_y, l_z). It should be noted that K_s is equal to or larger than the number of surface harmonics taken in the computational.

4. Repeat Step 1 and Step 3 with the velocity excitation by all other surface harmonics of unit amplitude to get all the columns of $\mathbf{\Omega}_s$.

The impedance $\mathbf{\Omega}_r$ can be obtained in an analogous way.

4.4 Approach Validation

This section analyses two computational cases to illustrate the proposed Harmonic technique. The first one used point sources in a rectangular room and thus is treated by analytical modelling. The other more complex case models the sound radiation of a vibrating box within an irregular space and the analysis is carried out by FEM modelling.

4.4.1 Characterisation of Point Sources in a Rectangular Room

In this section, a validation of sound prediction outlined will be made. The entire acoustical space is represented by a rectangular room of dimensions $2m \times 1m \times 1.2m$, Fig. 4.2. The physical source is taken to be a group of three monopoles located at $(0.2, 0.38, 0.55)m$, $(0.4, 0.78, 0.29)m$, $(0.35, 0.43, 0.8)m$. The volume velocities of the three monopoles are $(1, -i, -1)m^3/s$. The interface surface is created at $x = 0.7m$ which divides the room into two subsystems: the source space and the receiver space. The source space is thus a $0.7m \times 1m \times 1.2m$ room containing 3 monopoles while the receiver space is a $1.3m \times 1m \times 1.2m$ room. The response will be computed across a surface in the receiver space positioned at $x = 1.5m$. The sound speed of air in the room is $343m/s$, the mass density is $1.21kg/m^3$, the damping factor is 5×10^{-4}. The procedure of sound prediction outlined in Section 4.2.2 is applied in the following way:

1. Compute blocked pressure $\boldsymbol{P}_b$ in $K = 11 \times 13 = 143$ points across the interface surface due to 3 monopoles in the source space by Eq. (4.14). Compute the basis function $\boldsymbol{\Phi}_b$ using $H = (2 \times 2 + 1) \times (2 \times 3 + 1) = 35$ surface harmonics on the interface surface to get the blocked pressure amplitude $\boldsymbol{\Pi}_b$ by Eq. (4.12). Comments on the choice of these parameters will be provided in Section 4.5.

2. Compute harmonic impedances $\boldsymbol{\Omega}_s$ and $\boldsymbol{\Omega}_r$ using Eqs. (4.2)(4.13)(4.19). The two impedances are $H \times H$ matrices.

3. Compute $\boldsymbol{\Gamma}_c$ and $\boldsymbol{\Pi}_c$ using Eq. (4.7). The coupling velocity amplitudes follow from $\boldsymbol{V}_c = \boldsymbol{\Phi}\boldsymbol{\Gamma}_c$.

4. Compute $\boldsymbol{P}_r$ on the receiving surface by Eq. (4.19). The reference pressure response across the interface surface is computed directly.

Fig. 4.3 shows the computed descriptors at 350Hz: the blocked pressure $\mathbf{P}_b$ across the interface surface and the harmonics impedances $\boldsymbol{\Omega}_s, \boldsymbol{\Omega}_r$. Fig. 4.4 compares the predicted and reference pressures on $x = 1.5m$ at 350Hz. One can see that the predicted result well matches the reference values. The mismatch between two results will be explained in Section 4.5.

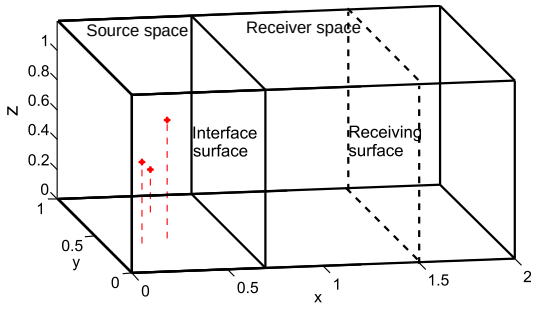

Fig. 4.2 Sound radiation due to monopoles in a room

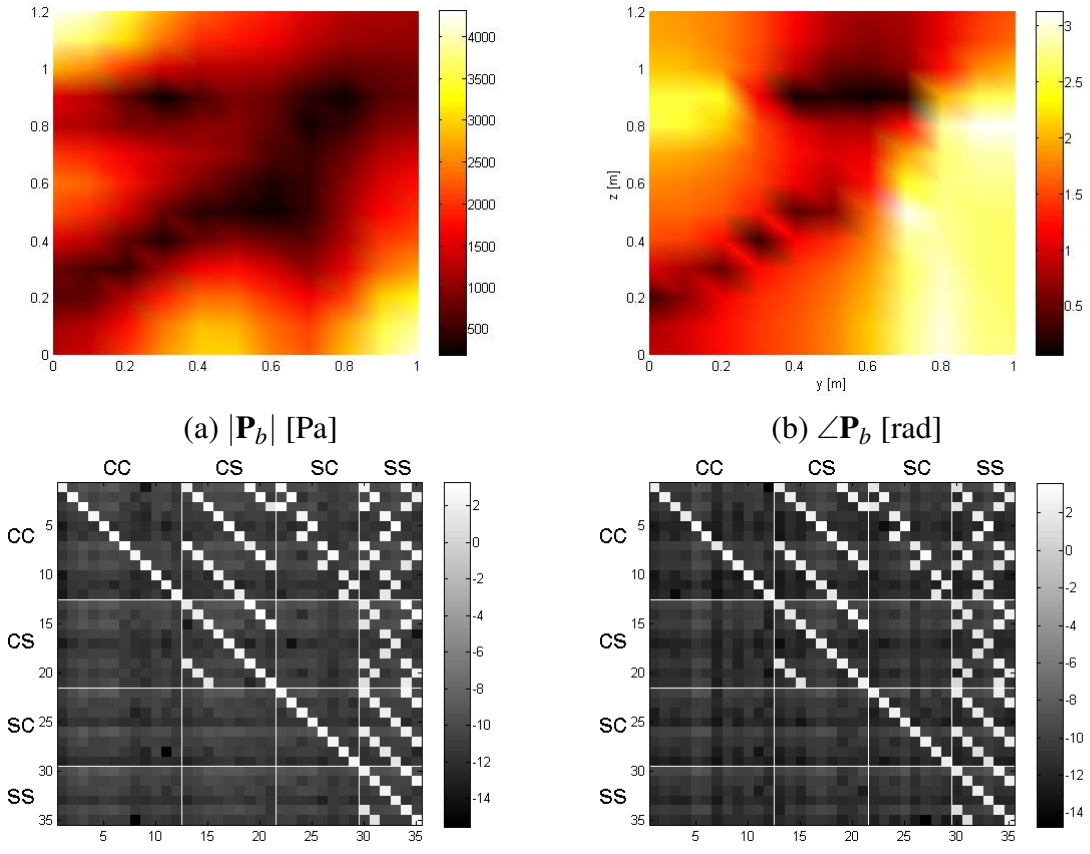

(a) $|\mathbf{P}_b|$ [Pa] (b) $\angle\mathbf{P}_b$ [rad]

(c) $\log_{10}(|\mathbf{\Omega}_s|)$ (d) $\log_{10}(|\mathbf{\Omega}_r|)$

Fig. 4.3 Descriptors at 350Hz. (a) Amplitude of blocked pressure $\mathbf{P}_b$, (b) Phase of blocked pressure $\mathbf{P}_b$, (c) Absolute value of $\mathbf{\Omega}_s$ in *log* scale, (d) Absolute value of $\mathbf{\Omega}_r$ in *log* scale

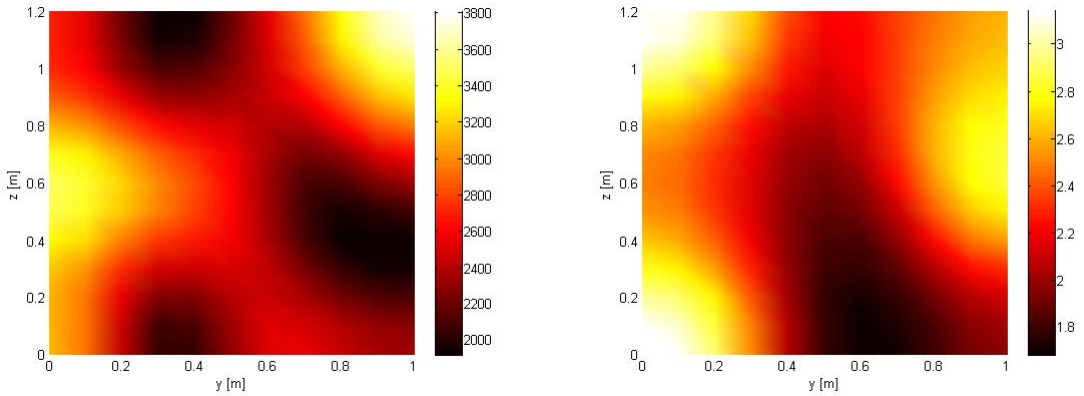

(a) $|P_r|$ [Pa] (b) $\angle P_r$ [rad]

(c) $|P_{r,ref}|$ [Pa] (d) $\angle P_{r,ref}$ [rad]

Fig. 4.4 Pressure maps on $x = 1.5m$ at 350Hz. Top: predicted, bottom: reference values; left: amplitude, right: phase.

Surface harmonic impedance Ω

Fig. 4.3 (b) and (c) indicate that the source and receiver surface harmonic impedances are upper triangular matrices. And it seems that two matrices have the same form. This may look odd and deserves further investigation as following.

As shown in Fig. 4.1, if the velocity excitation is applied to the entire surface at $x = 0$, the coefficient $B_{l,n}$ becomes

$$B_{l,n} = \underbrace{\int_0^b cos(\frac{l_y\pi}{b}y_e)cos(\frac{n_y\pi}{b}y_e)dy_e}_{①}\underbrace{\int_0^h sin(\frac{l_z\pi}{h}z_e)cos(\frac{n_z\pi}{h}z_e)dz_e}_{②} \tag{4.20}$$

Due to the orthogonal properties of trigonometric functions, in y direction, if $l_y = n_y$, ① $= \frac{b}{2}$, otherwise ① $= 0$; in z direction, if $l_z - n_z$ is odd number, ② $= \frac{2l_zh}{\pi(l_z+n_z)(l_z-n_z)}$, otherwise ② $= 0$, the detailed inferences are given in Appendix C.1. Concerning the values of ① and ②, Eq. (4.19) gives the pressure response on $x = 0$ plane as

$$\begin{aligned} P(x=0,y,z) &= \sum_{n'} A_{n'}\frac{b}{2}\frac{2l_zh}{\pi(l_z+n_z)(l_z-n_z)}cos(\frac{l_y\pi y}{b})cos(\frac{n_z\pi z}{h}) \\ &= \frac{b}{2}\underbrace{cos(\frac{l_y\pi y}{b})}_{③}\underbrace{\sum_{n'} A_{n'}\frac{2l_zh}{\pi(l_z+n_z)(l_z-n_z)}cos(\frac{n_z\pi z}{h})}_{④} \end{aligned} \tag{4.21}$$

with $n' = [n_x, n_y, n_z] = [n_x, l_y, n_z], n_z - l_z =$ odd number

According to Eq. (4.2), the pressure response on the interface surface $P(x = 0, y, z)$ is represented by a linear superposition of all the surface harmonics $[\mathbf{\Pi}^{cc}, \mathbf{\Pi}^{cs}, \mathbf{\Pi}^{sc}, \mathbf{\Pi}^{ss}]^t$. From Eq. (4.21), it can be seen that

- **In y direction**, $P(x = 0, y, z)$ can only be decomposed to *cos* function basis due to the *cos* velocity distribution, see ③, which means $\mathbf{\Pi}^{sc}, \mathbf{\Pi}^{ss}$ are equal to 0 with respect to both the source and receiver spaces.

- **In z direction**, $P(x = 0, y, z)$ can be decomposed to both *cos* and *sin* function basis due to the *sin* velocity distribution, see ④, which means $\mathbf{\Pi}^{cc}, \mathbf{\Pi}^{cs}$ are not equal to 0. Besides, assume that we use the same number of room modes and surface harmonics for the source and receiver spaces, namely l_z, n_z are the same with respect to the two spaces. And the height h of the source and receiver spaces is also the same, thereby only the constant $A_{n'}$ related to the room properties is different with respect to ④. Hence $\mathbf{\Pi}^{cc}, \mathbf{\Pi}^{cs}$ corresponding to the two spaces have linear relationship.

In conclusion, firstly, the source and receiver harmonic impedances $\mathbf{\Omega}_s, \mathbf{\Omega}_r$ have similar configuration. Secondly, the triangular form of non-zero values in impedance matrices are due to a particular character of parallelepipedic space excited over the entire wall surface. In this case, the velocity excitation of *cos* harmonics can only generate the pressure response of *cos* harmonics while *sin* harmonics velocity excitation can produce both *cos* and *sin* harmonics pressure response. Therefore, the surface harmonic impedance $\mathbf{\Omega}$ in this case is such a matrix having the following form:

$$\mathbf{\Omega} = \begin{array}{c} \\ cc \\ cs \\ sc \\ ss \end{array} \begin{array}{c} \begin{array}{cccc} cc & cs & sc & ss \end{array} \\ \begin{bmatrix} \times & \times & \times & \times \\ 0 & \times & 0 & \times \\ 0 & 0 & \times & \times \\ 0 & 0 & 0 & \times \end{bmatrix} \end{array} \tag{4.22}$$

where $\times$ means non zero value.

However, if the interface surface is not the entire cross section of the parallelepipedic room, the surface harmonic impedance is no longer a upper triangular matrix because the elements of the lower triangular part are not guaranteed to be zeros according to Eqs. (C.1) (C.6)–(C.8). So that impedance matrix is a non-symmetric full matrix. For example, with respect to the source and receiver spaces illustrated in Fig. 4.2, the harmonic impedances of a surface on $y-z$ plane and of size $0.6m \times 0.6m$ with one corner aligned to $(0.7, 0.1, 0.2)m$ in the two spaces are shown in Fig. 4.5 (a) and (b), respectively. From Fig. 4.5, we can see that both surface harmonic impedances are non-symmetric full matrices.

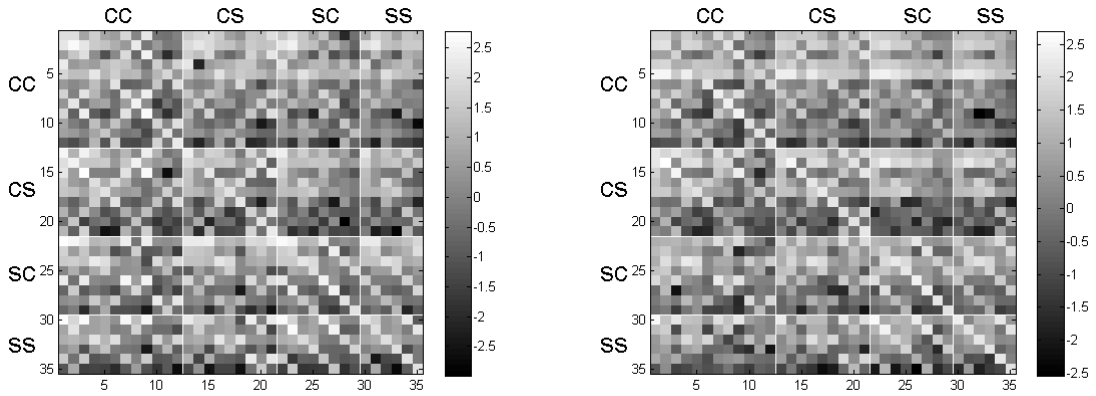

(a) $\log_{10}(|\mathbf{\Omega}_s|)$ (b) $\log_{10}(|\mathbf{\Omega}_r|)$

Fig. 4.5 Harmonic impedances of a surface of size $0.6m \times 0.6m$ with one corner aligned to $(0.7, 0.1, 0.2)m$ in the source (left) and receiver (right) spaces illustrated in Fig. 4.2.

4.4.2 Characterisation of a Vibrating Box in an Irregular Room

This section will demonstrate how can the characterisation using plane surface harmonics be applied to a more complex source – a vibrating box. The frequency response analysis is carried out by tool box based on the finite element method[1].

Fig. 4.6(a) shows the entire acoustical space. It is composed of two cavities separated by a plane wall with a rectangular opening. A vibrating box in the bigger cavity radiates sound. To characterise the vibrating box and carry out the sound prediction, a parallelepipedic interface surface is created to envelop the vibrating box and divides the entire space into source and receiver spaces, as shown in Fig. 4.6(b). Thus, the source space here is the parallelepipedic cavity within the interface surface with the vibrating box and the rest is the receiver space.

The entire acoustical space is of the size $2m \times 1m \times 1.2m$. The plane wall is at $x = 1.3m$. The opening is centered at $(1.3, 0.55, 0.35)m$ is of the size $0.5m \times 0.7m$. The prallelepipedic interface surface is centered at $(0.85, 0.55, 0.475)m$ is of the size $0.7m \times 0.5m \times 0.45m$. The vibrating box with $0.2m$ length, $0.3m$ width, $0.13m$ height is centered at $(0.8, 0.55, 0.565)m$. A uniform normal velocity distribution is applied to 6 surfaces of the box and the randomly selected velocities on the 6 box sides are listed in Table. 4.1.

Table 4.1 Velocity distribution on the 6 surfaces of the vibrating box

Surface position	$x = 0.7m$	$x = 0.9m$	$y = 0.4m$	$y = 0.7m$	$z = 0.5m$	$z = 0.63m$
Velocity $[m/s]$	2.8715 $+2.3766j$	1.4561 $+2.8785j$	2.4008 $+1.9672j$	0.4257 $+0.1071j$	1.2653 $+2.5474j$	2.7472 $+2.8020j$

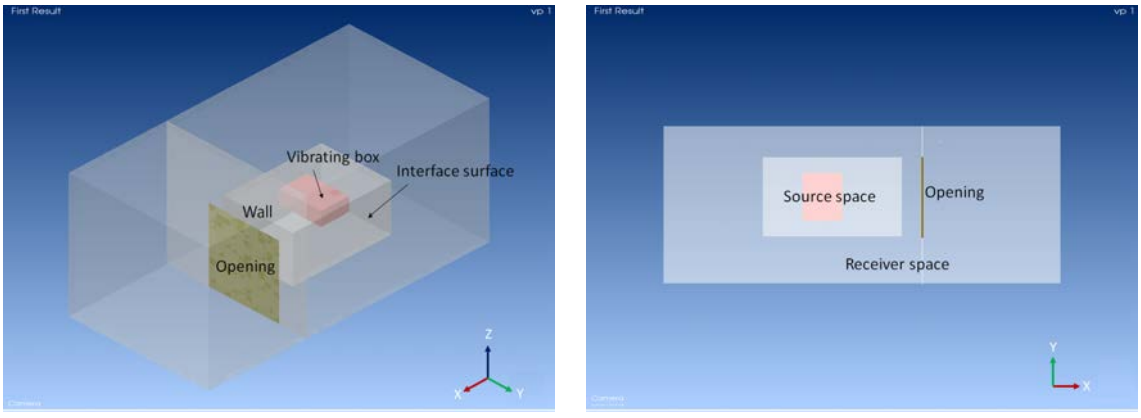

(a) (b)

Fig. 4.6 Sound radiation model. (a) ISO view, (b) Top view.

[1]Finite element models in the thesis are created by Hypermesh; the frequency response analysis is computed by Actran.

The characterisation of the vibrating box, including the identification of descriptors, realised through Actran has the same steps as described in Section 4.2.2. Specifically, the velocity excitation of any combination of sine and cosine functions can be applied by Actran across the interface surface for computing one column of impedance $\mathbf{\Omega}$. For example, a velocity with unit amplitude and $cos-sin$ distribution is applied to one side of the interface surface in the source space, as illustrated in Fig. 4.7. The pressure vector at all the sampling points on the interface surface due to the velocity excitation is $\mathbf{P} = [\mathbf{P}_1, \cdots, \mathbf{P}_6]^t$ where $\mathbf{P}_i$ is the pressure vector on the i^{th} rectangular surface. With the function basis $\mathbf{\Phi}_i$ corresponding to the i^{th} surface, $\mathbf{P}_i$ is developed into harmonics of amplitudes $\mathbf{\Pi}_i$ using $\mathbf{\Pi}_i = \mathbf{\Phi}_i^{-1}\mathbf{P}_i$ (Eq. (4.9)). Therefore the pressure vector $\mathbf{P}$ can be expressed by

$$\underbrace{\begin{bmatrix} \mathbf{P}_1 \\ \vdots \\ \mathbf{P}_6 \end{bmatrix}}_{\mathbf{P}} = \underbrace{\begin{bmatrix} \mathbf{\Phi}_1 & & \\ & \ddots & \\ & & \mathbf{\Phi}_6 \end{bmatrix}}_{\mathbf{\Phi}} \underbrace{\begin{bmatrix} \mathbf{\Pi}_1 \\ \vdots \\ \mathbf{\Pi}_6 \end{bmatrix}}_{\mathbf{\Pi}} \tag{4.23}$$

where the diagonal matrix $\mathbf{\Phi}$ is the function basis of the parallelepipedic interface surface. Since the excitation matches one of surface harmonics, $\mathbf{\Pi}$ is one column of the surface harmonic impedance $\mathbf{\Omega}$ in this case. 142 plane surface harmonics are used for the characterisation of the vibrating box, where the maximum indices of surface harmonics in x, y, z directions are $M_x = 3, M_y = 1, M_z = 2$.

The predicted pressure response compared to the reference result is shown in Fig. 4.8 for a point at $(1.3, 0.35, 0.25)m$. The overall matching between the predicted and reference results looks good. Nevertheless, some mismatch is seen which may be caused by several

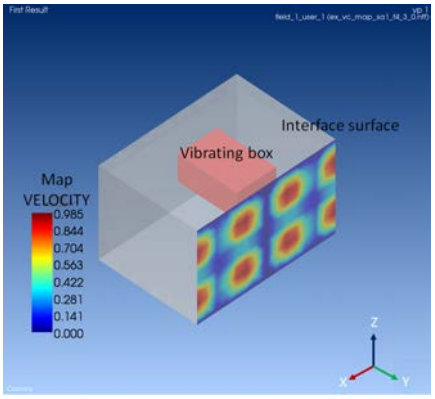

Fig. 4.7 Amplitude of velocity excitation of $cos-sin$ distribution applied to one side of the interface surface in the source space. The velocity is reported in m/s.

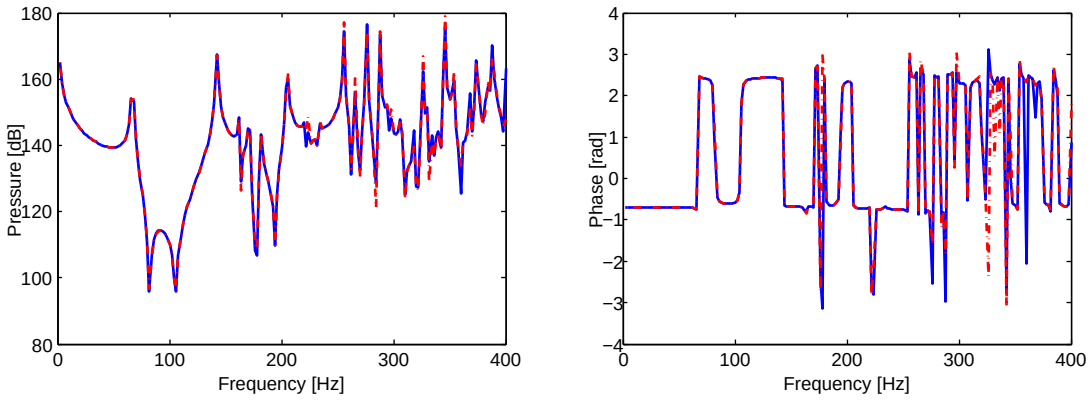

(a) (b)

Fig. 4.8 Pressure response at $(1.3, 0.35, 0.25)m$. Solid line: predicted using source characterisation; dashed line: reference. Left: amplitude, ref.$2 \times 10^{-5} Pa$; right: phase

.

factors, such as insufficient number of harmonics. The influence of these factors will be studied in the next section for better understanding of this approach.

4.5 Influence of Number of Surface Harmonics

This section analyses the influence of the number of harmonics on the predicted results. Since the sound radiation in the receiver space is predicted by applying the computed coupling velocity to the interface surface, this surface acts as an external vibrating source. If the predicted pressure response on the interface surface matches well the reference, the sound radiation in the receiver space can be well predicted. Therefore, Eq. (4.24) is used to characterise the matching between the predicted and reference results.

$$\varepsilon_h = \frac{\sqrt{\frac{1}{2}\sum_{i=1}^{K_p} |P_{c,i}|^2}}{\sqrt{\frac{1}{2}\sum_{i=1}^{K_p} |\hat{P}_{c,i}|^2}} \tag{4.24}$$

Here ε_h is called 'Characterisation error'; K_p is the number of receiving points on the interface surface; $P_{c,i}$ is the predicted coupling pressure of the i^{th} point while $\hat{P}_{c,i}$ is the reference coupling pressure at this point. A result predicted at only one receiving point can not provide a global judgement whether the source characterisation is good or bad. The more the receiving points covering the whole interface surface, the more reliable the characterisation error. The spacing between two adjacent points equal to $\frac{1}{6}\lambda$, referring to the mesh criterion of FEM, is considered to be sufficient for the error analysis.

The error analysis will be carried out using the radiation model in Fig. 4.2, we use 143 points covering the entire interface surface. The spacing between two adjacent points is 0.1m, about $\frac{1}{8}$ of λ_{min} corresponding to maximum frequency 400Hz. For the sake of studying the influence of the number of harmonics on the sound prediction, 20 cases have been employed with the number of harmonics varying from 9 to 99. Details of the 20 cases are displayed in Table. 4.2.

The wavelength of the (m_y, m_z) surface harmonic can be found by identifying the wavenumbers in y and z directions k_y, k_z: $k_y = \pi m_y/b$ and $k_z = \pi m_z/h$. The vector sum of the two vavenumbers defines the surface wavenumber $k_s = \sqrt{k_y^2 + k_z^2}$. With $\lambda_s = 2\pi/k_s$, this in turn gives the surface wavelength:

$$\lambda_s = \frac{2}{\sqrt{(\frac{m_y}{b})^2 + (\frac{m_z}{h})^2}} \tag{4.25}$$

Substituting the maximum values of indices M_y and M_z of the surface harmonic in both y and z directions into Eq. (4.25) yields the minimum wavelength $\lambda_{s,min}$ of the surface harmonics. Likewise, once the minimum wavelength of surface harmonic $\lambda_{s,min}$ is determined, the maximum values of indices M_y and M_z can be recognized through Eq. (4.25) by making the ratios $\frac{M_y}{b}$ and $\frac{M_z}{h}$ approximately equal. Thereby $\lambda_{s,min}$ is an equivalent measure of the number of harmonics. For the maximum frequency 400Hz, the minimum wavelength $\lambda_{s,min}$ of the surface harmonics of the 20 cases is between $0.4\lambda_{min}$ and $1.8\lambda_{min}$.

The scope of the characterisation error ε_h of 20 cases at [2, 400]Hz is displayed in Fig. 4.9. We can see that the number of harmonics influences the sound prediction at higher frequencies, i.e. [300,400]Hz, but have little influence on the lower frequencies. Fig. 4.10 plots the characterisation error ε_h of 20 cases at all the frequencies in [300,400]Hz, each line corresponds to one frequency. It can be seen that when $\lambda_{s,min}$ is larger than $\lambda_{min}/2$ (Case 14), the error fluctuates a lot, which means the predicted results varies a lot with the number of

Table 4.2 Twenty cases

N^o	$\lambda_{s,min}[m]$	$\frac{\lambda_{s,min}}{\lambda_{min}}$	(M_y, M_z)	N^o	$\lambda_{s,min}[m]$	$\frac{\lambda_{s,min}}{\lambda_{min}}$	(M_y, M_z)	N^o	$\lambda_{s,min}[m]$	$\frac{\lambda_{s,min}}{\lambda_{min}}$	(M_y, M_z)
1	1.54	1.80	(1,1)	8	0.58	0.68	(3,2)	15	0.45	0.52	(3,4)
2	1.03	1.02	(1,2)	9	0.57	0.66	(1,4)	16	0.43	0.5	(2,5)
3	0.92	1.07	(2,1)	10	0.51	0.59	(2,4)	17	0.42	0.49	(4,3)
4	0.77	0.90	(2,2)	11	0.51	0.59	(3,3)	18	0.39	0.45	(3,5)
5	0.74	0.86	(1,3)	12	0.49	0.57	(4,1)	19	0.38	0.44	(4,4)
6	0.64	0.75	(3,1)	13	0.47	0.55	(1,5)	20	0.35	0.4	(4,5)
7	0.62	0.72	(2,3)	14	0.46	0.54	(4,2)				

harmonics; below this value, ε_h is practically a constant, which means the increasing number of surface harmonics has little influence on the predicted results. Besides, we find that the condition number of $\mathbf{\Omega}_s$ and $\mathbf{\Omega}_r$ increases with number of harmonics, which is indicated in Fig. 4.11. To avoid the error from the matrix inverse, the number of surface harmonics should not be too large.

Hence, even from physical point of view, the more the number of surface harmonics, the better the sound prediction, from computational point of view, the number of surface harmonics should not be too large. From above discussion, the minimum wavelength of surface harmonic $\lambda_{s,min}$ approximate to $\frac{1}{2}$ sound wavelength λ could be served as a rule to determine the number of surface harmonics. Once the minimum wavelength of surface harmonic $\lambda_{s,min}$ is determined, the maximum values of indices M_y and M_z can be recognized through Eq. (4.25) by making the ratios $\frac{M_y}{b}$ and $\frac{M_z}{h}$ approximately equal. Moreover, since the minimum wavelength of surface harmonic $\lambda_{s,min}$ is related to the sound wavelength λ, the number of surface harmonics can be adjusted according to frequency bands. In other words, less number of surface harmonics is needed at low frequencies than that at high frequencies.

Last but not least, from Fig. 4.9, we can see that the characterisation error λ_h is large around a few resonance frequencies, such as 192Hz and 282Hz, and varies little as the number of surface harmonics increasing. Take the sound prediction around 192Hz and 282Hz as an example. When the minimum wavelength of surface harmonic $\lambda_{s,min}$ is $0.35m$ (Case 20), which is smaller than $\frac{1}{2}\lambda$ with respect to the two frequencies, the predicted and reference pressure responses at $(0.7, 0.05, 0.95)m$ around the two frequencies are as the dashed lines shown in Fig. 4.12. The predicted pressure levels at 192Hz and 282Hz are 6.77dB and 11.05dB higher than the corresponding reference values. However, if we increase the frequency resolution from 2Hz to 0.1Hz, the predicted and reference pressure responses around 192Hz and 282Hz are as the solid lines shown in Fig. 4.12. It can be seen that the amplitude peaks of predicted and reference pressure responses for both cases are at the same level but with a small frequency shift, which means the mismatch between the predicted and reference results is related to the frequency shift. As increasing number of surface harmonics cannot decrease the frequency shift of predicted results any more, the mismatch varies little with the number of surface harmonics. That is why the characterisation error ε_h of the last 7 cases at [300,400]Hz stays stable, see Fig. 4.10. However, the frequency shift is inherent for source characterisation via enveloping surface [78], as the continuous global 'source – receiver' system is represented by discrete coupling, i.e. a finite number of harmonics and measuring points.

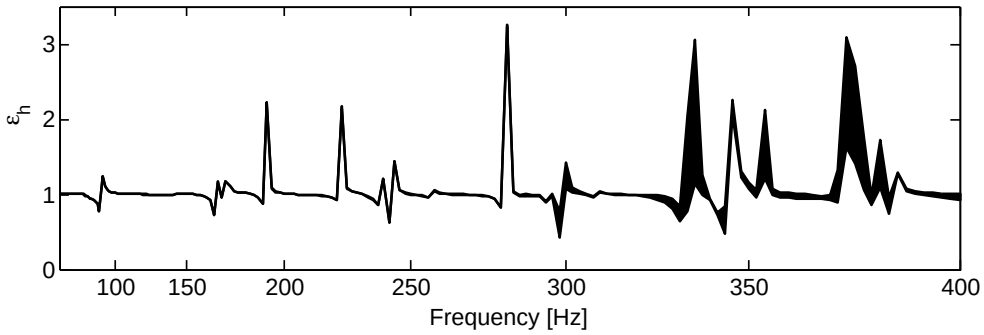

Fig. 4.9 Influence of number of surface harmonics on response pressure matching

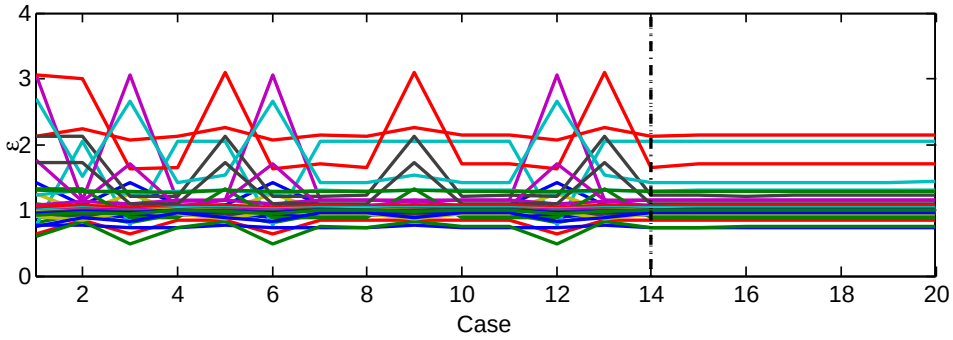

Fig. 4.10 ε_h of 20 cases at all the frequencies in [300,400]Hz

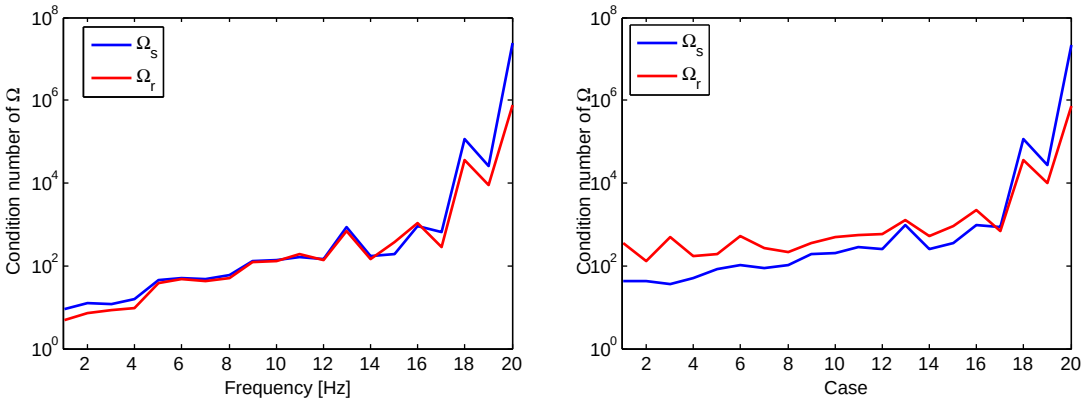

(a) (b)

Fig. 4.11 Condition numbers of $\boldsymbol{\Omega}_s$ and $\boldsymbol{\Omega}_r$ at 100Hz (left) and 350Hz(right)

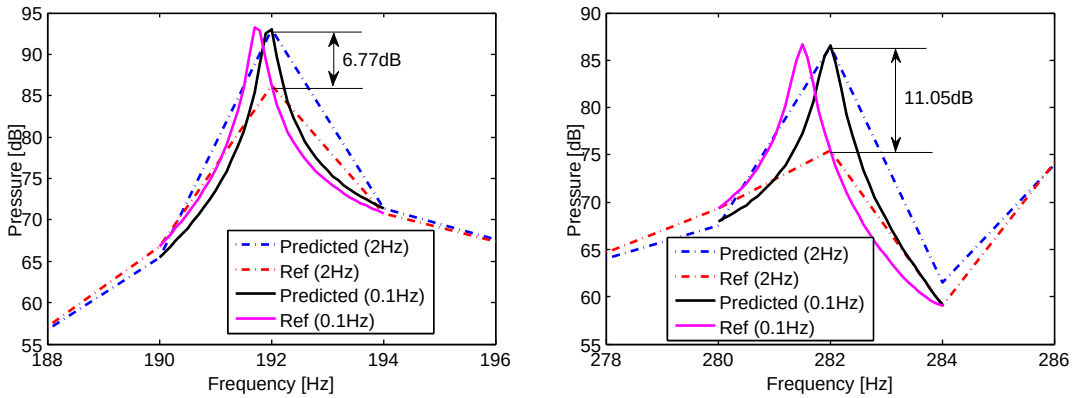

(a) 192Hz (b) 282Hz

Fig. 4.12 Pressure response at (0.7,0.05,0.95)m. Frequency resolution: solid line 0.1Hz, dashed line 2Hz.

4.6 Conclusions

Using an interface surface consisting of one or several rectangular surfaces, the sound field across each surface is expanded into plane surface harmonics – sine and cosine functions. Using plane surface harmonics, the blocked pressure is represented as a vector of complex amplitudes of harmonics, while the impedance is represented as a matrix of pressure/velocity amplitude ratios. The chapter has demonstrated how to characterise the source and get the predicted sound pressure using the blocked pressure and surface impedance of the source.

Analytical computation of the source descriptors in a parallelepipedic cavity was done first to demonstrate the principle of the approach. The sound prediction in a more realistic case of a vibrating box coupled to two different acoustical spaces is then carried out to illustrate the feasibility of the developed surface technique. The error analysis about the influence of number of surface harmonics shows that the minimum wavelength of surface harmonic $\lambda_{s,min}$ is approximate $\frac{1}{2}$ of sound wavelength λ. This can be serve as a criterion for selecting the number of surface harmonics.

The next chapter will introduce an alternative technique – 'Patch surface coupling technique' (Patch technique) to carry out the source characterisation.

Chapter 5

Source Characterisation using Patch Surface Coupling Technique

This chapter will introduce an alternative technique – 'Patch surface coupling technique' – to identify the source and receiver descriptors, i.e., blocked pressure, source impedance and receiver impedance. The main idea of the Patch technique is dividing an interface surface into a number of patches and subsequently considering each patch as a discrete point. The blocked pressure is expressed by the pressures and normal velocities averaged across the concerned patches. Thus by using N_p patches, the blocked pressure is represented by a N_p complex vector while the two impedances are represented by corresponding $N_p \times N_p$ matrices.

This chapter will first present the patch concept as well as the procedure of identification of the descriptors using the Patch technique. Then we will study two cases to demonstrate the feasibility of sound prediction through the Patch technique. The first case is simply the characterisation of point sources in a rectangular room as used in Chapter 4. Specifically, we will investigate the influence of patch size to the predicted result, followed by a discussion on the imperfect patch averaging. The second case is on the characterisation of a vibrating box in a rectangular room. By changing the velocity distribution on the vibrating box, the source limitation of the Patch technique will be investigated at the end of this chapter. Moreover, the sound radiation of a vibrating box in an irregular room studied in Chapter 4 shown by the model in Fig. 4.6, will be predicted using the Patch technique. This will enable a comparison between the Patch and Harmonic techniques with respect to the computational and experimental perspectives.

5.1 Identification of Descriptors Using Patches

Take the model of point sources in a rectangular room in Section 4.4.1 as an example. The patch technique suggests dividing the interface surface into several patches, as shown in Fig. 5.1. The acoustical state across each patch will be represented by two scalar quantities: the sound pressure and the normal component of particle velocity, each of these averaged over the surface of the patch. Thus, a decrease in patch size will produce better representation of pressure and velocity, but will in turn result in a larger number of patches.

According to the Patch concept, the source and receiver descriptors can be identified as below.

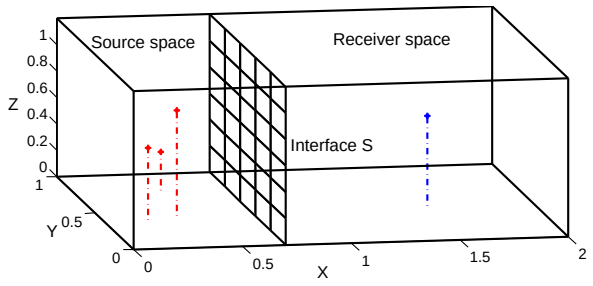

Fig. 5.1 Patch concept

5.1.1 Identification of Descriptors

- **Blocked pressure**

With respect to the N_p patches of the interface surface, the blocked pressure $\mathbf{P}_b$ due to the operating source, i.e., the pressure across the immobile interface surface in the source space, is represented by the discrete values of pressures averaged across each patch.

$$\mathbf{P}_b = [< P_{b,1} >_{\Delta S}, \cdots, < P_{b,i} >_{\Delta S}, \cdots, < P_{b,N_p} >_{\Delta S}]^t, i = 1, \cdots, N_p \tag{5.1}$$

where ΔS denotes the patch area; $< P_{b,i} >_{\Delta S}$ is the pressure amplitude averaged across the i^{th} patch. Hence the blocked pressure $\mathbf{P}_b$ is a $N_p \times 1$ vector.

- **Source and receiver impedances**

The source impedance $\mathbf{Z}_s$ or the receiver impedance $\mathbf{Z}_r$ of the interface surface is represented by the coupling impedances among all the patches. A normal velocity $< V_{z,m_2} >_{\Delta S}$

applied uniformly to the m_2^{th} patch with all other patches immobile produces the pressure response averaged across the m_1^{th} patch $< P_{z,m_1} >_{\Delta S}$. This gives the coupling impedance between the m_1^{th} and m_2^{th} pathes as

$$Z_{m_1 m_2} = \frac{< P_{z,m_1} >_{\Delta S}}{< V_{z,m_2} >_{\Delta S}}, m_1, m_2 = 1, \cdots, N_p \tag{5.2}$$

which is the $(m_1, m_2)^{th}$ element of the surface impedance $\mathbf{Z}_{s|r}$. The latter is thus a $N_p \times N_p$ matrix.

- **Coupling velocity**

According to the principle of impedance coupling (Eq. (3.5)), we can obtain the coupling velocity with the three identified descriptors. Like the blocked pressure, the coupling velocity $\mathbf{V}_c$ is also a $N_p \times 1$ vector,

$$\mathbf{V}_c = [< V_{c,1} >_{\Delta S}, \cdots, < V_{c,i} >_{\Delta S}, \cdots, < V_{c,N_p} >_{\Delta S}]^t, i = 1, \cdots, N_p \tag{5.3}$$

where $< V_{c,i} >_{\Delta S}$ is the velocity which will be applied to the i^{th} patch to reconstruct the sound radiation in the receiver space. The coupling velocity reads [78]:

$$\mathbf{V}_c = (\mathbf{Z}_s + \mathbf{Z}_r)^{-1} \mathbf{P}_b \tag{5.4}$$

5.1.2 Procedure of Sound Prediction

The computational procedure of sound prediction via the Patch technique can be summarized as:

1. In the source space, with the source operating and the interface surface is blocked, compute the pressure responses averaged across each of the N_p patches, that is the blocked pressure vector $\mathbf{P}_b$ ($N_p \times 1$).

2. In the source space, switch the source off, apply the unit normal velocity excitation to the i^{th} patch only and measure the pressure responses averaged across each patch. This yields the i^{th} column of the source impedance $\mathbf{Z}_s$. Repeat the computation N_p times by applying the velocity excitation to all patches. In this way, all the columns of the source impedance $\mathbf{Z}_s$ ($N_p \times N_p$) will be created.

3. Similarly to the previous step, compute the receiver impedance $\mathbf{Z}_r$ ($N_p \times N_p$) in the receiver space.

4. With the identified descriptors $\mathbf{P}_b, \mathbf{Z}_s, \mathbf{Z}_r$, calculate the coupling velocity $\mathbf{V}_c$ ($N_p \times 1$) by Eq. (5.4).

5. Apply the coupling velocity to the patches of the receiver space to obtaine the sound pressure at a discrete point.

5.1.3 Analytical Modelling

Pavić [78] has studied the source and receiver descriptors using the Patch technique. Similarly to the Harmonic technique, referring to Eq. (4.14), the pressure response averaged across a patch ΔS centered at $\mathbf{r}$ to an excitation of strength Q_e uniformly spread over a patch ΔS centered at $\mathbf{r}_e$ is

$$< P(\mathbf{r}) >_{\Delta S} = \frac{j\omega\rho_0 c^2}{U} Q_e(\mathbf{r}_e) \sum_{n=1}^{N} \frac{< \phi_n(\mathbf{r}) >_{\Delta S} < \phi_n(\mathbf{r}_e) >_{\Delta S}}{\omega_n^2 - \omega^2 + 2j\varepsilon\omega} \tag{5.5}$$

where $< \phi_n >_{\Delta S} = \frac{1}{\Delta S} \int_{\Delta S} \phi_n dS$. For a parallelepipedic room the averaged volume of eigenfunction $< \phi_n(\mathbf{r}) >_{\Delta S}$ reduce to the product of cardinal sines as shown in [78]. Besides, with $< \phi_n(\mathbf{r}) >_{\Delta S}$ replaced by $\phi_n(\mathbf{r})$, the right-hand side of Eq. (5.5) gives the pressure response at a point $\mathbf{r}$ due to a patch excitation; with $< \phi_n(\mathbf{r}_e) >_{\Delta S}$ replaced by $\phi_n(\mathbf{r}_e)$, the right-hand side of Eq. (5.5) gives the patch pressure response due to the point source excitation. In brief, Eq. (4.14) can be used to compute the pressure response due to point source excitation (*Point-to-Point*), while Eq. (5.5) can be used to compute the pressure response in other 3 cases: patch pressure response to patch velocity excitation (*Patch-to-Patch*), patch pressure response to point source excitation (*Patch-to-Point*), point pressure response to patch velocity excitation (*Point-to-Patch*).

According to Eq. (5.5), the coupling impedance between driving and receiving patches is computed by

$$\begin{aligned} Z(\mathbf{r}, \mathbf{r}_e) &= \frac{< P(\mathbf{r}) >_{\Delta S}}{< V(\mathbf{r}_e) >_{\Delta S}} = \frac{< P(\mathbf{r}) >_{\Delta S}}{Q_e(\mathbf{r}_e)/\Delta S} \\ &= \Delta S \frac{j\omega\rho_0 c^2}{U} \sum_{n=1}^{N} \frac{< \phi_n(\mathbf{r}) >_{\Delta S} < \phi_n(\mathbf{r}_e) >_{\Delta S}}{\omega_n^2 - \omega^2 + 2j\varepsilon\omega} \end{aligned} \tag{5.6}$$

5.2 Approach Validation

This section studies two computational cases - the point sources in a prallelepipedic room as analysed in Chapter 4 and a vibrating box in a parallelepipedic room.

5.2.1 Characterisation of Point Sources in a Rectangular Room

The first simple example of the Patch technique uses the model shown in Section 4.4.1, i.e., to reconstruct sound radiation of three point sources in a rectangular room. The interface surface is divided into patches as shown in Fig. 5.1. The three descriptors – blocked pressure, source impedance, receiver impedance – can be directly computed by Eqs. (5.5)(5.6). Then we can calculate the expected normal velocity across the interface surface and employ it as the equivalent source model. With the interface surface divided in to $5 \times 6 = 30$ patches, the predicted pressure response at 300Hz across the plane $x = 1.816m$ in the receiver space is shown in Fig. 5.2. Compared with the pressure response computed directly, it can be seen that the Patch technique can produce acceptable results.

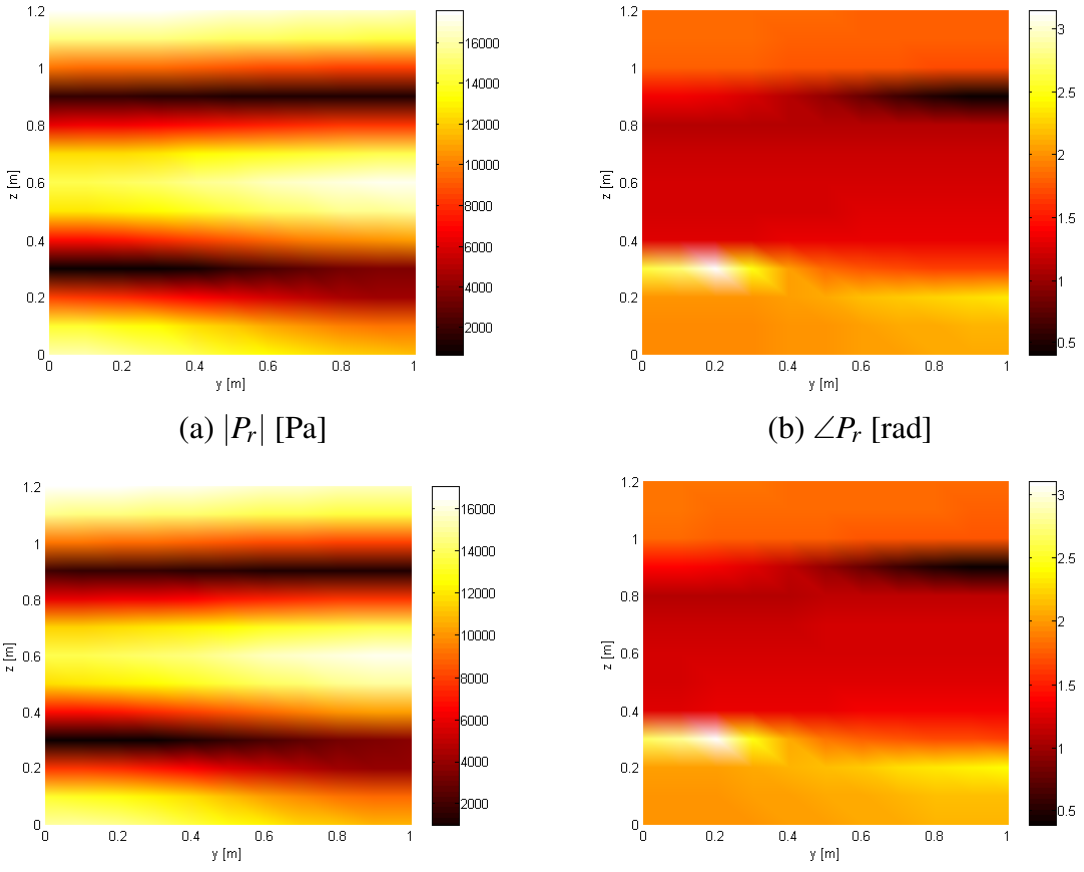

(a) $|P_r|$ [Pa] (b) $\angle P_r$ [rad]

(c) $|P_{r,ref}|$ [Pa] (d) $\angle P_{r,ref}$ [rad]

Fig. 5.2 Pressure response at 300Hz on the plane at $x = 1.816m$. Top: predicted, bottom: reference values; left: amplitude, right: phase.

Patch Size

The influence of patch size on the predicted results has been discussed in [79]. It has been found that the patch size of $\frac{1}{3}\lambda$ which enables acceptable sound prediction can serve as a rule for sectioning the interface surface. To present the influence of patch size on predicted results, we carry out the sound prediction due to the point sources in the parallelepipedic room with the interface surface divided into various numbers of patch. For a narrow frequency band between 450Hz and 480Hz, the ratio between the patch size (i.e., length of a side) and the wavelength λ stays approximately the same for all frequencies. We successively change the patch size from $\lambda/2$ to $\lambda/6$, and plot corresponding pressure responses at the point $(1.816, 0.6058, 0.7072)m$ in Fig. 5.3. One can notice a slight frequency shift between the reference and coupled results. Concerning the frequency shift between the predicted results and the reference, all the predicted results of a patch size smaller than or equal to $\lambda/3$ are very close to the reference. However, as smaller patch size means a larger number of patches, the dimension of the surface impedances will be larger, which results in more computational time and more measuring work. Therefore, the patch size of $\frac{1}{3}\lambda$ is appropriate for sectioning the interface surface.

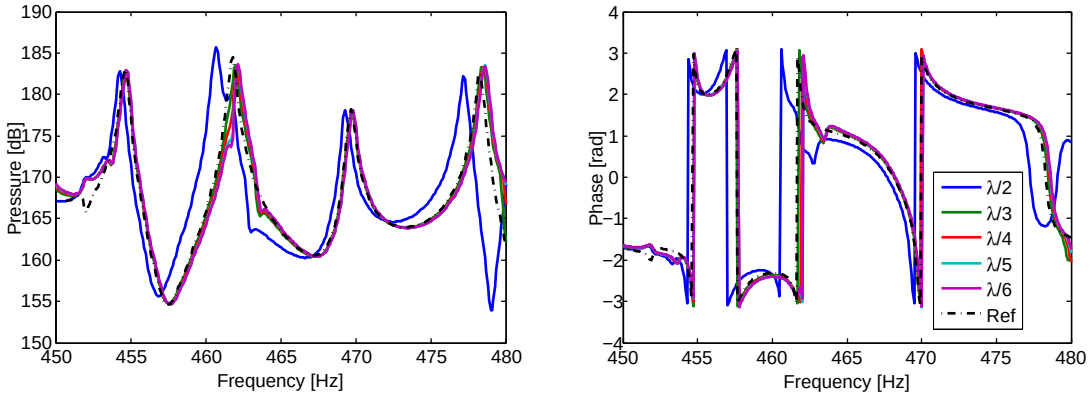

(a) (b)

Fig. 5.3 Pressure responses at $(1.816, 0.6058, 0.7072)m$ due to point sources. Solid lines: predicted results, dashed line: reference; Left: amplitude level, ref, 20μ Pa), right: phase.

Patch Averaging

Unlike the current example that directly calculates the three descriptors by Eq. (5.6), there is no analytical solution for complex cases, where the Patch technique actually adopts *patch averaging* to compute the descriptors. The pressure averaged across a patch will be therefore

estimated by the mean values of pressures at discrete points across the patch. Theoretically, the more the discrete measuring points, the better the estimation. In other words, the spacing between the adjacent points should be small enough in order to well estimate the averaged pressure across a patch. Now we show the largest threshold of the adjacent spacing for the estimation.

Instead of directly computing the pressure response averaged across a patch by Eq. (5.5), we now estimate it by the mean value of pressures at discrete points on the patch, where the pressure response at a single point due to either the patch or point excitation is calculated by Eq. (5.5). Using the example in Fig. 5.1, when the patch size is set to $\frac{1}{3}\lambda$ with respect to frequencies between 450Hz and 480Hz, the interface surface is divided into 30 patches (5×6). Each patch is represented by 4 different combinations of points, ranging from 1 to 12, as shown in Fig. 5.4. Accordingly, the spacing between adjacent points changes from $\frac{1}{3}\lambda$ to $\frac{1}{12}\lambda$.

First, we compute the mismatch of the predicted and exact sound pressure levels at $(1.816, 0.6058, 0.7072)m$ obtained through patch averaging and direct computation, as shown in Fig. 5.5 (a). We can see that the mismatch decreases as the spacing between points reducing, indicating that the more the discrete points, the better the predicted result. In addition, we compare the descriptors estimated via patch averaging to the descriptors directly computed by analytical modelling. On the patch centered at $(0.7, 0.375, 1.08)m$, the curves of the blocked pressure, its self impedance in source and receiver spaces are plotted in Figs. 5.5 (b), (c) and (d), respectively. The solid lines are those results estimated via patch averaging, the dashed line denotes the reference computed by analytical modelling. From the three figures, we can observe that when the spacing between adjacent points is smaller than or equal to $\lambda/6$, the estimations well approximate the reference values, thus we conclude that the spacing between adjacent measuring points is better to be no larger than $\lambda/6$.

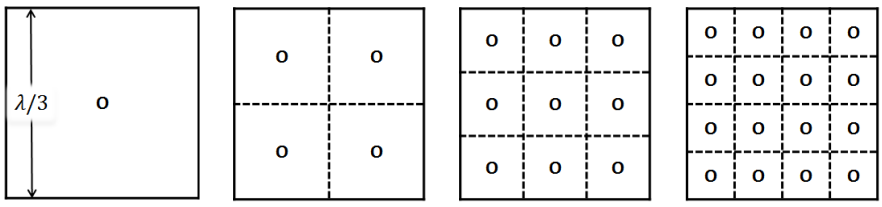

Fig. 5.4 Discrete points on a patch, denoted by ○. Spacing between adjacent points from left to right: $\lambda/3$, $\lambda/6$, $\lambda/9$, $\lambda/12$

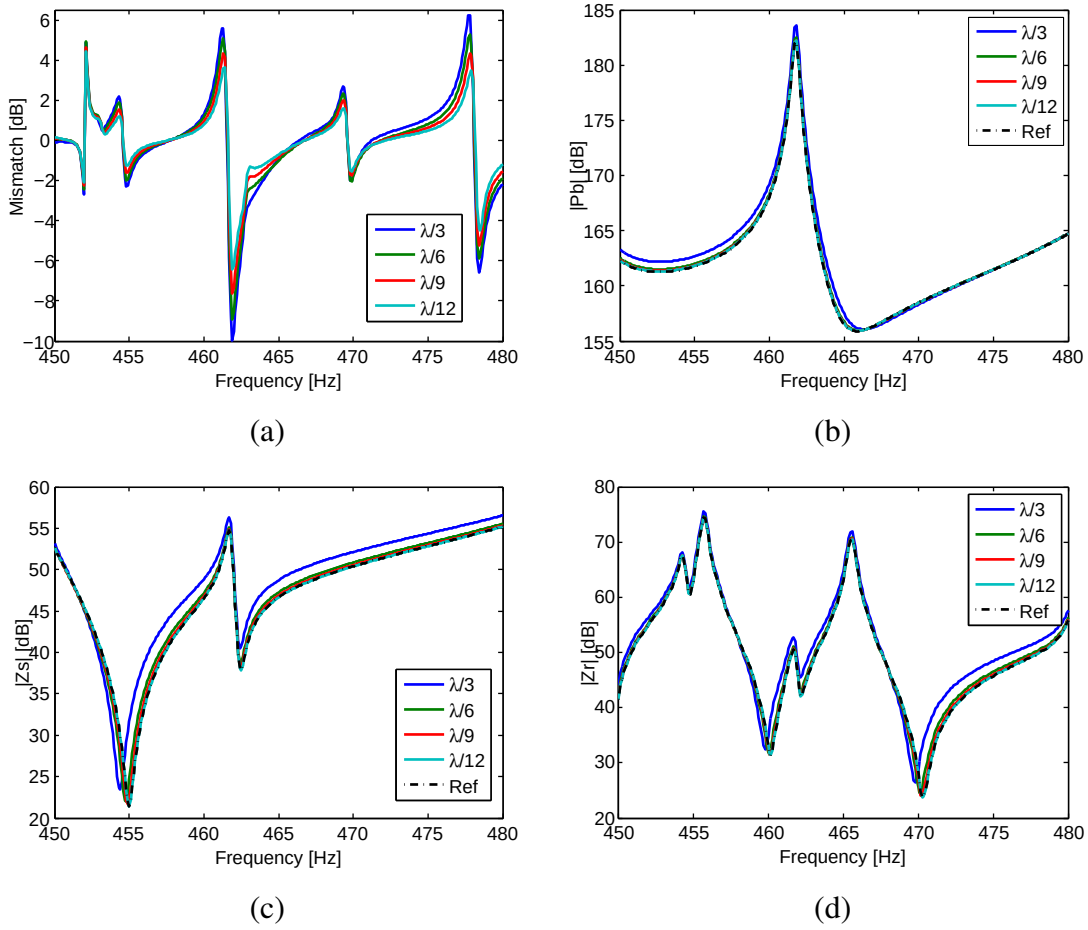

Fig. 5.5 Influence of patch averaging. (a) Mismatch between the predicted and exact sound pressure levels at $(1.816, 0.6058, 0.7072)m$, (b) pressure responses averaged across the patch centered at $(0.7, 0.375, 1.08)m$ due to point sources in source space, (c) and (d) its self impedances in source and receiver spaces. Solid line: estimated through discrete points, dashed line: reference values

5.2.2 Characterisation of a Vibrating Box in a Rectangular Room

Fig. 5.6 shows the second example: that of a vibrating box in a rectangular room. A parallelepipedic surface, i.e., an interface surface consisting of six rectangular surfaces, divides the entire room into source and receiver spaces. The entire room is of the size $2m \times 1m \times 1.2m$. The vibrating box centered at $(0.8, 0.55, 0.565)m$ is of the size $0.2m \times 0.3m \times 0.13m$. Unit normal velocity directing to the room is applied to the six faces of the box. The interface surface centered at $(1, 0.5, 0.6)m$ is of the size $1m \times 0.5m \times 0.6m$.

According to the established patch size criterion, the patch size is set to be about $\frac{1}{3}\lambda$. Specifically, for the frequency band $[2,\ 440]$Hz, the interface surface is divided into 62

patches, i.e., 5, 2, 3 patches in x, y, z directions, respectively. The pressure averaged across a patch is estimated by the mean value of the pressures at several discrete points across the patch. As we have discussed above, the spacing between two adjacent discrete points is set to the usual mesh criterion, $\frac{1}{6}\lambda$. Fig. 5.7 plots the predicted and reference pressure responses at $(0.3, 0.2, 0.15)m$ in the receiver space. The predicted result matches well the reference but shows a small frequency shift at high frequencies.

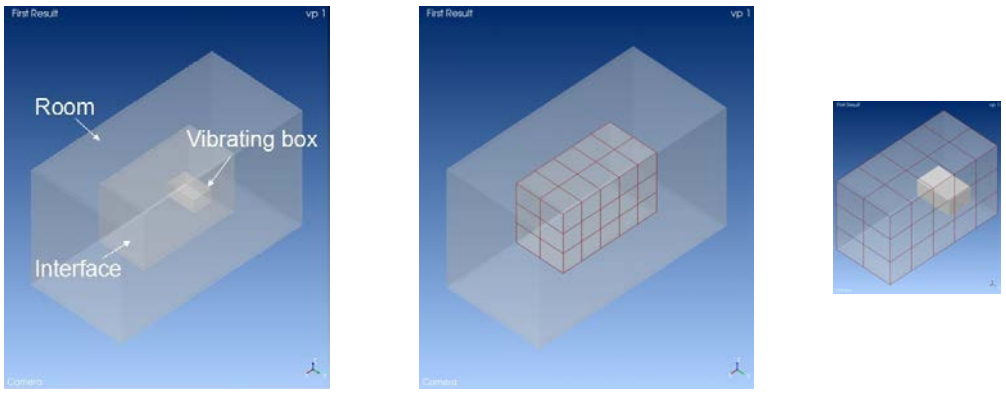

(a) (b) (c)

Fig. 5.6 A rectangular room with a vibrating box. (a) Global system, (b) Receiver space, (c) Source space.

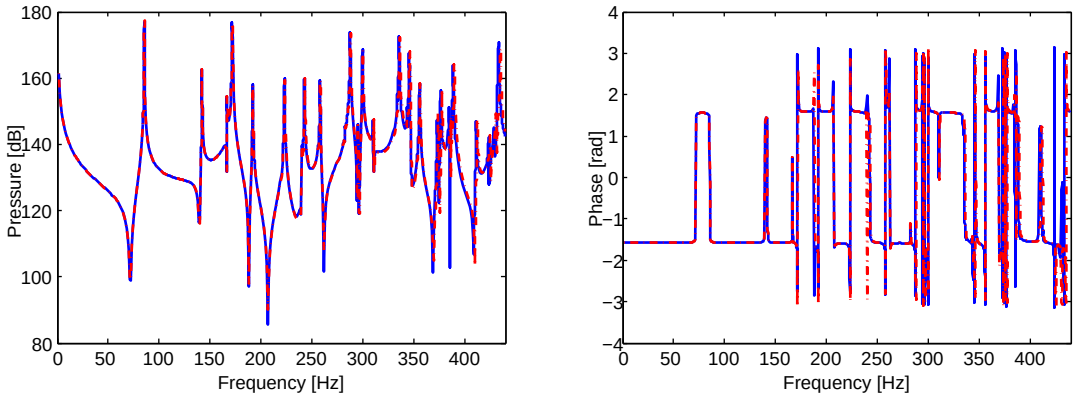

(a) (b)

Fig. 5.7 Pressure response of a vibrating box at $(0.3, 0.2, 0.15)m$ in a rectangular room. Solid line: predicted result, dashed line: reference; Left: amplitude (ref, 2×10^{-5} Pa), right: phase.

5.3 Comparison to the Harmonic Technique

Using the Patch technique, we re-predict the pressure response due to the vibrating box at the same point in the irregular room shown in Fig. 4.6. The interface surface is divided into $32 = 2 \times (3 \times 2 + 3 \times 2 + 2 \times 2)$ patches, as shown in Fig. 5.8. The predicted and reference responses are given in Fig. 5.9. Remind that the results of the Harmonic technique has been given in Fig. 4.8. It can be seen that the predicted responses by the two techniques match the exact reference well.

With respect to the reference response, the mismatches of the two techniques are summarized in Fig. 5.10. It seems that the Patch technique gives larger mismatch than the Harmonic technique. Actually, we found that the mismatches of both the techniques are due to frequency shift to the exact response. For example, between 386Hz and 392Hz, the predicted pressure responses obtained by the two techniques as well as the reference values at $(1.3, 0.35, 0.25)m$ are shown in Fig. 5.11. We can see that the pressure resonance peaks are at the same level, but the frequency shifts caused by the Patch and Harmonic techniques are different. The frequency shift of the former is obviously larger than that of the latter, therefore larger mismatch by the Patch technique is observed. For example, at 389Hz, the mismatches between the predicted sound pressure level and the reference value are 11.1dB and 5.3dB for the Patch technique and the Harmonic technique, respectively. The larger frequency shift by the Patch technique is probably because it represents the sound field across the interface surface using discrete patches. Compared with the Harmonic technique that always consider the sound field as a continuous entirety, it is the discretization of sound field that causes more shift to the predicted results. However, for either the Patch technique or the Harmonic technique, the frequency shift can be often ignored e.g. when the sound is broad-band or when the results are represented in frequency bands. Concerning the similar performance of the predicted response amplitude, we consider the two techniques comparably effective for sound prediction.

In spite of the similar prediction performance, some differences exist between the two techniques. Where application to measurement is concerned, the Patch technique looks simpler than the Harmonic technique, e.g., for a square surface of the size λ, the Patch technique divides the surface into $9(= 3 \times 3)$ patches according to the criterion of patch size $\frac{1}{3}\lambda$, which means 9 measurements are required for the identification of source or receiver impedance $\mathbf{Z}_s$, $\mathbf{Z}_r$. According to the criterion of minimum wavelength of surface harmonic $\lambda_{s,min} = \frac{1}{2}\lambda$, the maximum indices of surface harmonics of the square surface is $2\sqrt{2} \approx 3$ estimated through Eq. (4.25), therefore we need $49(= (2 \times 3 + 1)^2)$ surface harmonics, which means 49 measurements, to get all the elements of harmonic impedances. In brief, the Harmonic technique needs 5.4 times more measurements as the Patch technique. The

Patch technique being simpler, we will apply it in experimental validation in the next chapter. Before that, we examine the limitations of the Patch technique as a complementary study.

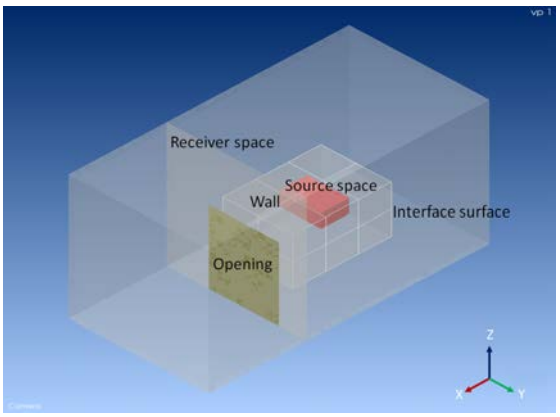

Fig. 5.8 Interface surface separated into patches.

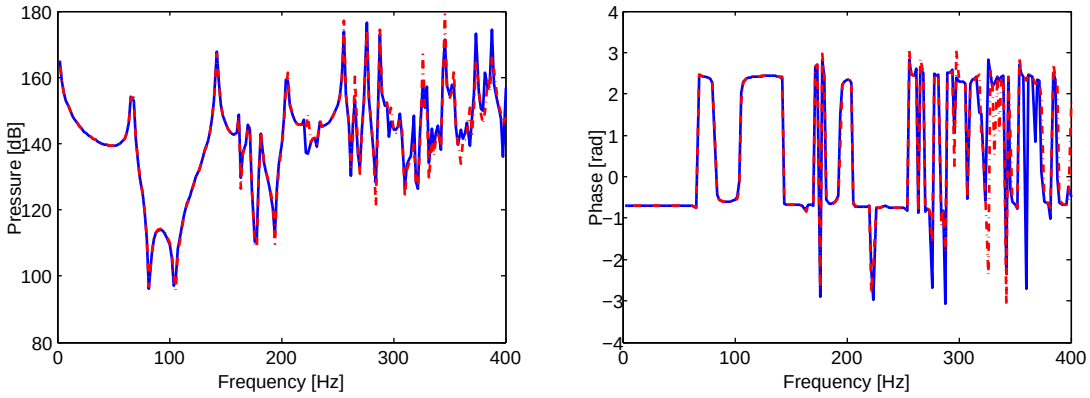

(a) (b)

Fig. 5.9 Pressure response at $(1.3, 0.35, 0.25)m$ using Patch technique. Solid line: predicted; dashed line: reference. Left: amplitude ref.$2 \times 10^{-5} Pa$; Right: phase

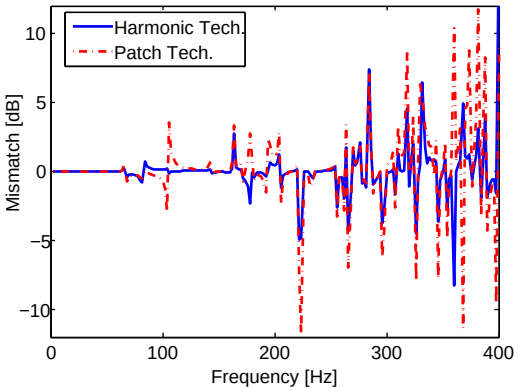

Fig. 5.10 Mismatch between the reference sound pressure level and the predicted values using the Patch and Harmonic techniques. Solid line: Harmonic, dashed line: Patch

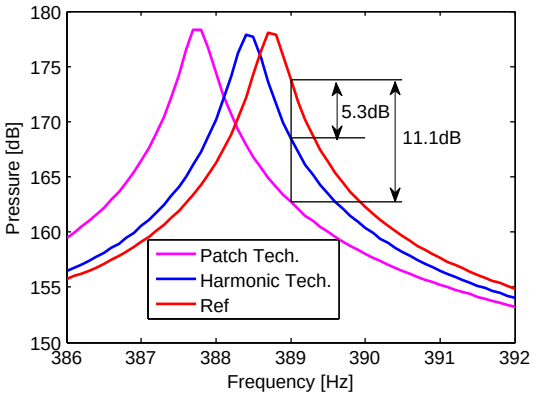

Fig. 5.11 Pressure response $(1.3, 0.35, 0.25)m$ between 386Hz and 392Hz.

5.4 Discussion: Source Limitation

In the previous examples, we have examined specific source configuration, point sources and vibrating boxes. It has been found that the Patch technique is likely be a simpler procedure for sound prediction. Now we investigate source limitations on the source, i.e. source configurations where the characterisation via the Patch tech becomes problematic.

5.4.1 On the Vibrating Box

A. Source configuration

We first perform the investigation on the vibrating box model in Fig. 5.6 by changing the source configuration. For the vibrating box of six faces, pressure amplitude P_r at a given

point in the receiver space is a linear combination of the pressure response $P_{r,i}$ due to the i^{th} face with unit normal velocity.

$$P_r = \sum_{i=1}^{6} \alpha_i P_{r,i} \tag{5.7}$$

where the coefficient α_i can be interpreted as the vibrating velocity of the i^{th} face. Note that a positive α_i indicates that the direction of the velocity is towards inside of the source space. The volume velocity of the vibrating box is simply the sum of volume velocities on each face,

$$Q_{vb} = \sum_{i=1}^{6} \alpha_i S_i \tag{5.8}$$

here S_i is the area of the i^{th} face. For the vibrating box, the position and area of its six faces are summarized in Table. 5.1.

For each vibrating velocity α_i, we select one of 4 amplitudes ($|\alpha_i| = 0,1,2,3\ m/s$) and 4 phases ($\angle\alpha_i = 0, \frac{\pi}{2}, \pi, \frac{3}{2}\pi$). Hence the number of different vibrating combinations, i.e., sources of different excitations, is 4,826,809 ($= (1+4\times 3)^6$).

Table 5.1 Area and position of the six faces of the vibrating box

Face	1	2	3	4	5	6
Area(m^2)	0.039	0.039	0.026	0.026	0.06	0.06
Position	$x = 0.7m$	$x = 0.9m$	$y = 0.4m$	$y = 0.7m$	$z = 0.5m$	$z = 0.63m$

B. Error analysis

The frequency shift of resonant frequencies is inherent to the Patch technique. The shift can produce larger level differences between the responses obtained by interface coupling and reference values. The way to remove the local effect of the shift is to use *band-averaging*. Here one should be careful because not all quantities can be band-averaged. Only the quadratic ones can, like the RMS square value (simple RMS cannot). Usual band-averaging is octave or 1/3 octave. These types of analyses are standardised and a lot used in industry. However, the octave-type analysis is not well adapted to the features of room acoustics, since the number of resonance frequencies D_{f_c} in a frequency band Δf centred at f_c in a room increases with frequency square:

$$D_{f_c} \approx \frac{4\pi f_c^2 U}{c^3} \Delta f \tag{5.9}$$

where U – room volume, c – speed of sound. For example, a room of $50m^3$ will statistically have about 3 resonances in a band of $\Delta f = 20$Hz centred at f_c=100Hz, but in same band centred at 500Hz there will be about 78 resonances (5^2 times more). A resonance density increasing with frequency does not fit well the band width which also increases with frequency. Reducing band width with frequency would be best from the computational point of view, but would go against the acoustics of human ear. Thus where room acoustic is concerned the type of averaging using constant band width would be probably the most appropriate.

The RMS square value in a frequency band centred at f_c is computed by [84]:

$$P_{RMS}^2 = \frac{1}{2}\int_{f_c-\frac{B}{2}}^{f_c+\frac{B}{2}} |P_r|^2 df \tag{5.10}$$

Eq. (5.10) allows us to obtain the reference and predicted RMS square values, P_{RMS}^2 and $\widetilde{P}_{RMS}^2$, respectively. Thus the RMS error ε_p of the predicted and reference results is characterised by the following equation:

$$\varepsilon_p = 20 \times \log_{10}\left(\sqrt{\frac{\widetilde{P}_{RMS}^2}{P_{RMS}^2}}\right) \ ([dB]) \tag{5.11}$$

C. Frequency resolution

Linked to band averaging comes the frequency resolution. To carry out the error analysis correctly the response peaks should not be missed, because low frequency resolution may give poor results. The lower the damping, the higher the gradient of the frequency response of the room and thus the finer the resolution needed.

A direct way is applying a high frequency resolution to the whole frequency band in our analysis but it demands high computation cost, so we only increase the frequency resolution around the resonance peaks. We found that the Patch technique causes various frequency shifts at these peaks with respect to the predicted results. Therefore around each exact resonance peak, we seek a frequency range to cover the exact peak and the frequency shift so that the predicted resonance peak will also appear in this range. According to the exact resonance peaks and frequency shifts shown in Fig. 5.7, we list in Table. 5.2 the frequency ranges that needs finer resolution. Specially, the frequency resolution in these ranges is set to 0.05Hz, otherwise it is 1Hz.

Table 5.2 Frequency ranges of resolution 0.05Hz

[84,86], [141,143], [166,168], [170,172], [191,194], [221,224], [241,244], [256,259], [280,289], [294,297], [299,301], [308,312], [333,342], [349,357], [371,380], [384,391], [409,414], [421,426], [431,440]

D. Results

For all the 4,826,809 cases of the vibrating box, we compute the RMS error of the predicted pressure at the position of $(0.3, 0.2, 0.15)m$ by Eq. (5.11). All the cases are divided into 5 error groups and ranged from 8 frequency error bands with respect to the frequency. The numbers of cases in different groups and bands are listed in Table. 5.3. We observe that most of the cases are of an error smaller than 1dB, indicating that the Patch technique works well most of the times.

However, it is strange that there are still 64 (=4+12+20+20+8) cases of an error larger than 3dB, especially at low frequencies rather than at high frequencies. We list four ill cases as examples: the velocities on the six faces of the vibrating box in Table. 5.4, the predicted and reference pressure responses in Fig. 5.12. When we check these 64 cases and their pressure responses, we find that they have a common feature: all these source excitations, i.e., the volume velocities, are extremely low. We guess that maybe the Patch technique could not give acceptable sound prediction at low frequencies for some sound sources of extremely low volume velocity. The next section will confirm this discover using a typical zero volume velocity source – the dipole source. Nevertheless, as the industrial products mainly generate sound in the middle frequency band, we endorse the Patch technique to industrial applications.

Table 5.3 Statistics of cases with different error scales

f(Hz)	Error band(dB)				
	(0,1]	(1,2]	(2,3]	(3,4]	(4,5]
	Cases	Cases	Cases	Cases	Cases
1-55	4826805	0	0	4	0
55-110	4826557	188	32	12	20
110-165	4826493	248	36	20	8
165-220	4826809	0	0	0	0
220-275	4826793	4	12	0	0
275-330	4826785	20	4	0	0
330-385	4826809	0	0	0	0
385-440	4070329	749420	7060	0	0

Table 5.4 Velocity distribution on the vibrating box of four ill examples

Case	1	2	3	4	5	6	Q_{vb}
	α_1	α_2	α_3	α_4	α_5	α_6	(m^3/s)
1	3	3	-3	1	0	-3	0.002
2	3j	3j	-2j	0	-j	-2j	0.002j
3	3j	3j	-j	-j	-j	-2j	0.002j
4	2j	2j	-j	2j	-j	-2j	0.002j

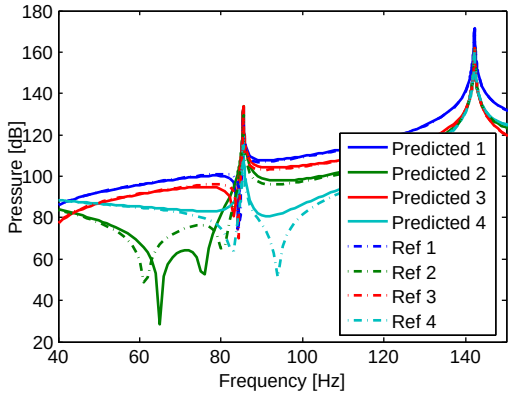

Fig. 5.12 Pressure responses of four ill examples

5.4.2 Dipole excitation

To confirm the discovery of the problem on some sound sources of low volume velocity, we study the characterisation of a typical zero volume velocity source – the dipole source. A dipole is placed in a rectangular room and the characterisation is carried out by analytical modelling.

A. Analytical modelling

A dipole at a point $\mathbf{r}_e = (x_e, y_e, z_e)$ radiates sound in a rectangular room of size $a \times b \times h$. The dipole consists of two point sources with strength Q_e opposite in phase and separated by an infinitesimal distance d. The pressure response at the point $\mathbf{r} = (x, y, z)$ due to the dipole can be expressed by the sum of the pressure responses due to the two point sources, that is

$$P(\mathbf{r}) = \lim_{d \to 0} [P_+(\mathbf{r}) - P_-(\mathbf{r})] \tag{5.12}$$

and the dipole strength is $D_d = Q_e d$. If this dipole of strength D_d is in the direction shown in Fig. 5.13. The strength in x, y, z directions is

$$\begin{aligned} D_{dx} &= D_d sin\psi cos\theta \\ D_{dy} &= D_d sin\psi sin\theta \\ D_{dz} &= D_d cos\psi \end{aligned} \tag{5.13}$$

where ψ and θ denote the angles shown in the figure. Then the pressure response $P(\mathbf{r})$ can be decomposed as the sum of three components,

$$P(\mathbf{r}) = P(\mathbf{r})|_x + P(\mathbf{r})|_y + P(\mathbf{r})|_z \tag{5.14}$$

where $P(\mathbf{r})|_x$ represents the pressure response due to the dipole of strength D_{dx} in x direction, and so on. Substituting Eq. (4.14) into Eq. (5.12) yields

$$P(\mathbf{r})|_x = jD_{dx}\frac{\omega\rho_0 c^2}{U}\sum_n^N \frac{\phi_n(\mathbf{r})}{\omega_n^2 - \omega^2 + 2j\varepsilon\omega}\left[\frac{\partial\phi_n(\mathbf{r}_e)}{\partial x_e}\right] \tag{5.15a}$$

$$P(\mathbf{r})|_y = jD_{dy}\frac{\omega\rho_0 c^2}{U}\sum_n^N \frac{\phi_n(\mathbf{r})}{\omega_n^2 - \omega^2 + 2j\varepsilon\omega}\left[\frac{\partial\phi_n(\mathbf{r}_e)}{\partial y_e}\right] \tag{5.15b}$$

$$P(\mathbf{r})|_z = jD_{dz}\frac{\omega\rho_0 c^2}{U}\sum_n^N \frac{\phi_n(\mathbf{r})}{\omega_n^2 - \omega^2 + 2j\varepsilon\omega}\left[\frac{\partial\phi_n(\mathbf{r}_e)}{\partial z_e}\right] \tag{5.15c}$$

The pressure response averaged across the patch ΔS centered at $\mathbf{r}$ due to the dipole is

$$< P(\mathbf{r}) >_{\Delta S} = < P(\mathbf{r}) >_{\Delta S}|_x + < P(\mathbf{r}) >_{\Delta S}|_y + < P(\mathbf{r}) >_{\Delta S}|_z \tag{5.16}$$

Replacing $\phi_n(\mathbf{r})$ in Eq. (5.15) by $\frac{1}{\Delta S}\int_{\Delta S}\phi_n(\mathbf{r})dS$ yields $< P(\mathbf{r}) >_{\Delta S}|_x, < P(\mathbf{r}) >_{\Delta S}|_y, < P(\mathbf{r}) >_{\Delta S}|_z$. The formula derivation is shown in Appendix C.2.

B. Characterisation results

Now we present the computation for the dipole model. In a rectangular room of $2m \times 1m \times 1.2m$, three dipoles with strength $D_d = 1m^4/s$ located in three different positions with different directions. Information about the three dipoles are summarized in Table. 5.5. We create an interface surface at $x = 0.7m$ and analyse the sound radiation in the frequency band [1,500]Hz. As usual, the targeted patch size is kept at $\frac{1}{3}\lambda_{min}$, so the interface surface is divided into 5×6 patches. Results of predicted and reference responses at three different points in the receiver space are shown in Fig. 5.14. We can see that at low frequencies, even

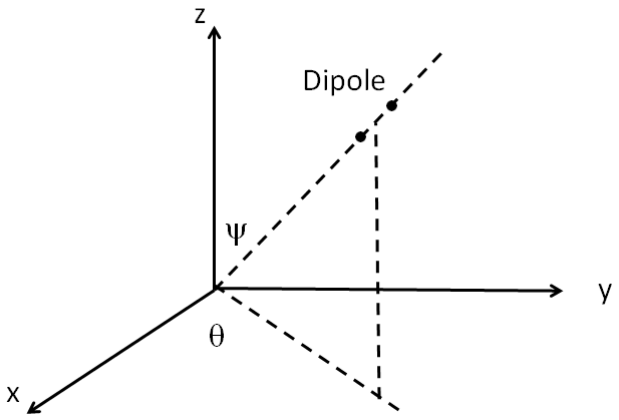

Fig. 5.13 Position of a dipole

though the patch size is fairly reasonable, the predicted and reference responses do not match well. Thus we conclude that one should be careful if the source has extremely low volume velocity, because the Patch technique will produce large prediction error at low frequencies.

Table 5.5 Information of three dipoles

Dipole	Position	Direction (ψ, θ)	Receiving point
1	(0.2,0.38,0.55)	$(\frac{\pi}{3}, \frac{\pi}{4})$	(1.816,0.6058,0.7072)
2	(0.1,0.43,0.78)	$(\frac{4\pi}{6}, 0)$	(0.882,0.704,1.13)
3	(0.65,0.24,0.18)	$(0, \frac{2\pi}{3})$	(0.73,0.45,0.38)

5.5 Conclusions

This chapter introduced patch concept to identify source and receiver descriptors based on the Patch technique. The characterisation of point sources in a rectangular room was carried out at first, on one hand to demonstrate the feasibility of sound prediction by source characterisation using the Patch technique, on the other hand to display the influence of patch size on the prediction. Considering practical measurements, we also studied patch averaging to figure out the appropriate spacing between two adjacent measuring points. We have found that the patch size should be no larger than $\lambda/3$ and the point spacing should be no larger than $\lambda/6$, sound radiation of a vibrating box in rectangular and irregular rooms were conducted, in order to justify the effectiveness of the Patch technique on complex cases. Thirdly, the Patch and Harmonic techniques were compared from the computational and experimental aspects. We concluded that the Patch technique should be more suitable for experimental validation because of its efficiency and simplicity of measurements. Finally,

the limitation on the source due to the Patch technique was investigated. It has been found that the characterisation using the Patch technique may not give good predictions at low frequencies for some sound source of extremely small volume velocity. Nevertheless, as the industrial products mainly generate sound in the middle frequency band, we believe that the Patch technique is useful for industrial applications.

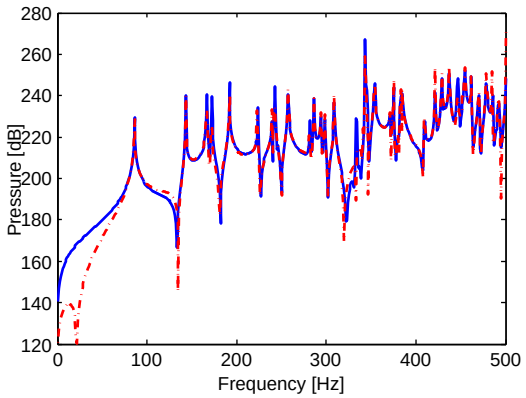

(a) Dipole 1

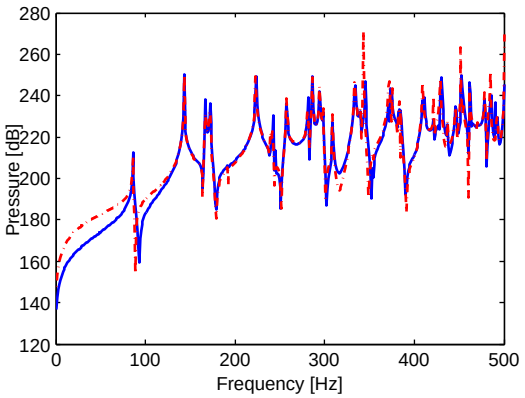

(b) Dipole 2

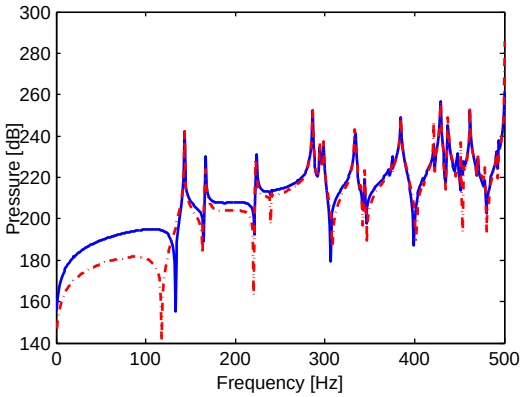

(c) Dipole 3

Fig. 5.14 Pressure response due to dipoles. Solid line: predicted, dashed line: reference.

Chapter 6

Experimental Validation of Source Characterisation Approach

In the previous three chapters, we have studied the surface coupling approach and introduced the Harmonic and Patch techniques to identify the source and receiver descriptors. We demonstrated that the Patch technique should be more suitable for practical implementation than the Harmonic technique. This chapter will carry out experimental validation of source characterisation using the Patch technique.

Since the blocked pressure as well as source and receiver impedances are defined across a virtual interface surface, the identification of these descriptors has to be carried out at this surface. Both the blocked pressure identification and impedance identification require this surface to be immobile. This means that the measurements of descriptors have to be done by installing a stiff cover (shield) around the physical source, the inner surface of which coincides with the interface surface.

In the case of blocked pressure measurement, the surface should incorporate microphones. In the case of impedance measurement, the surface should accommodate a vibrating patch and simultaneously allow sound pressure measurement across it. The challenges regarding the rigid surface are:

1. How to design and manufacture the surface? A good coupling surface should satisfy two conditions: (1) it should be rigid enough to prevent creating a secondary sound field comparable to the measured field; (2) it should allow use in both the source and receiver spaces.

2. How to create a driving patch on the rigid surface? The key problem is to apply an uniform velocity excitation to a patch and measure it simultaneously.

Bearing these two problems in mind, the two descriptors – blocked pressure and source impedance – characterising a vibrating box will be identified by measurement and then the sound pressure at several receiving points will be predicted to validate the characterisation using the Patch technique.

6.1 Measurement Set-up

Fig. 6.1(a) shows a global view of our system. It consists of two box-like cavities coupled via the opening. Two cross sectional views of the system are shown in Fig. 6.1 (b) and (d). A vibrating box – the audio speaker in Fig. 6.1 (c) – is used as a physical source. Together with the lower cavity (Cavity A) it represents the source space. The upper cavity representing the receiver space (Cavity C) has an irregular inner shape.

The parallelepipedic Cavity A is of length $0.5m$, width $0.6m$ and height $0.7m$. The audio speaker is of length $0.24m$, width $0.15m$, height $0.4m$, and is located at the corner of Cavity A. The inner surfaces of the lower cavity are hard while those of the upper cavity are covered by absorbing material.

As shown in Fig. 6.1 (b), a rectangular PVC plate (Plate B) was produced to insert between the two cavities. The Plate B is of width $0.53m$, length $0.63m$, thickness $0.04m$ and the square opening on it is of size $0.34m$. In particular, the Plate B can be separated into two parts: a bigger cover frame and a smaller circular frame as shown in Figs. 6.2 (a) and (b) respectively. A groove of diameter $0.5m$ and depth $0.02m$ was made on the cover frame to exactly accommodate the circular frame. The smaller circular frame is of diameter $0.5m$ and thickness $0.02m$, the square opening on it is of size $0.34m$. Such a specific design of Plate B is for the characterisation of the physical source in the source space, which will be explained in the incoming section.

A recorded diesel engine noise or white noise signals will be generated by a computer, amplified by an amplifier and played by the audio speaker. The sound volume of the speaker is kept unchanged during various measurements. Microphones in the irregular Cavity C are used to measure pressure responses. These responses will serve to compare the noise levels measured directly when the two cavities are coupled and indirectly using the prediction based on source and receiver descriptors obtained through separate measurements.

Following the principle of source characterisation via surface coupling, we create the interface surface S at the horizontal center of Plate B, as shown in Fig. 6.1(b). The interface surface divides the entire acoustical space into two spaces: the lower source space and the upper receiver space. According to the Patch concept, the interface surface is meshed into several patches.

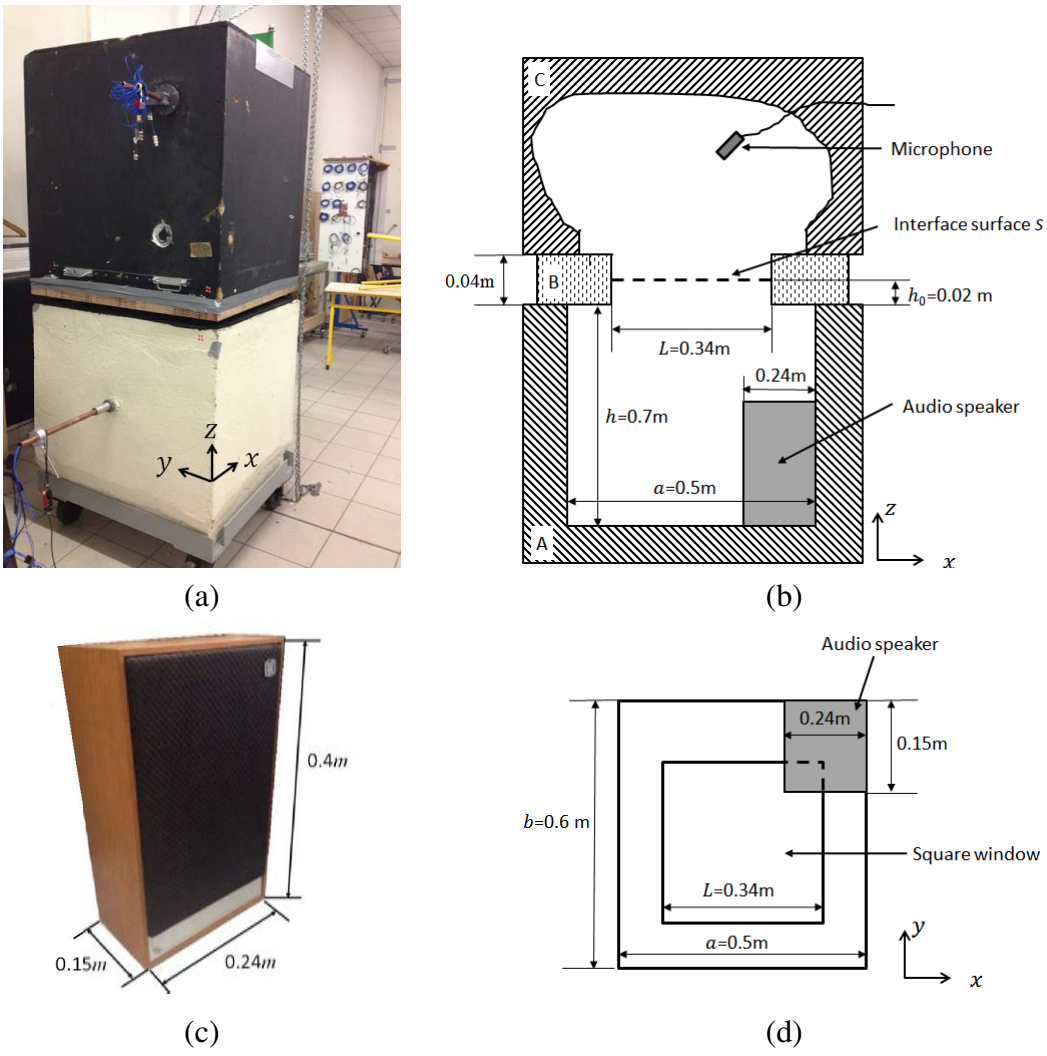

Fig. 6.1 Global system of the 3-dimensional experiment: (a) acoustical receiver, (b) cross sectional view, (c) audio speaker, (d) bottom-up view

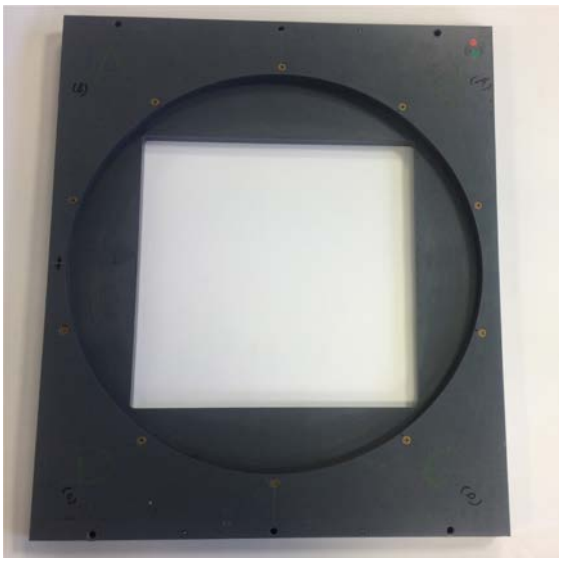

(a) Cover frame

(b) Circular frame

Fig. 6.2 Plate B can be separated into two parts: (a) a cover frame and (b) a circular frame.

In practice, our measuring work consists of the following steps:

- **Measurement of reference pressure response in the entire space**

1. In the global system, switch on the physical source (audio speaker) and record the pressure responses at the receiving points of interest in the receiver space, those are the reference pressures.

- **Characterisation of source**

2. Install the rigid cover plate to block the source space, i.e., Cavity A.
3. Switch on the physical source and measure the blocked pressure P_b across the plate.
4. Switch off the physical source. Apply a normal velocity to one of the patches which thus becomes the driving patch; the remaining patches are receiving patches. Measure the velocity of the driving patch and pressure responses on the receiving patches including that on the driving patch itself. Repeat the measurement for all patches as driving patches. And then calculate coupling impedances between driving and receiving patches in the source space, that is the source impedance matrix Z_s.

- **Sound prediction**

5. Move the rigid cover plate to block the receiver space interface, i.e., Cavity C. Like the measurement procedure of source impedance matrix Z_s, compute the receiver impedance Z_r, i.e., coupling impedances between the driving and receiving patches in the receiver space.

6. For the receiving points of interest in the receiver space, measure the coupling impedance Z_{rp} between the interface surface and these points.

7. With the descriptors P_b, Z_s, Z_r, Z_{rp} computed, predict the pressure responses at the receiving points and compare them with the reference pressures.

6.2 Design of Cover Interface Surface

From the above outline of measurement, one can see that the rigid cover plate plays a major role in our experiment. First of all, in order to realize the rigid surface, a circular revolving plate, see Fig. 6.3 (b) and (d), can be inserted into the cover frame (Fig. 6.2(a)) of Plate B, so that the source space (Cavity A) or the receiver space (Cavity B) are blocked. The groove of the cover frame is of the thickness 0.02m, i.e., half of the Plate B (0.04m), so that the cover frame and the revolving plate together can be fitted to either the lower cavity or to the upper cavity for keeping the interface surface at the same position.

The revolving plate is of diameter $0.5m$ and thickness $0.02m$, as shown in Fig. 6.4 (a). Only the $0.34m \times 0.34m$ square area will be open to the inner space of the two cavities (see Fig. 6.3 (b) and (d)) while the bordering area outside the square area will stay shielded by the cover frame. *This square area (surface) is the interface surface we need.*

In this area, we carve a square open window of size $0.17m \times 0.17m$, i.e., one quadrant of the whole area (see Fig. 6.4 (a)). When we measure the blocked pressure due to the operating source, we put a small square PVC plate (the fill-in plate without driver in Fig. 6.4 (b)) to fill in the window. When we measure the surface impedances, i.e., measure velocity and pressure responses on the driving and receiving patches, we alternatively use another small square plate with integrated piezoceramic speaker (the driver plate with driver in Fig. 6.4 (c)) to provide the normal velocity. The procedure of measuring blocked pressure and source or receiver impedance will be given in detail in the incoming sections.

The entire interface surface area is divided into 16 ($= 4 \times 4$) patches and the small square plate contains 4 ($= 2 \times 2$) patches. The holes on these patches represent discrete measuring points where microphones are fitted to estimate the patch pressure. Each patch has two measuring points. Thereby for the entire interface surface, 32 ($= 16 \times 2$) measuring points are required. However, concerning the symmetry of the large and small squares, by making

(a)

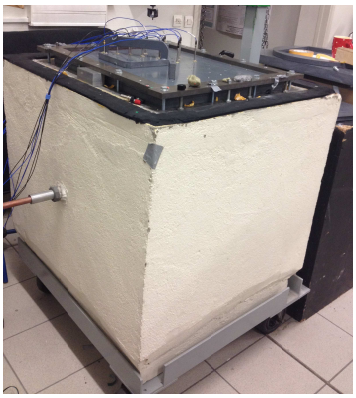

(c)

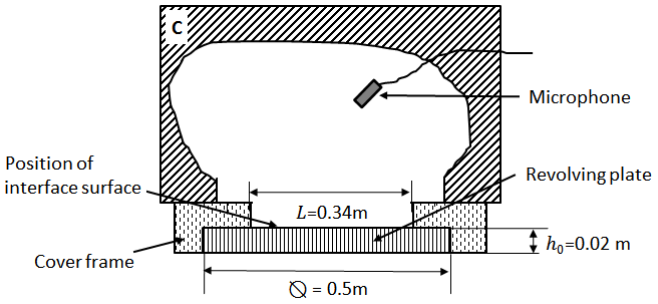

(b)

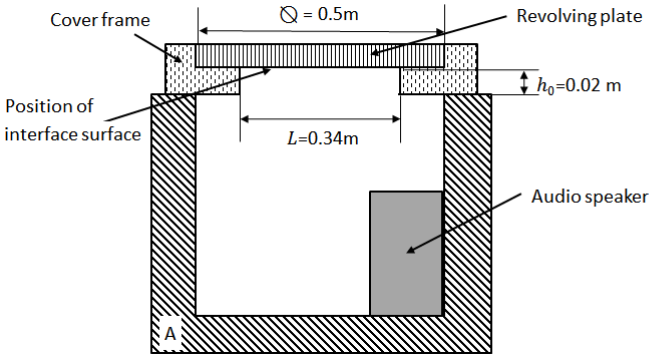

(d)

Fig. 6.3 Top: Receiver space, bottom: Source space.

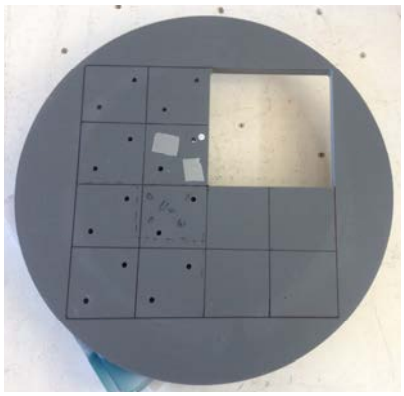

(a)

(b)

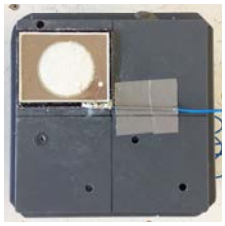

(c)

Fig. 6.4 (a) Revolving plate. The inscribed square area of the round plate acts as the interface surface; (b) driver plate with driver; (c) fill-in plate without driver.

the large round plate and the small square plate revolving, the number of microphones can be reduced to 16.

6.3 Coupling Impedance between Patches

According to the Patch technique and the definition of surface impedance, we apply a normal velocity excitation to one of the patches and measure the pressure responses averaged across this and other patches. The ratios between the pressure response amplitudes and the velocity amplitudes compose one column of the surface impedance matrix. The problem is how to generate a velocity excitation to a patch and measure the mean velocity of this patch.

6.3.1 Design of Driving Patch

Designing a driving patch is the first step to carry out the measurement of coupling impedance between patches.

Lindberg and Pavić [85] introduced the compression chamber method and the blocked pipe method to measure the volume velocity of a back-enclosed driver with no assumptions about the shape or the vibration distribution of the driver's diaphragm. The authors defined the coupling impedance Z^q as the ratio between the pressure response P at a receiving point and the volume velocity Q of a driver,

$$Z^q = \frac{P}{Q} \tag{6.1}$$

where $[\cdot]^q$ indicates a term related to the volume velocity, as distinguished from the usually used velocity.

For the driver with an enclosed back cavity, a reference microphone is fixed inside its back cavity, as shown in Fig. 6.5. Since the volume velocity Q is unknown, we rewrite the above equation with respect to the reference microphone as

$$Z^q = \frac{P}{Q} = \frac{P(\mathbf{i})}{Q}\frac{P}{P(\mathbf{i})} = \Psi^q \Xi^q \tag{6.2}$$

where $\mathbf{i}$ is the position of the reference microphone and $P(\mathbf{i})$ is the pressure response inside the back cavity. Ψ^q is called Source function while Ξ^q is called Space function. Specifically, the space function Ξ^q can be simply obtained by measuring the two pressures P and $P(\mathbf{i})$. For the source function $\Psi^q = \frac{P(\mathbf{i})}{Q}$, if the back cavity is rigid and its volume is small, the sound pressure $P(\mathbf{i})$ is effectively proportional to the volume displacement $\frac{Q}{j\omega}$ when the diaphragm

(see Fig. 6.5) compresses and expands the interior air, i.e., $P(\mathbf{i}) \propto \frac{Q}{j\omega}$. In practice, both the compression chamber method and the blocked pipe method in [85] can be employed to identify the source function Ψ^q, and then the coupling impedance Z^q and the volume velocity Q can be known.

The compression chamber method requires fixing a compression chamber in front of the diaphragm of the driver, as shown in Fig. 6.5, and measuring the pressure $P(\mathbf{e})$ inside the compression chamber by another microphone, i.e., the measurement microphone in Fig. 6.5. With the two measured pressures $P(\mathbf{i})$, $P(\mathbf{e})$, the source function is estimated by

$$\Psi^q = \frac{\rho_0 c^2}{j\omega U_0} \frac{P(\mathbf{i})}{P(\mathbf{e})} \tag{6.3}$$

here U_0 is the volume of the compression chamber.

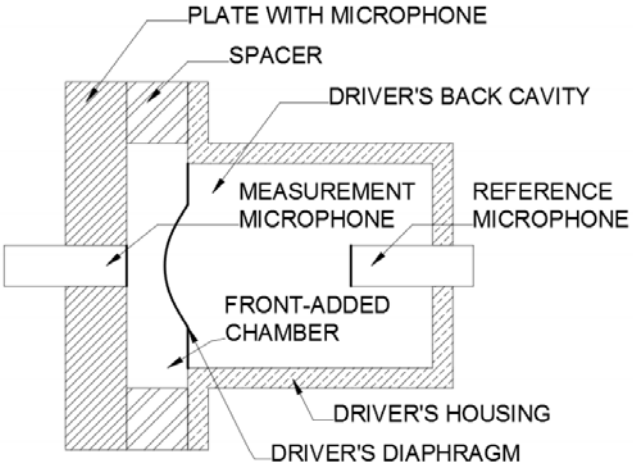

Fig. 6.5 Schematic view of measuring the source function using a compression chamber [85].

Inspired by the idea of Lindberg and Pavić [85], we use a specific driver as a driving patch, as shown in Fig. 6.6 (b): Sonitron piezoceramic driver (SPS-68-T00)[1] of size $0.835m \times 0.68m$ is fixed on the plate using adhesive tape and the diaphragm – the metal area – is of $0.753m \times 0.58m$. A rectangular cavity of the size $0.753m \times 0.58m \times 0.0052m$ is behind the diaphragm, as shown in Fig. 6.6 (a). *The back cavity and the operating piezoceramic speaker together compose a driving patch.*

In our experiment, we use the compression chamber method to identify the source function of the driving patch and carry out the measurement of surface impedances. However, we also demonstrate the way to identify source function by the blocked pipe method in Appendix D.

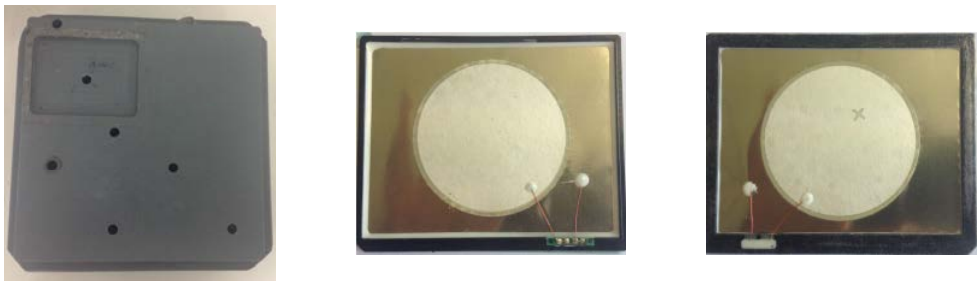

(a) (b) (c)

Fig. 6.6 Driving patch comprising a rectangular cavity and a Sonitron piezoceramic speaker (SPS-68-T00): (a) back cavity, (b) front of the speaker, (c) back of the speaker.

6.3.2 Measurement on Patches

The coupling impedance between a driving patch centered at $\mathbf{r}_s$ and a receiving patch centered at $\mathbf{r}$ is

$$Z(\mathbf{r},\mathbf{r}_s) = \frac{< P(\mathbf{r}) >_{\Delta S}}{< V(\mathbf{r}_s) >_{\Delta S}} \tag{6.4}$$

With the volume velocity of the driving patch $Q(\mathbf{r}_s) = \Delta S < V(\mathbf{r}_s) >_{\Delta S}$, the equation is rewritten as

$$Z^q(\mathbf{r},\mathbf{r}_s) = \frac{Z(\mathbf{r},\mathbf{r}_s)}{\Delta S} = \frac{< P(\mathbf{r}) >_{\Delta S}}{Q(\mathbf{r}_s)} \tag{6.5}$$

[1] http://www.sonitron.be/useruploads/files/DatasheetSPS-29-41-53-68-T00Series.pdf

According to the definitions in Eq. (6.2), the corresponding source and space functions of the driving patch read

$$\Psi^q = \frac{P(\mathbf{i})}{Q(\mathbf{r}_s)}, \quad \Xi^q = \frac{< P(\mathbf{r}) >_{\Delta S}}{P(\mathbf{i})} \tag{6.6}$$

Briefly, we made a back rigid cavity and a compression chamber for a piezoceramic speaker. The piezoceramic speaker and the back rigid cavity together act as a driving patch. On one hand, with the compression chamber method, the source function of the driving patch can be estimated. On the other hand, by operating a driving patch and measuring the pressures on all the patches, the space functions between patches are obtained. Finally, the impedances Z^q are simply the products of the identified source and space functions.

On the driving patch shown in Fig. 6.6, according to the compression chamber method, we further mount a small rigid chamber made of PVC material in front of the diaphragm using silicon rubber, as shown in Fig. 6.7. The compression chamber is of the size $0.753m \times 0.58m \times 0.0054m$, With one microphone in the back cavity and one in the compression chamber in Fig. 6.7 (a), the pressures $P(\mathbf{i})$ and $P(\mathbf{e})$ are measured and the source function is computed by Eq. (6.3). Fig. 6.8 plots the source function in our measurement: Fig. 6.8(b) is the imaginary part of source function, the frequency behaviour of which is dominated by a compliance law as expected, i.e.$\Psi^q = \frac{P(\mathbf{i})}{Q} \propto \frac{1}{j\omega}$. Fig. 6.8(a) is the real part of source function, which theoretically should be zero. The non-zero real part may be due to sound leakage caused by the imperfect attachment between the piezoceramic speaker and the compression chamber. However, the real part can be ignored since it is about 40dB lower than the imaginary part.

As we have mentioned above, to obtain the space function Ξ^q, we use microphones to estimate the pressure responses $< P(\mathbf{r}) >_{\Delta S}$ on a driving patch or a receiving patch. The position of microphones on the driving patch and receiving patches is shown in Fig. 6.9. Generally, for a receiving patch, two microphones are placed on the centers of two opposite quadrants, as shown in the right lower part of Fig. 6.9; for a driving patch in the left upper part, the microphones are moved away a little further to avoid the mounted speaker. For either a driving patch or a receiving patch, the pressure is the mean value of the pressures measured by the two microphones. Referring to the discussion about the imperfect patch averaging in Section 5.2.1, the spacing between measuring points on a patch should be no larger than $\frac{1}{6}\lambda$, which means to use at least four microphones per patch as illustrated in Fig. 5.5 (b). Due to limited number of microphones, we have used two microphones per patch for the sake of tradeoff between work effect and accuracy. Actually, the experimental result have confirmed that such a setting was reasonable.

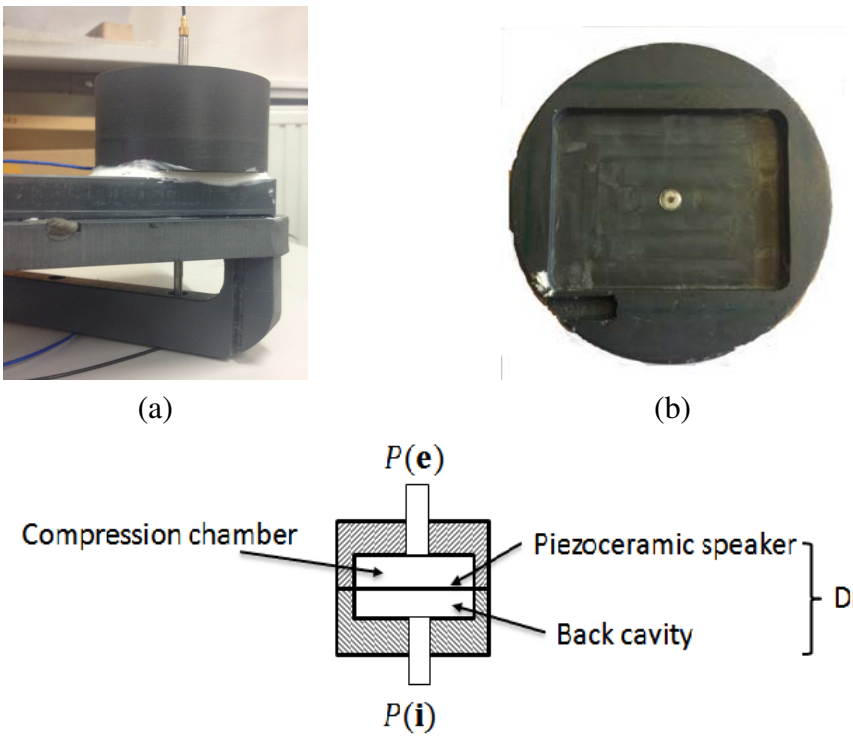

Fig. 6.7 Measurement of source function using the compression chamber method. (a) global view of measurement set-up, (b) compression chamber, (c) cross sectional view of measurement set-up.

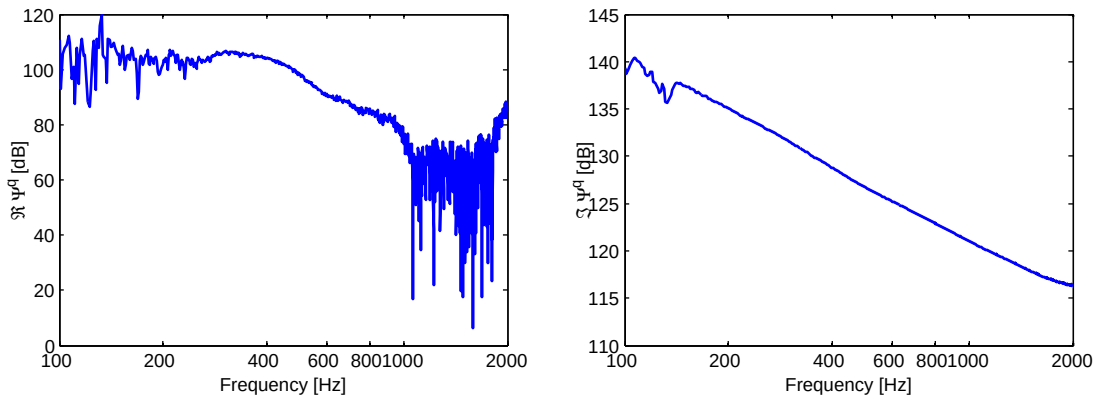

Fig. 6.8 Source function Ψ^q of our driving patch. Left: real part, right: imaginary part.

To check the feasibility of the proposed method for the measurement of coupling impedances, we have first measured coupling impedance between patches in the source space by removing the audio speaker. In this way, a space of simple geometry and a rigid inner surface was obtained, which could be modelled by numerical computation and thus validate our measurement. With no audio speaker in the source space, the space functions Ξ^q between Patch 4 and itself, Patch 8 and Patch 11, are shown in Fig. 6.10. The positions of patches are illustrated in Fig. 6.11. With the obtained source and space functions Ψ^q, Ξ^q, the self impedance of Patch 4 and the coupling impedance between Patch 8 and Patch 11 are calculated by Eq. (6.2) and as the solid lines shown in Fig. 6.12 and Fig. 6.13.

The numerical model is shown in Fig. 6.11. For the numerical computation, the sound speed is $343 m/s$, the fluid density is $1.21 kg/m^3$ and the damping factor of this numerical model is 5×10^{-4}. The self impedance of Patch 4 and the coupling impedance between Patch 8 and Patch 11 obtained by the numerical computation are shown by the dashed lines in Fig. 6.12 and Fig. 6.13. Comparing the measured and computed results, we can see that the general tendency of the measured coupling impedance well matches the computed reference except at high frequencies. We find that the amplitudes at resonance frequencies have a noticeable discrepancy, which may be caused by the underestimated damping factor of the numerical model.

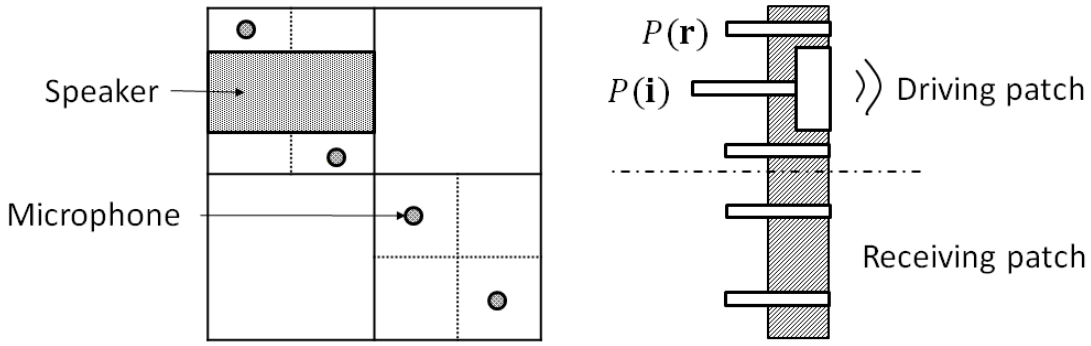

Fig. 6.9 Measurement of space function.

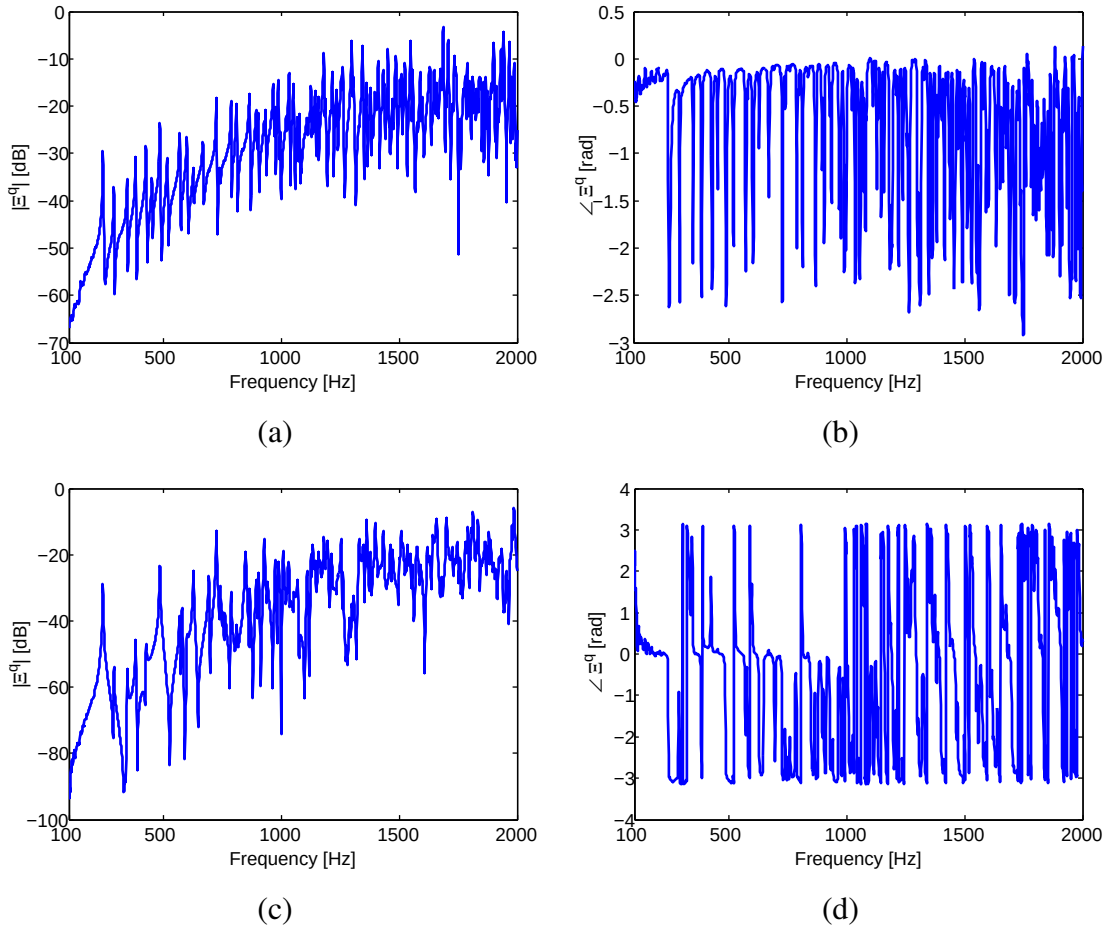

Fig. 6.10 Space functions Ξ^q between patches. Top: between Patch 4 and itself, bottom: between Patch 8 and Patch 11. Left: amplitude, right: phase.

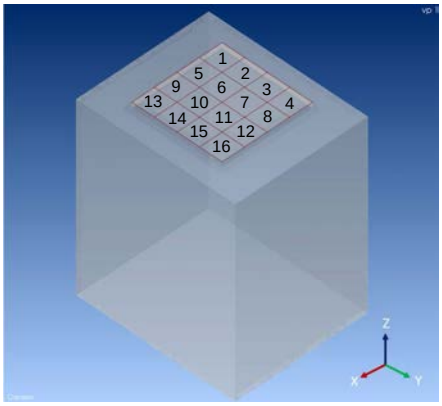

Fig. 6.11 Numerical model of source space without audio speaker.

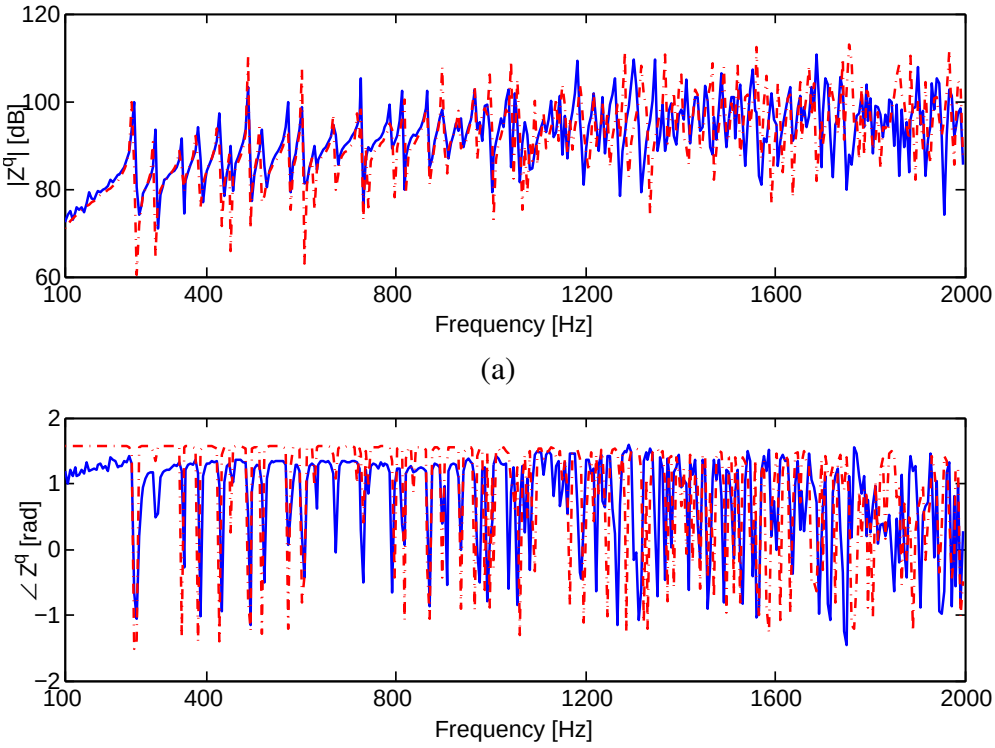

Fig. 6.12 Self impedance Z^q of Patch 4. Top: amplitude, ref $kg \cdot m^{-4} \cdot s^{-1}$, bottom: phase. Solid lines: measured results, dashed lines: computed results.

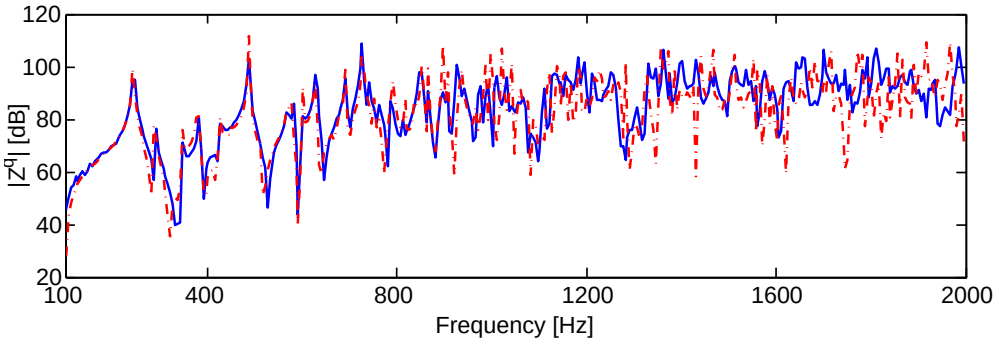

(a)

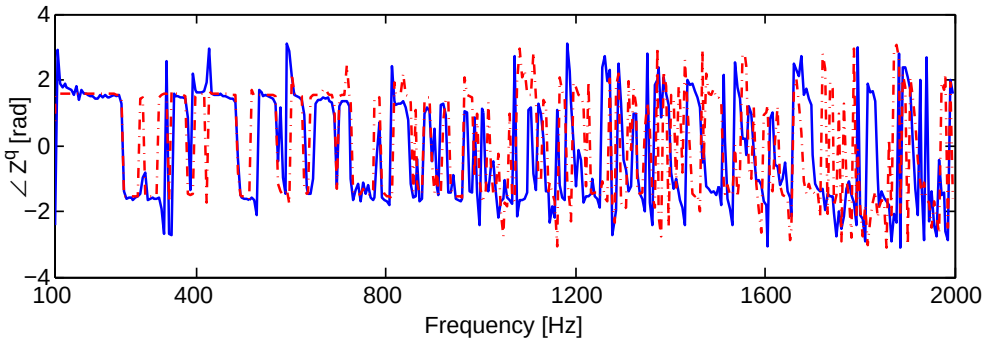

(b)

Fig. 6.13 Coupling impedance Z^q between Patch 8 and Patch 11. Top: amplitude, ref $kg \cdot m^{-4} \cdot s^{-1}$, bottom: phase. Solid lines: measured results, dashed lines: computed results.

6.4 Measurement of Descriptors and Sound Prediction

6.4.1 Source and Receiver Impedances

Using the designed cover surface and driving patch, we now carry out the measurement of source and receiver impedances in the source and receiver spaces, respectively.

The driver plate with driver (Fig. 6.4 (c)) is placed in the square hole of the round plate (Fig. 6.4 (a)). The inscribed square region on the round plate, comprising 16 patches, acts as the interface surface to block the source space (Cavity A) or the receiver space (Cavity C). Fig. 6.14 (a) gives a global view of the interface surface.

Since the round plate and the square plate are revolving, apart from the reference microphone fixed inside the back cavity of the driving patch, we need other 14 microphones more to complete our measurement: 8 on the round plate, 6 on the square plate including 2 on the driving patch itself. At each time, the 14 microphones are planted on 7 patches and the space functions between the driving patch and the corresponding patches are measured, as shown in Fig. 6.14 (b). The holes on the plate without microphones have been filled to ensure rigid boundary condition. Turning the square plate changes the position of the driving patch; turning the round plate changes the positions of driving and receiving regions. By iterative operations, the space functions between all the 16 patches are recorded. With the known source function of our driving patch (see Fig. 6.8 and Eq. (6.2)), we can calculate the coupling impedances between all the patches, i.e., the source impedance measured in the source space and the receiver impedance measured in the receiver space.

Fig. 6.15 – Fig. 6.19 illustrate some examples of the measured impedances. First, we measure the coupling impedances between Patch 12 and Patch 15 in the source space or the receiver space. Moreover, by setting the Patch 12 or the Patch 15 to be the driving patch, we examine the reciprocity principle of the impedance between two patches. Either in the source space (Fig. 6.15) or in the receiver space (Fig. 6.16), we can observe good agreement between the solid lines (driving Patch 12) and the dashed lines (driving Patch 15). It is this reciprocity principle that enables not having to plant microphones on all the 16 patches. Fig. 6.17 and Fig. 6.18 plot the self impedances of Patch 1 in the two spaces, respectively. Fig. 6.19 shows the coupling impedances between Patch 6 with four receiving points of interest in the receiver space. Comparing the identified impedances in the source space and that in the receiver space, we find that the impedances in the receiver space do not show any matched peaks. This is because that the irregular receiver space is covered by absorbing material while the inside walls of the source space are rigid.

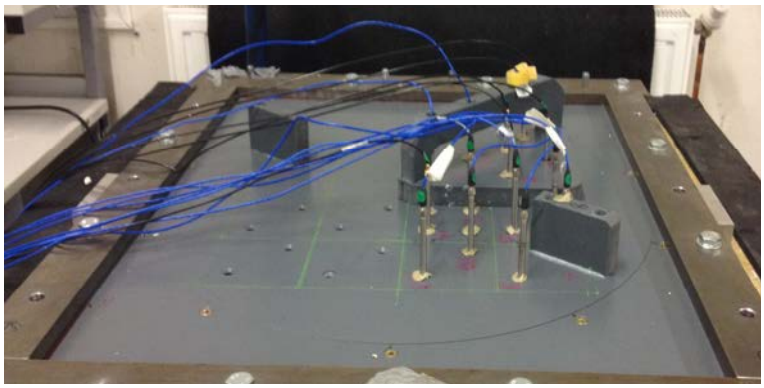

(a)

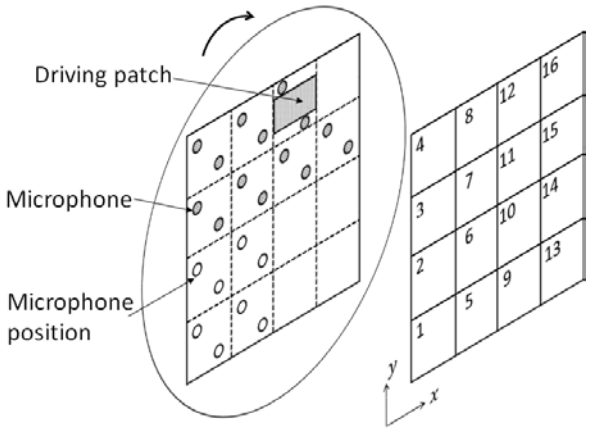

(b)

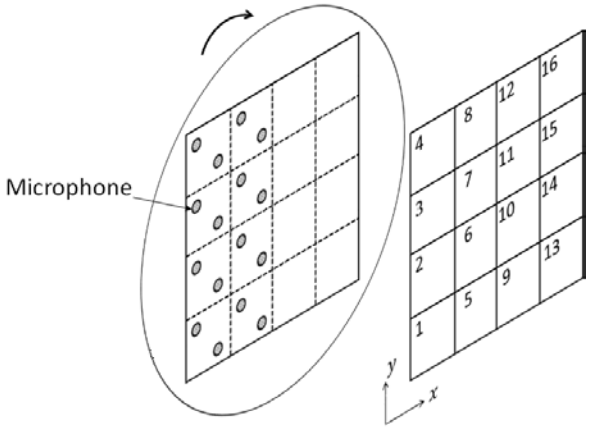

(c)

Fig. 6.14 Interface surface. Top: global view; middle: layout of patches for measuring the impedances; bottom: layout of patches for measuring the blocked pressure.

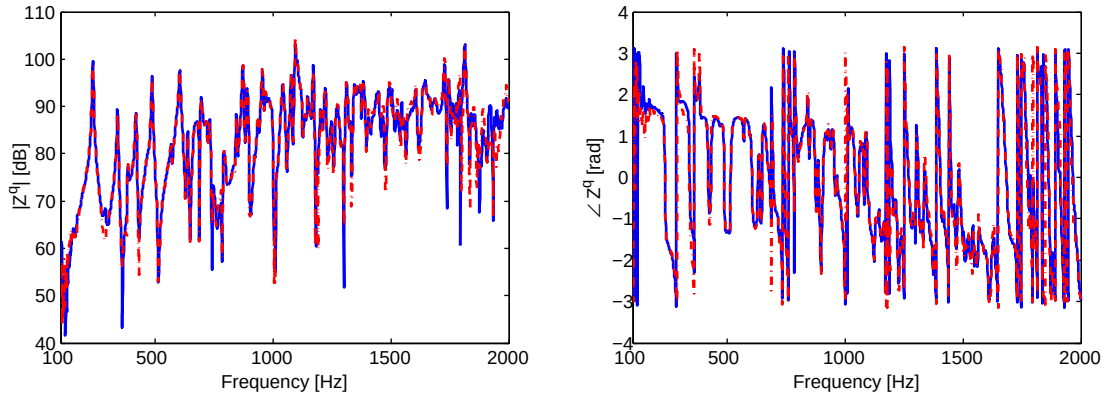

(a) (b)

Fig. 6.15 Coupling impedance Z^q between Patch 12 and Patch 15 in the source space. Left: amplitude, ref, $1kg \cdot m^{-4} \cdot s^{-1}$, right: phase. Solid line: Patch 12 is the driving patch, dashed line: Patch 15 is the driving patch.

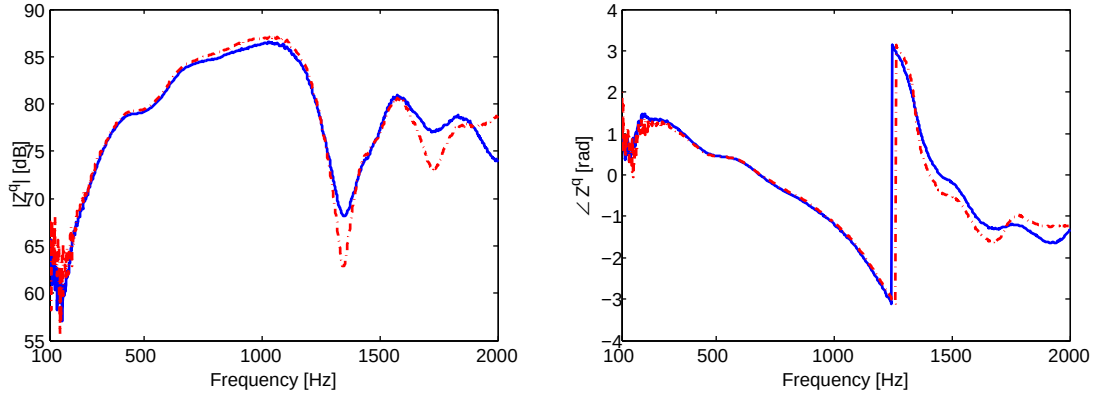

(a) (b)

Fig. 6.16 Coupling impedance Z^q between Patch 12 and Patch 15 in the receiver space. Left: amplitude, ref, $1kg \cdot m^{-4} \cdot s^{-1}$, right: phase. Solid line: Patch 12 is the driving patch, dashed line: Patch 15 is the driving patch.

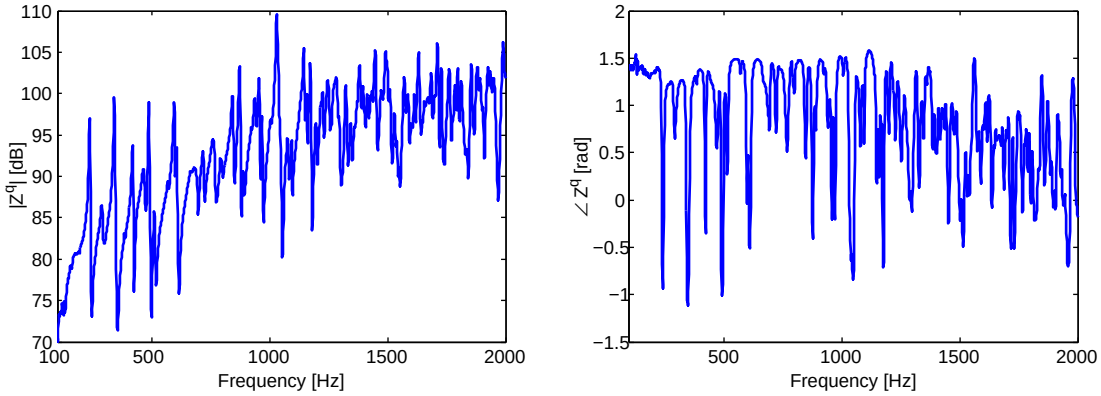

(a) (b)

Fig. 6.17 Self impedance Z^q of Patch 1 in the source space. Left: amplitude, ref, $1kg \cdot m^{-4} \cdot s^{-1}$, right: phase.

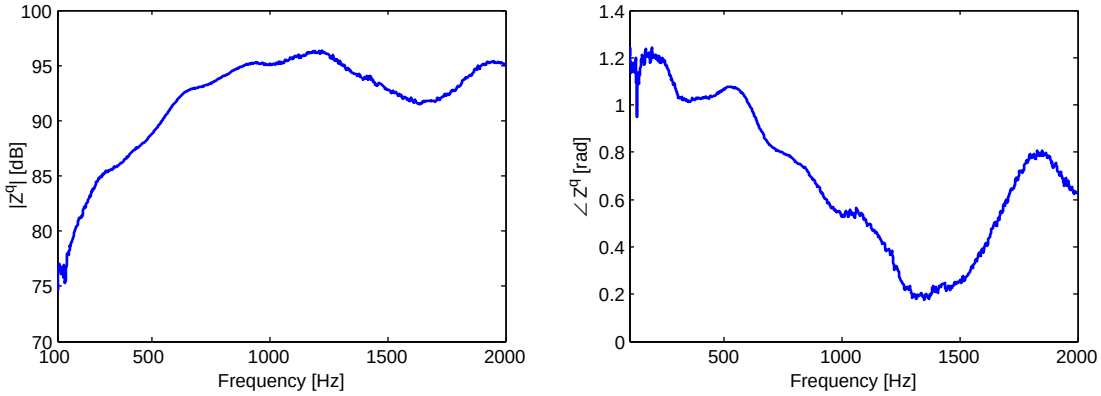

(a) (b)

Fig. 6.18 Self impedance Z^q of Patch 1 in the receiver space. Left: amplitude, ref, $1kg \cdot m^{-4} \cdot s^{-1}$, right: phase.

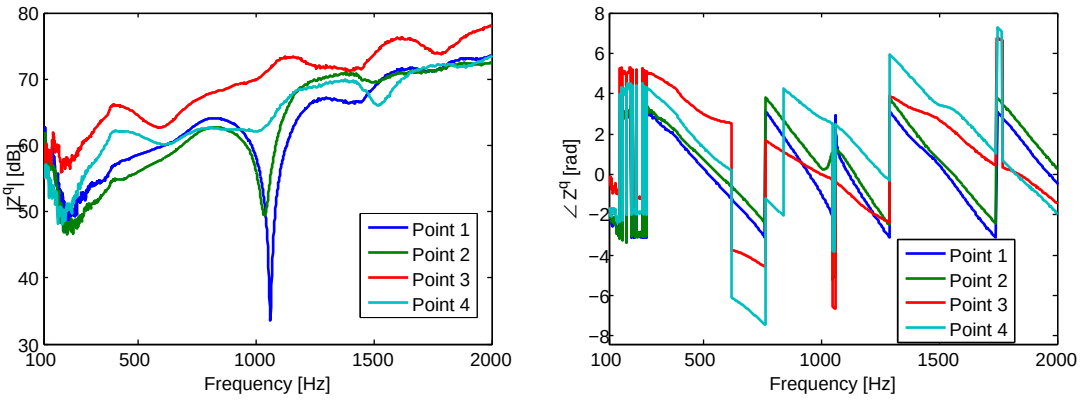

(a) (b)

Fig. 6.19 Coupling impedance Z^q between Patch 6 and 4 receiving points in the receiver space. Left: amplitude, ref, $1kg \cdot m^{-4}/s$, right: phase.

6.4.2 Blocked Pressure

To measure the blocked pressure, we put a small square plate – the one shown in Fig. 6.4 (b) – in the square hole of the round plate. The rigid surface blocks the source space (Cavity A) and 16 microphones are fixed on 8 patches of the surface, as shown in Fig. 6.14 (c). By turning the round plate, the pressures averaged across each of the 16 patches can be measured.

However, since we do not measure the pressure responses on all the patches at the same time, the relative phases of pressures on different patches can not be captured. To avoid this problem, we represent the blocked pressure by auto and cross spectra of measured pressures. Formally, the blocked pressure $\mathbf{P}_b$ in terms of auto and cross spectra of pressures on all the patches $\mathbf{G}_b$, where $\mathbf{G}_b$ is a 16×16 matrix. G_{mn}, the $(m,n)^{th}$ element of $\mathbf{G}_b$, denotes the cross spectra between the pressures $< P_m >_{\Delta S}$ and $< P_n >_{\Delta S}$ that are averaged across the m^{th} and n^{th} patches, respectively.

For any two patches in the same measurement, the cross spectrum reads

$$\begin{aligned} G_{mn} &\Leftrightarrow < P_m >_{\Delta S} < P_n >^*_{\Delta S} \\ &= \frac{1}{2}(P_{m1} + P_{m2})\frac{1}{2}(P_{n1} + P_{n2})^* \\ &\Leftrightarrow \frac{1}{4}(G_{m1,n1} + G_{m1,n2} + G_{m2,n1} + G_{m2,n2}) \end{aligned} \tag{6.7}$$

where $[\cdot]^*$ means conjugate transpose, $P_{m(n)1(2)}$ is the pressure measured by one of the two microphones on the m^{th} or n^{th} patch, $G_{m1(2),n1(2)}$ is the corresponding cross spectrum of the

pressure. And the $(m,m)^{th}$ element of $\mathbf{G}_b$, G_{mm}, is

$$G_{mm} = \frac{1}{4}(G_{m1,m1} + 2\Re\{G_{m1,m2}\} + G_{m2,m2}) \tag{6.8}$$

here $\Re\{G_{m1,m2}\}$ indicates the real part of the cross spectrum between the two measured pressures on the m^{th} patch.

In view of the full coherence between the signals originating from a single source, the cross spectrum between two patches activated in different measurements is indirectly computed with the help from another patch:

$$\begin{aligned} G_{mn} &\Leftrightarrow < P_m >_{\Delta S} < P_n >^*_{\Delta S} \\ &= \frac{< P_m >_{\Delta S} < P_i >^*_{\Delta S} < P_i >_{\Delta S} < P_n >^*_{\Delta S}}{< P_i >_{\Delta S} < P_i >^*_{\Delta S}} \\ &\Leftrightarrow \frac{G_{mi} G_{in}}{G_{ii}} \end{aligned} \tag{6.9}$$

where the m^{th} and n^{th} patches are activated in two different measurements, but the i^{th} patch is active in each measurement. Fig. 6.20 plots the cross spectra between Patch 6 and Patch 11, as well as the auto spectra of Patch 11. The spectra driven by the diesel engine noise is denoted by the blue solid lines and that driven by the white noise is denoted by the red dashed lines. From Fig. 6.20 (b), on the phases of the cross spectra between Patch 6 and Patch 11, we can see that the two phases of different noises well match each other. This result is in accordance with the fact that the sound is created by a single fully coherent source.

6.4.3 Sound Prediction

For sound prediction at 4 receiving points of interest, we refer to Eq. (3.6), i.e., $P_{rp} = Z_{rp}(Z_s + Z_r)^{-1} P_b$. With respect to the volume velocity used in the current experiment, this equation almost remains the same

$$\mathbf{P}_{rp} = \mathbf{Z}^q_{rp}(\mathbf{Z}^q_s + \mathbf{Z}^q_r)^{-1}\mathbf{P}_b \tag{6.10}$$

where only the receiver impedance term is changed. Let $\mathbf{T}$ denote the entire impedance term, $\mathbf{T} = \mathbf{Z}^q_{rp}(\mathbf{Z}^q_s + \mathbf{Z}^q_r)^{-1}$. The auto spectrum of the pressure $\mathbf{P}_{rp}$ is

$$\mathbf{G}_{rp} = \mathbf{T}\mathbf{G}_b\mathbf{T}^* \tag{6.11}$$

where $\mathbf{G}_b$ is the full spectral matrix of blocked pressure across all the 16 patches. With the $\mathbf{G}_{rp}$ is calculated, the sound prediction is done.

Sound prediction of diesel engine noise and white noise at 4 receiving points are shown in Fig. 6.21 and Fig. 6.23, respectively. The reference spectrum is the actual pressure directly measured at these receiving points when the source space and the receiver space are coupled. The errors between the prediction and the reference in 1/3 octave band are shown in Fig. 6.22 and Fig. 6.24. Generally, the predicted results are acceptable except at frequencies higher than 1.6k Hz. The mismatch at high frequencies is probably caused by the limited number of patches which cannot reconstruct the acoustical state well engough. Since we have used only 16 patches on our interface surface, the frequency limit by our system is about 1.3kHz. The reason why the error of Point 1 and Point 2 at the central frequency of 400Hz is large remains unknown and should be clarified in the future.

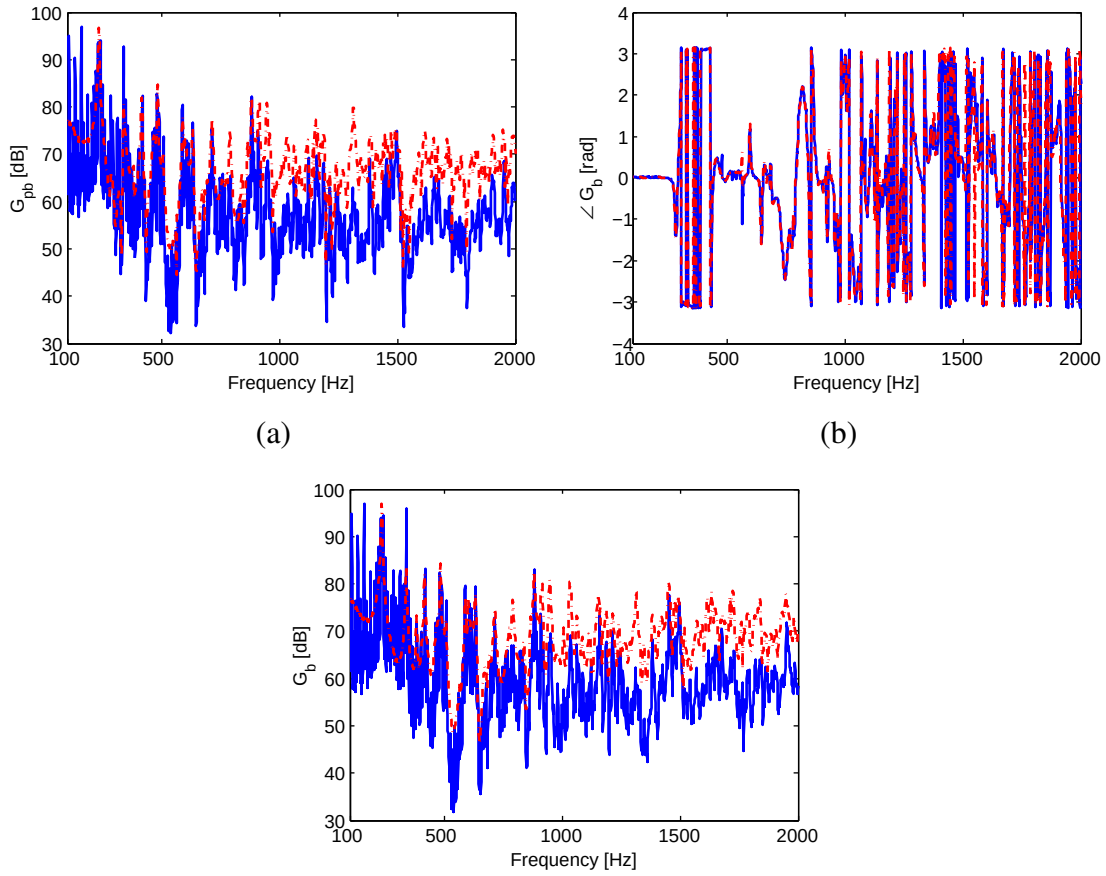

Fig. 6.20 Spectra of blocked sound patch pressures. Solid line: measured spectra with diesel engine noise, dashed line: measured spectra with white noise. Top: cross spectra between Patch 6 and Patch 11: (a) amplitude; (b) phase. Bottom: auto spectra of Patch 11: (c).

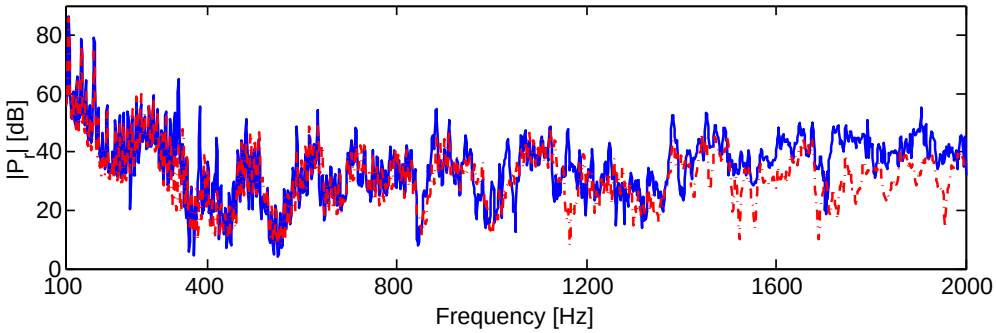

(a) Point 1

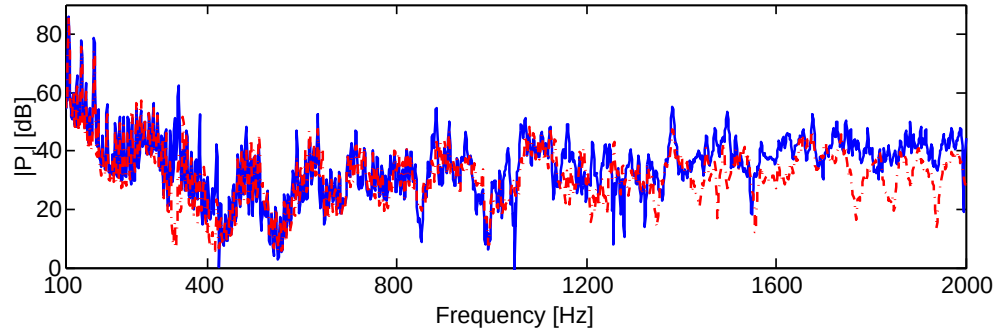

(b) Point 2

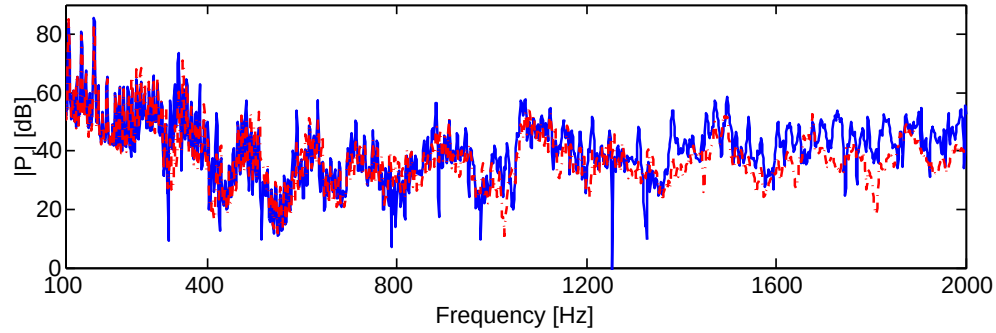

(c) Point 3

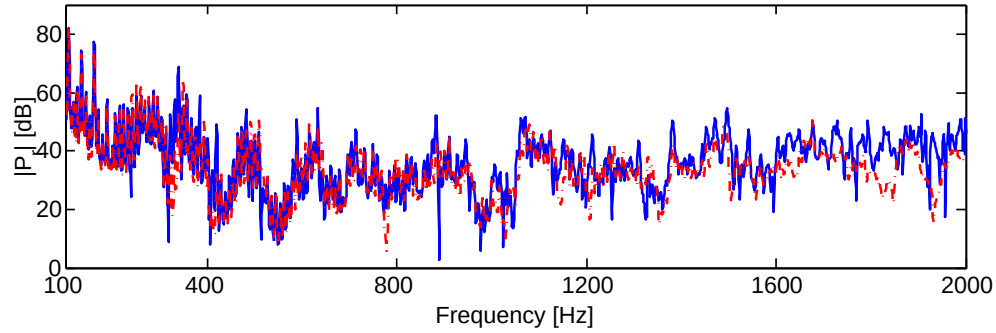

(d) Point 4

Fig. 6.21 Pressure response P_{rp} due to diesel engine noise. Solid line: predicted result, dashed line: reference.

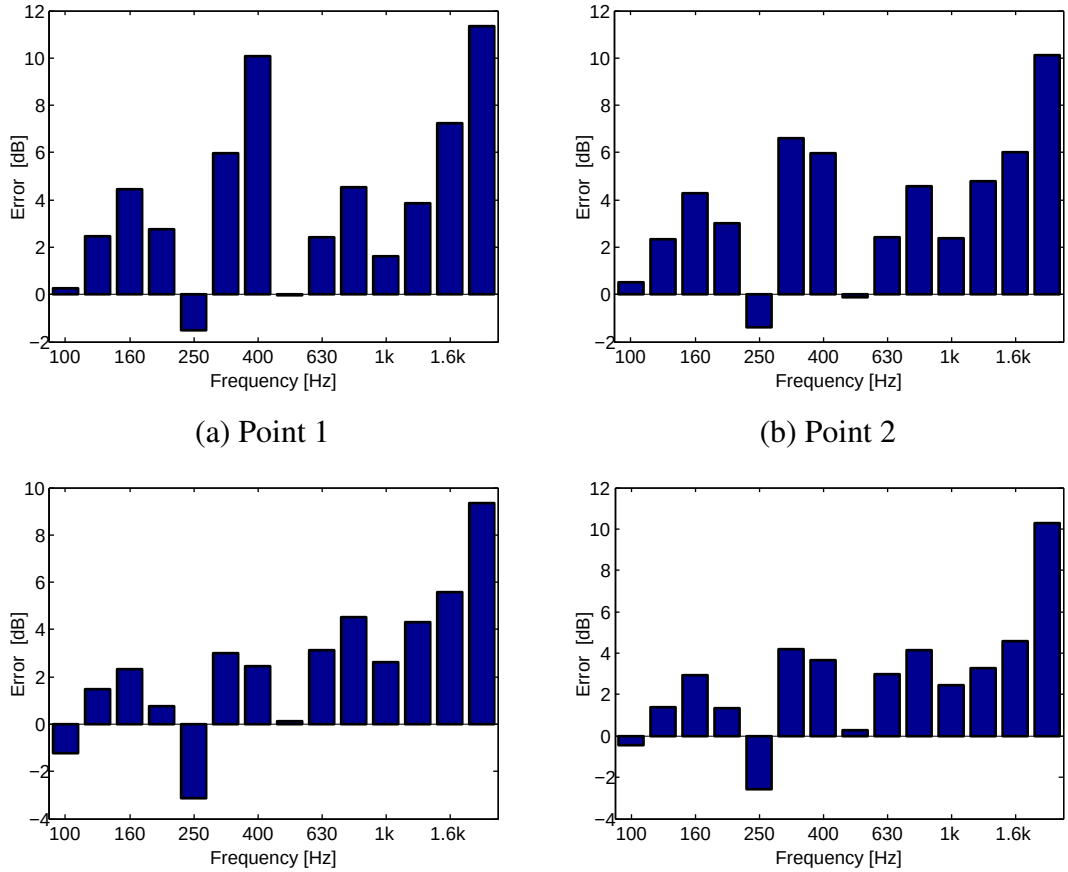

(a) Point 1 (b) Point 2

(c) Point 3 (d) Point 4

Fig. 6.22 Error between prediction and reference in 1/3 octave band of diesel engine noise.

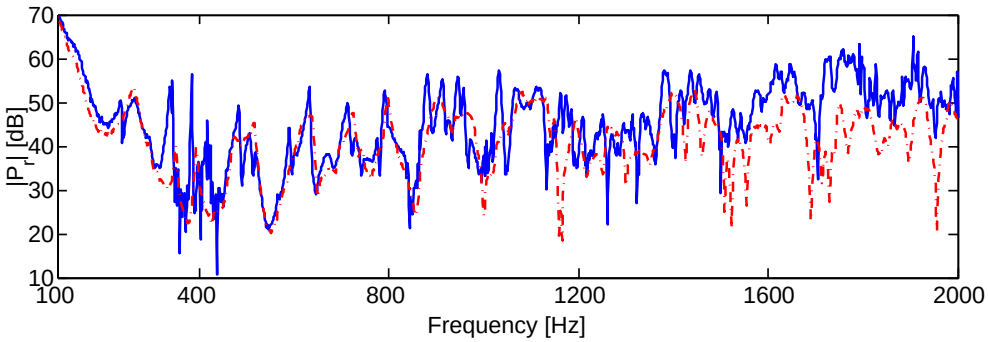

(a) Point 1

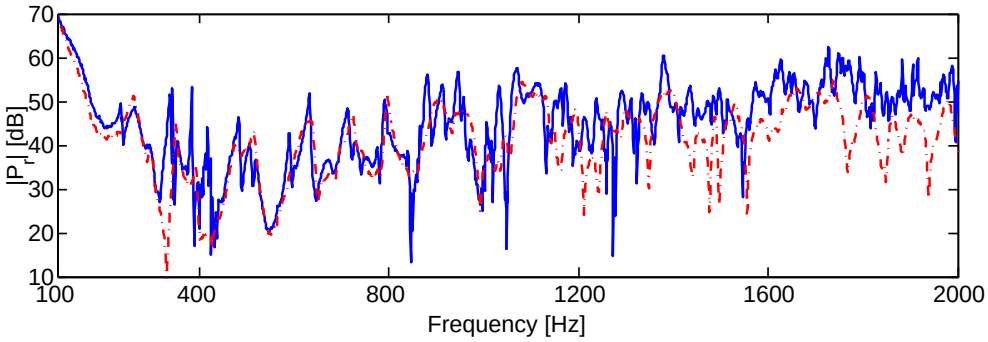

(b) Point 2

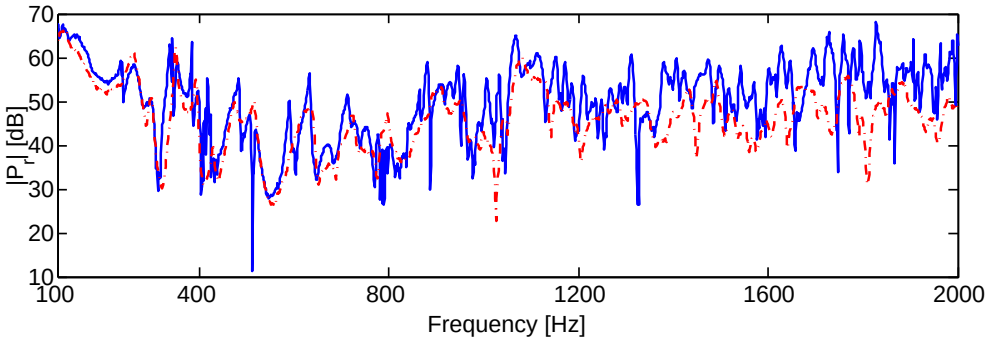

(c) Point 3

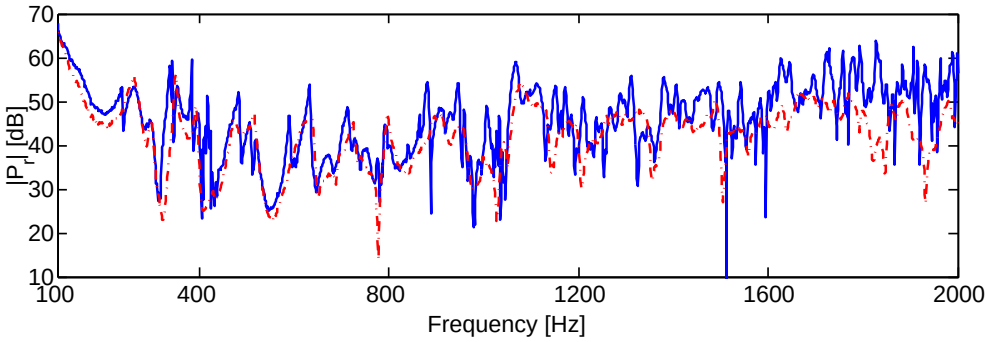

(d) Point 4

Fig. 6.23 Pressure response P_{rp} due to white noise. Solid line: predicted result, dashed line: reference.

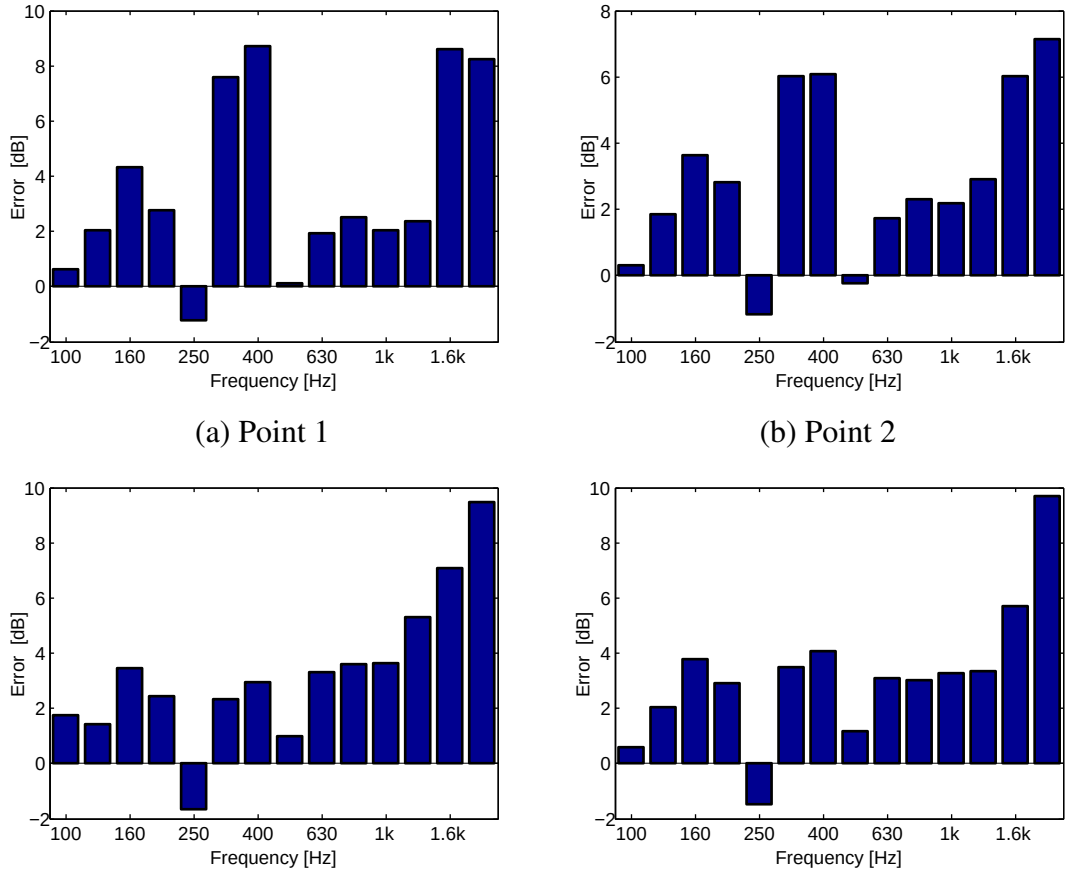

(a) Point 1

(b) Point 2

(c) Point 3

(d) Point 4

Fig. 6.24 Error between prediction and reference in 1/3 octave band of white noise.

6.5 Conclusions

In this chapter, we have validated a general technique of source characterisation via surface coupling. Concretely, we experimentally validated the characterisation of two noise sources and their sound radiation in an irregular cavity using the Patch technique. Two different noise sources in the cavity are recorded diesel engine noise and white noise played by an audio speaker. The characterisation work was accomplished step by step:

Firstly, a rigid cover interface surface was carefully designed and manufactured for carrying out the measurement of source and receiver descriptors which are defined on a virtual interface surface.

Secondly, a specific driver was designed to act as a driving patch for the sake of the identification of the coupling impedance between patches. The driving patch is composed of a piezoceramic speaker and a rigid back cavity. With a compression chamber mounted in front of the piezoceramic speaker, the coupling impedance between the driving patch and a receiving patch or point was identified in an indirect way, i.e., by the compression chamber method.

Finally, we successfully predicted the pressure responses at four receiving points due to the diesel engine noise and white noise in the cavity, with the measured blocked pressure, source and receiver impedances, as well as the coupling impedance between all the patches and the four receiving points.

Chapter 7

Sound Prediction in Multiple Connected Spaces via Surface Coupling

The key subject of the thesis is source characterisation. However, the surface coupling techniques can be applied for other purposes, such as prediction of sound sources in complex spaces. This will be illustrated in this chapter. The principle of modeling using surface coupling techniques will be described through two cases. Then we will carry out the validation of the results obtained by coupling techniques and by classical computation.

7.1 Principle of Surface Coupling

7.1.1 Case 1

The first case is an irregular room containing a physical source, as shown in Fig. 7.1 (a). Concerning the source position and the room structure, two coupling interface surfaces S_1, S_2 is created to divide the room into three subspaces: Space C, Space D and Space E. Specifically, Space C containing the source is the source space; the remaining spaces D and E are the receiver spaces.

According to its definition, the blocked pressure $\mathbf{P}_b$ is the pressure response across the coupling interface surface S with respect to the operating source:

$$\mathbf{P}_b = [P_{b1}, P_{b2}]^t \tag{7.1}$$

where P_{b1} and P_{b2} denote the blocked pressures across the surfaces S_1 and S_2, respectively. $[\cdot]^t$ means the matrix transpose. Since Space C is completely blocked by the surface S_1, the pressure response due to the source at the surface S_2 is 0, i.e., $P_{b2} = 0$. Before discussing the

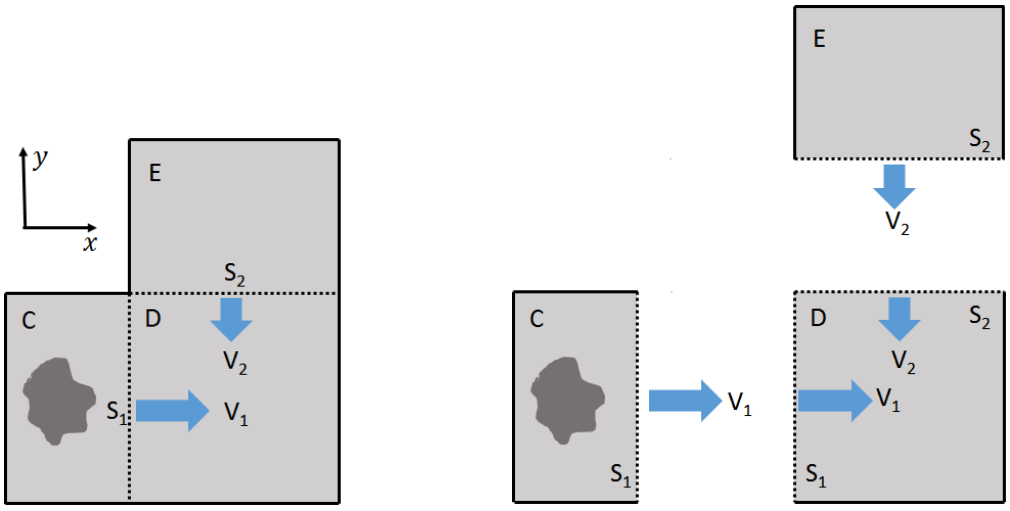

(a) Sound radiation model (b) Surface coupling

Fig. 7.1 Case study 1 of acoustical coupling via surface coupling.

source and receiver impedances, we first assume that the coupling velocity $\mathbf{V}_c$ at the coupling interface surface S is

$$\mathbf{V}_c = [V_1, V_2]^t \tag{7.2}$$

where, for simplicity, V_1 and V_2 either represent the velocities at the surfaces S_1 and S_2 in the acoustical receiver (see Fig. 7.1 (a)), or represent the velocities applied to the surfaces S_1 and S_2 in the corresponding subspaces by their adjacent space(s) (see Fig. 7.1 (b)).

According to the continuity conditions across each surface, the pressures at the surfaces S_1 and S_2 in different subspaces are computed by

$$P_{1,C} = P_{b1} + (-1) \times Z_{11,C} V_1 \tag{7.3a}$$
$$P_{1,D} = Z_{11,D} V_1 + Z_{12,D} V_2 \tag{7.3b}$$
$$P_{2,D} = Z_{21,D} V_1 + Z_{22,D} V_2 \tag{7.3c}$$
$$P_{2,E} = (-1) \times Z_{22,E} V_2 \tag{7.3d}$$

where $P_{1,C}$ is the pressure response at the surface S_1 in Space C, and so on; $Z_{12,D}$ denotes the coupling impedance between the surfaces S_1 and S_2 in Space D, etc. According to the reciprocity principle, $Z_{12,D}$ and $Z_{21,D}$ are equal to each other. Since we take that the direction of surface impedance is towards the inner space where the surface is located, $Z_{11,C} V_1$ is multiplied by a factor of -1 as the directions of $Z_{11,C}$ and V_1 are opposite, so is $Z_{22,E} V_2$. The

pressure continuity at the surfaces S_1 and S_2 gives

$$P_{1,C} = P_{1,D} \tag{7.4a}$$

$$P_{2,D} = P_{2,E} \tag{7.4b}$$

The matrix form by combining Eqs. (7.3) and (7.4) reads

$$\underbrace{\begin{bmatrix} P_{b1} \\ 0 \end{bmatrix}}_{\mathbf{P}_b} = \underbrace{\begin{bmatrix} Z_{11,C}+Z_{11,D} & Z_{12,D} \\ Z_{21,D} & Z_{22,D}+Z_{22,E} \end{bmatrix}}_{\mathbf{Z}} \underbrace{\begin{bmatrix} V_1 \\ V_2 \end{bmatrix}}_{\mathbf{V}_c} \tag{7.5}$$

Finally, the velocities V_1 and V_2 can be simply obtained by $\mathbf{V}_c = \mathbf{Z}^{-1}\mathbf{P}_b$. Here the impedance $\mathbf{Z}$ can be decomposed to the sum of three components with respect to the three subspaces,

$$\mathbf{Z} = \mathbf{Z}_C + \mathbf{Z}_D + \mathbf{Z}_E \tag{7.6a}$$

$$\mathbf{Z}_C = \begin{bmatrix} Z_{11,C} & 0 \\ 0 & 0 \end{bmatrix}, \mathbf{Z}_D = \begin{bmatrix} Z_{11,D} & Z_{12,D} \\ Z_{21,D} & Z_{22,D} \end{bmatrix}, \mathbf{Z}_E = \begin{bmatrix} 0 & 0 \\ 0 & Z_{22,E} \end{bmatrix} \tag{7.6b}$$

where $\mathbf{Z}_C, \mathbf{Z}_D, \mathbf{Z}_E$ present the impedances of the coupling surfaces in Spaces C, D and E, respectively. The $(m,n)^{th}$ element of the impedance $\mathbf{Z}_{C(D,E)}$ is the coupling impedance between the coupling surfaces S_m and S_n, $m,n = 1$ or 2, in the corresponding subspace. Alternatively, like the general case in Eq. (3.5), the impedance $\mathbf{Z}$ can be represented as the sum of source impedance and receiver impedance, that is

$$\mathbf{Z} = \mathbf{Z}_s + \mathbf{Z}_r \tag{7.7}$$

where the source impedance $\mathbf{Z}_s = \mathbf{Z}_C$ and the receiver impedance $\mathbf{Z}_r = \mathbf{Z}_D + \mathbf{Z}_E$.

Eqs. (7.5)(7.6)(7.7) hold true by replacing the field variables P, V and Z with corresponding harmonic parameters. Thus $\mathbf{P}_b$ is replaced by the corresponding harmonic amplitude $\mathbf{\Gamma}_b$, and $\mathbf{Z}$ is replaced by harmonic impedance $\mathbf{\Omega}$, that is

$$\underbrace{\begin{bmatrix} \Pi_{b1} \\ 0 \end{bmatrix}}_{\mathbf{\Pi}_b} = \underbrace{\begin{bmatrix} \Omega_{11,C}+\Omega_{11,D} & \Omega_{12,D} \\ \Omega_{21,D} & \Omega_{22,D}+\Omega_{22,E} \end{bmatrix}}_{\mathbf{\Omega}} \underbrace{\begin{bmatrix} \Gamma_1 \\ \Gamma_2 \end{bmatrix}}_{\mathbf{\Gamma}_c} \tag{7.8}$$

with

$$\mathbf{\Omega} = \mathbf{\Omega}_C + \mathbf{\Omega}_D + \mathbf{\Omega}_E \tag{7.9a}$$

$$\mathbf{\Omega}_C = \begin{bmatrix} \Omega_{11,C} & 0 \\ 0 & 0 \end{bmatrix}, \mathbf{\Omega}_D = \begin{bmatrix} \Omega_{11,D} & \Omega_{12,D} \\ \Omega_{21,D} & \Omega_{22,D} \end{bmatrix}, \mathbf{\Omega}_E = \begin{bmatrix} 0 & 0 \\ 0 & \Omega_{22,E} \end{bmatrix} \tag{7.9b}$$

where $\mathbf{\Gamma}_c$ is the harmonic amplitude of the coupling velocity $\mathbf{V}_c$, $\mathbf{\Omega}_{21,C}$ is the harmonic impedance between S_1 and S_2 in Space C, etc.

7.1.2 Case 2

While the previous case has connected receiver subspaces, this case will show a case of separated receiver subspaces. Fig. 7.2 (a) shows a sound radiation model containing a physical source. By defining a coupling interface surface S, the room is divided into four isolated subspaces: Space C, D, E and F. Specifically, the coupling interface surface S consists of three surfaces S_1, S_2 and S_3, i.e., $S = S_1 \bigcup S_2 \bigcup S_3$. Space C is the source space and the rest comprises the receiver space. We can see that the subspace D is separated from the other two subspaces E and F. In similarity with the previous case, the blocked pressure P_{b3} at the surface S_3 is 0 since the sound source is blocked by the other two surfaces S_1 and S_2. The directions of the coupling velocities at the positions of the surfaces are assumed in Fig. 7.2 (b). Given the valid blocked pressures P_{b1}, P_{b2} and the coupling impedances between different surfaces in different subspaces, the equilibrium equations of this case read

$$P_{1,C} = P_{b1} - Z_{11,C}V_1 - Z_{12,C}V_2 \tag{7.10a}$$

$$P_{2,C} = P_{b2} - Z_{21,C}V_1 - Z_{22,C}V_2 \tag{7.10b}$$

$$P_{1,D} = Z_{11,D}V_1 \tag{7.10c}$$

$$P_{2,E} = Z_{22,E}V_2 + Z_{23,E}V_3 \tag{7.10d}$$

$$P_{3,E} = Z_{32,E}V_2 + Z_{33,E}V_3 \tag{7.10e}$$

$$P_{3,F} = -Z_{33,F}V_3 \tag{7.10f}$$

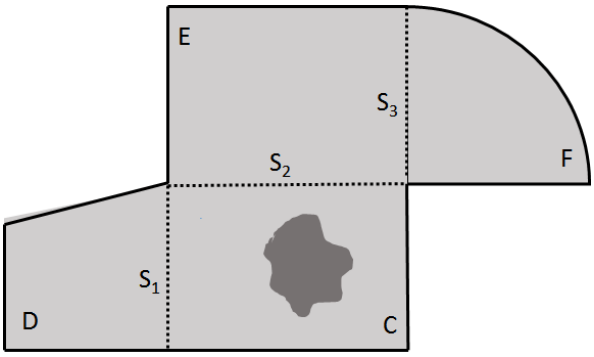

(a) Sound radiation model

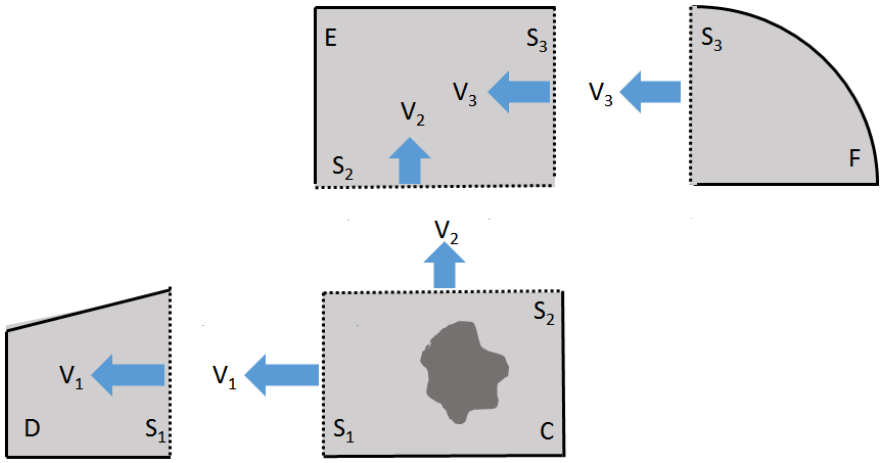

(b) Surface coupling

Fig. 7.2 Case study 2 of acoustical coupling via surface coupling.

The continuity conditions at the coupling surfaces make $P_{1,C} = P_{1,D}$, $P_{2,C} = P_{2,E}$, $P_{3,E} = P_{3,F}$, so the above equations can be rewritten as

$$\underbrace{\begin{bmatrix} P_{b1} \\ P_{b2} \\ 0 \end{bmatrix}}_{\mathbf{P}_b} = \underbrace{\begin{bmatrix} Z_{11,C}+Z_{11,D} & Z_{12,C} & 0 \\ Z_{21,C} & Z_{22,C}+Z_{22,E} & Z_{23,E} \\ 0 & Z_{32,E} & Z_{33,E}+Z_{33,F} \end{bmatrix}}_{\mathbf{Z}} \underbrace{\begin{bmatrix} V_1 \\ V_2 \\ V_3 \end{bmatrix}}_{\mathbf{V}_c} \tag{7.11}$$

In this case, the impedance $\mathbf{Z}$ is the sum of four components with respect to the four subspaces,

$$\mathbf{Z} = \mathbf{Z}_C + \mathbf{Z}_D + \mathbf{Z}_E + \mathbf{Z}_F \tag{7.12a}$$

$$\mathbf{Z}_C = \begin{bmatrix} Z_{11,C} & Z_{12,C} & 0 \\ Z_{21,C} & Z_{22,C} & 0 \\ 0 & 0 & 0 \end{bmatrix}, \mathbf{Z}_D = \begin{bmatrix} Z_{11,D} & 0 & 0 \\ 0 & 0 & 0 \\ 0 & 0 & 0 \end{bmatrix} \tag{7.12b}$$

$$\mathbf{Z}_E = \begin{bmatrix} 0 & 0 & 0 \\ 0 & Z_{22,E} & Z_{23,E} \\ 0 & Z_{32,E} & Z_{33,E} \end{bmatrix}, \mathbf{Z}_F = \begin{bmatrix} 0 & 0 & 0 \\ 0 & 0 & 0 \\ 0 & 0 & Z_{33,F} \end{bmatrix} \tag{7.12c}$$

Similarly with the previous example, the source impedance $\mathbf{Z}_s$ and the receiver impedance $\mathbf{Z}_r$ can be interpreted as $\mathbf{Z}_s = \mathbf{Z}_C$ and $\mathbf{Z}_r = \mathbf{Z}_D + \mathbf{Z}_E + \mathbf{Z}_F$, respectively.

With the field variables replaced by corresponding surface harmonic parameters, Eqs. (7.11) (7.14) are rewritten as

$$\underbrace{\begin{bmatrix} \Pi_{b1} \\ \Pi_{b2} \\ 0 \end{bmatrix}}_{\mathbf{\Pi}_b} = \underbrace{\begin{bmatrix} \Omega_{11,C}+\Omega_{11,D} & \Omega_{12,C} & 0 \\ \Omega_{21,C} & \Omega_{22,C}+\Omega_{22,E} & \Omega_{23,E} \\ 0 & \Omega_{32,E} & \Omega_{33,E}+\Omega_{33,F} \end{bmatrix}}_{\mathbf{\Omega}} \underbrace{\begin{bmatrix} \Gamma_1 \\ \Gamma_2 \\ \Gamma_3 \end{bmatrix}}_{\mathbf{\Gamma}_c} \tag{7.13}$$

with

$$\mathbf{\Omega} = \mathbf{\Omega}_C + \mathbf{\Omega}_D + \mathbf{\Omega}_E + \mathbf{\Omega}_F \tag{7.14a}$$

$$\mathbf{\Omega}_C = \begin{bmatrix} \Omega_{11,C} & \Omega_{12,C} & 0 \\ \Omega_{21,C} & \Omega_{22,C} & 0 \\ 0 & 0 & 0 \end{bmatrix}, \mathbf{\Omega}_D = \begin{bmatrix} \Omega_{11,D} & 0 & 0 \\ 0 & 0 & 0 \\ 0 & 0 & 0 \end{bmatrix} \tag{7.14b}$$

$$\mathbf{\Omega}_E = \begin{bmatrix} 0 & 0 & 0 \\ 0 & \Omega_{22,E} & \Omega_{23,E} \\ 0 & \Omega_{32,E} & \Omega_{33,E} \end{bmatrix}, \mathbf{\Omega}_F = \begin{bmatrix} 0 & 0 & 0 \\ 0 & 0 & 0 \\ 0 & 0 & \Omega_{33,F} \end{bmatrix} \tag{7.14c}$$

Implementation Remarks

During computing, one should take care of the directions of coupling impedances and velocities. We have shown the default setting of directions in Fig. 7.1 (b) and Fig. 7.2 (b) for the two examples. Our setting can be summarized as:

1. For the coupling interface surface consisting of several sub-surfaces, the surface impedance of any sub-surface is defined such that the driving velocity is oriented towards the inner space to which the sub-surface is assigned.

2. (a) In each subspace, the directions of coupling velocities across the sub- surfaces are either towards the inner space or towards the outside. For example, as shown in Fig. 7.2, the directions of V_2, V_3 in Space E are towards the inner space; the directions of V_1, V_2 are towards the outside of Space C.

   (b) Generally, we suggest that the directions of the coupling velocities in the source space are always towards the outside of the source space. And then the directions of the velocities in the remaining subspaces can be specified by following the previous criterion (a).

7.2 Numerical modelling

Based on the principle described in the previous section, this section will carry out the sound radiation by a vibrating box and a point source in two complex spaces via computation of surface coupling.

7.2.1 Example 1

The first example concerns the sound radiation by a vibrating box in an irregular acoustical space in Fig. 7.3. The height of the acoustical space is 0.6m and other sizes of the acoustical space are given in Fig. 7.3(b). The vibrating box of $0.2m \times 0.24m \times 0.4m$ is centered at $(0.2, 0.22, 0.3)m$. Unit normal acceleration is applied to the six faces of the box. Due to the vibrating box, the pressure responses at 400Hz across two planes at $x = 1.2m$ in Space B and at $y = 1.5m$ in Space C are computed by Actran, as shown in Fig. 7.3.

A coupling interface surface S is taken to divide the entire space into three subspaces, i.e., Space A, B and C. as shown in Fig. 7.3. The coupling interface surface S consists of two rectangular surfaces S_1 and S_2. Space A with the source is the source space while Space B and Space C are the receiver space. The descriptors in the source and receiver spaces can be identified by following the steps described in Chapter 4 and Chapter 5 with respect to

the Harmonic and Patch techniques, respectively. With the identified descriptors, the sound radiation in the receiver space can be reconstructed based on the principle introduced in the previous sections.

Referring to the criterion of selecting number of harmonics and patches, we use 60 harmonics[1] and 18 patches[2],with respect to the Harmonic and Patch techniques, to reconstruct the sound radiation. Fig. 7.4 plots the reconstructed pressure responses at 400Hz across

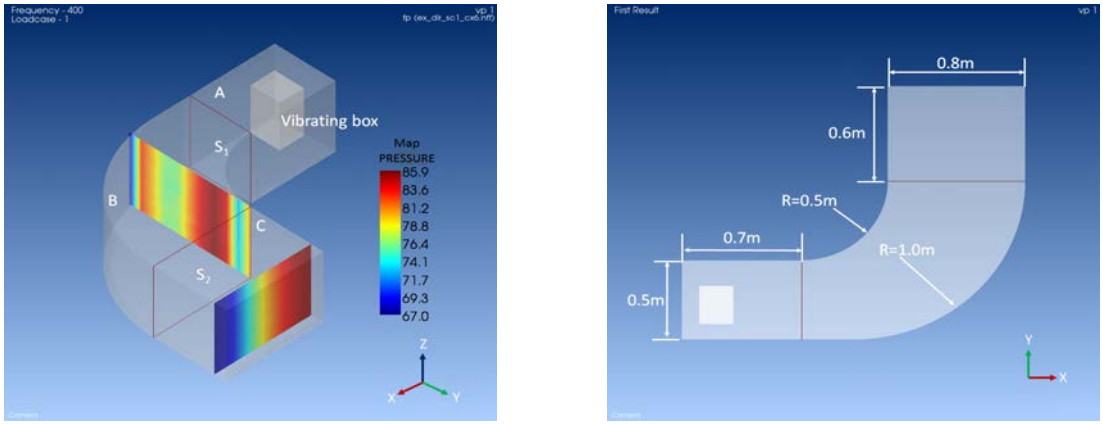

(a) (b)

Fig. 7.3 Sound radiation of a vibrating box in an irregular room. Left: 3D view, right: top view. The pressure is reported in dB.

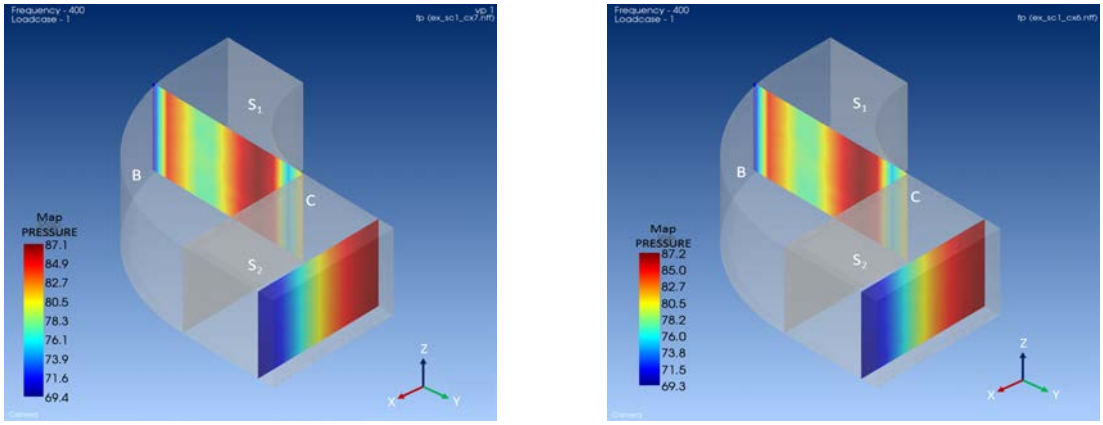

(a) (b)

Fig. 7.4 Sound reconstruction on the planes at $x = 1.2m$ in Space B and at $y = 1.5m$ in Space C using the Harmonic (left) and Patch techniques (right). The pressure is reported in dB.

[1] $25 = (2\times2+1)\times(2\times2+1)$ harmonics of the interface S_1 and $35 = (2\times3+1)\times(2\times2+1)$ harmonics of the interface S_2 are employed, in total there are 60 harmonics.

[2] The interface S_1 is divided into $6 = 2\times3$ patches while the interface S_2 is divided into $12 = 4\times3$ patches, in total there are 18 patches

the same planes in Space B and Space C. It can be observed that both predicted results match their references well when using the two techniques. Hence, with surface coupling techniques, the sound radiation can be predicted before the receiver space coupled with the source space.

7.2.2 Example 2

Another example is to show the reconstruction of a point source in an acoustical space through surface coupling. As shown in Fig. 7.5(a), the entire acoustical space is composed of three parallelepipedic spaces – Space A, Space B and Space C. Three spaces are coupled through two rectangular openings S_1 and S_2. Three spaces are of $3m$ height and two openings are of $2m$ height and $1m$ width. Other sizes of the room are illustrated in Fig. 7.5(b). The point source is located at $(2.5, 3.5, 2)m$ in Space B and its pressure amplitude is 1Pa defined by Actran. The sound radiation due to the point source in the entire coupled space can be computed by Actran.

Using coupling surface techniques, we take two openings S_1 and S_2 as the coupling interface surface S, namely $S = S_1 \bigcup S_2$. The coupling interface surface S divides the entire coupled space into the source space, i.e., Space B and the receiver space, i.e., Space A and Space C. The source and receiver descriptors can be identified using the Harmonic and Patch techniques. Thereby the sound radiation in the receiver space can be reconstructed with the identified descriptors.

With respect to the two techniques, we use 90 surface harmonics[3] and 90 patches[4] to reconstruct the pressure response at $(1.1, 1.79, 1.34)m$ in Space A and $(3.66, 1.1, 1.66)m$ in Space C, as shown in Fig. 7.6. Compared with the reference, the predicted results in Space A and Space C have shown considerable agreement when using the Harmonic and Patch techniques.

7.3 Conclusions

Besides the source characterisation via surface coupling, this chapter demonstrated another application of surface coupling techniques – sound prediction in multiple connected spaces. The principle of modeling sound prediction using surface coupling techniques has been described. Based on this principle, the sound radiation of a vibrating box and a point source in two complex spaces was reconstructed. The reconstructed sound radiation matched well

[3] $45(= 2 \times 2 + 1)(2 \times 4 + 1)$ harmonic of two interfaces S_1, S_2 are taken, in total there are 90 harmonics

[4] Both interfaces are divided into $45(= 5 \times 9)$ patches, in total there are 90 patches

the reference, which indicated that the sound radiation can be predicted through surface coupling techniques before coupling the subspaces together to form an entire acoustical space.

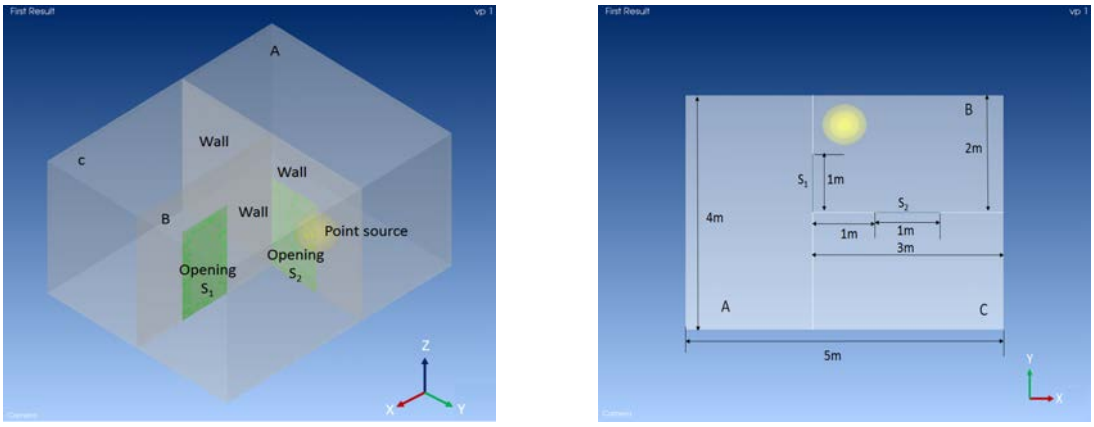

(a) (b)

Fig. 7.5 Sound radiation of a point source in a irregular room. (a) ISO view, (b) Top view.

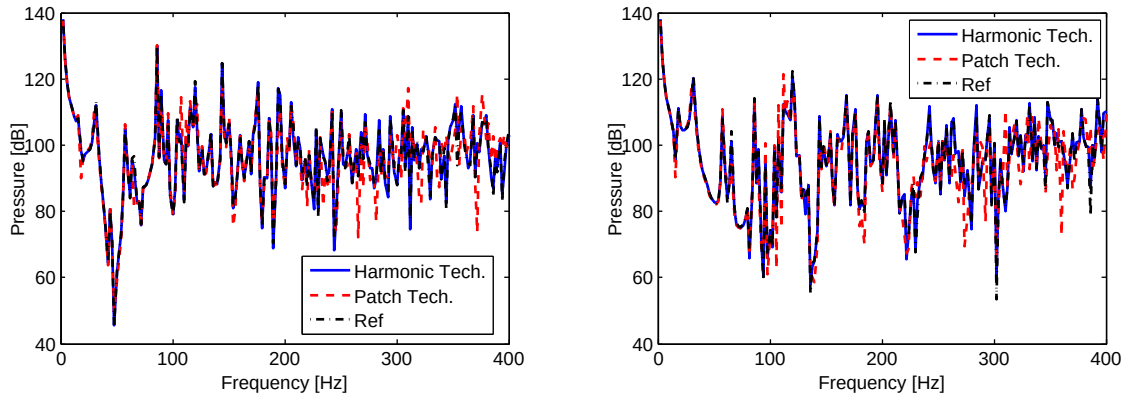

(a) (b)

Fig. 7.6 Sound reconstruction at $(1.1, 1.79, 1.34)m$ in Space A and at $(3.66, 1.1, 1.66)m$ in Space C using the Harmonic and Patch techniques.

Chapter 8

Conclusions and Perspectives

8.1 Conclusions

We investigated source characterisation via an enveloping surface as a method that provides a source model independent of surrounding acoustical space. The source model intrinsically characterises the acoustical properties of a physical source, so that the sound radiation from the source in an arbitrary acoustical space can be predicted. The main contribution of this thesis is studying source characterisation via enveloping surface and applying it for sound prediction. Two surface coupling techniques have been investigated and various sound prediction cases have been examined by analytical modeling, numerical modeling as well as experimental validation.

The principle of source characterisation via enveloping surface is to conceive an interface surface enveloping a physical source and to identify at this surface two source descriptors: its blocked pressure and its impedance. The physical source and the medium between it and the enveloping surface compose 'source space'. The source is characterised in this way by two descriptors: an active one, the blocked pressure, which defines the excitation capacity of the source and a passive one, the source impedance. Both descriptors are continuous functions of the enveloping surface. Such a characterisation permits dealing with sound sources which do not necessarily create sound by vibration, such as fans.

To predict the sound radiation due to the physical source in a given acoustical space, the same enveloping surface is applied to this space and a 'receiver space' established in this way. Like the source impedance characterising the source space, a compatible receiver impedance has to be defined to characterise the receiver space. With the identified blocked pressure, source impedance and receiver impedance, the coupling normal velocity can be obtained across the enveloping surface. The enveloping surface with the prescribed velocity

can be then considered as an equivalent source driving the receiver space, and the prediction of sound radiation due to the original source in the receiver space can be then obtained.

The identification of the descriptors is done by two surface coupling techniques – 'Continuous surface coupling technique' and 'Patch surface coupling technique'. Both techniques are defined in frequency domain.

The continuous technique, also named 'Harmonic technique', expands the sound field on the interface surface into a number of surface harmonics. The pressure and the normal particle velocity on the interface surface are represented by the vectors of complex amplitudes of the prescribed harmonics. The surface impedance can be then defined as the matrix having the ratios of pressure and velocity amplitudes as elements. The second technique, also named 'Patch technique', divides the interface surface into patches. The pressure and particle velocity on the interface surface are expressed by the values of amplitudes averaged across each patch. In this way the pressure and velocity amplitudes are again taken as vectors while the surface impedance is expressed as a matrix. The major difference between the two techniques is that the former considers the sound field to be continuous while the latter discretises it in points positioned at patch centres.

In order to validate the two techniques, sound field created by point sources and by a vibrating box in various acoustical spaces was modelled by analytical and numerical approaches. Good agreement was observed between the fields computed directly and by coupling the source to the receiver space. These examples have demonstrated that both techniques could give acceptable predicted results if the characterisation is carried out using correctly selected parameters: number of harmonics or patch size. For the Harmonic technique, it has been found that the wavelength of surface harmonics equal to $\frac{1}{2}$ of the sound wavelength could serve for selecting the number of harmonics. For the Patch technique, the patch size should be not larger than $\frac{1}{3}$ of the sound wavelength. If the averaged values of pressure across a patch are estimated by using discretely spaced sensors (microphones), the spacing between adjacent sampling points of a patch should be not larger than $\frac{1}{6}$ of wavelength to achieve reliable estimation.

Between the results obtained directly and by coupling, a frequency shift is observed. The shift is inherent for both surface coupling techniques, because the continuous global 'source–receiver' system is represented by a finite degrees of freedom coupling, i.e., either by a finite number of harmonics or by discretising the sound field. Increasing the number of harmonics and patches should reduce the frequency shift but leads to loss of matrix conditioning. However, the frequency shift caused by the two techniques can be often ignored e.g. when the sound is broad-band or when the results are represented in frequency

bands. However, it has been found that the Patch technique can produce poor results where some sound sources of extremely low volume velocity are concerned.

In terms of practical measurement, comparing the Harmonic technique to the Patch technique, it has been found that the former demands far more work than the latter because it requires more data to achieve correct characterisation. Thereby the Patch technique was preferred and applied for the experimental characterisation using a vibrating box as a source.

A simple measurement set-up using straight tubes was used to demonstrate the experimental feasibility of coupling approach. The final validation was one on a 3D set-up. According to the principle of surface coupling, the blocked pressure as well as source and receiver impedances were defined via an immobile plane surface. The biggest challenge of measurement was the design and manufacture of the enveloping surface needed to identify these descriptors. To validate the coupling approach, a rigid cover interface surface was carefully designed to enable measurements at the virtual surface. In addition a specific patch driver, a piezoceramic speaker was employed to provide patch excitation of known velocity for the sake of identifying the coupling impedance between patches. A recorded engine noise and white noise played by an audio speaker in an irregular cavity was predicted using the three descriptors. The experimental validation has produced acceptable predicted results with respect to sound pressure measured directly and has thus demonstrated the Patch technique could provide means of characterising the source.

The coupling technique by surface impedance was tested with an alternative objective in mind: computing the response of a complex acoustical space built up of smaller spaces of simple shape. Good results were obtained once more demonstrating the versatility of the surface coupling approach.

8.2 Perspectives

Due to limited time, many problems have remained open and should be considered in future work.

- We have finished the experimental validation of the Patch technique, but the experimental validation of the Harmonics technique remains missing. It would be interesting to complete this part and figure out the differences between the two techniques. Like in this thesis, there are possible problems in the future experiment, including but not limited to: how to drive the interface surface to compute the harmonic impedances, the number of measuring points on the entire surface, the distribution of microphones at the measuring points.

- We have experimented with laboratory sound sources such as compression driver and audio speaker. In contrast, experimenting with industrial sound sources such as a car engine will be more challenging. One of the challenges should be the design of the interface surface. Instead of using a single plate to separate the source space in our experiments, a real situation would probably require a parallelepipedic interface surface to fully envelop the original source. According to our experience, a major effort should be expected in producing an appropriate rigid surface as well as in designing the driving and receiving patches.

- We have also shown in Chapter 7 that the surface coupling technique – either the Harmonic technique or the Patch technique – could be useful for sound prediction in multiple connected spaces. However, this work has been limited to numerical modelling of a few simple cases using parallelepipedic surfaces. It could be extended to other surface shapes, such as cylindrical or spherical, for which the analytical solution is known.

References

[1] R. H. Lyon. *Statistical energy analysis of dynamical systems: theory and applications*. MIT press Cambridge, 1975.

[2] ISO 3744 acoustics–determination of sound power levels and sound energy levels of noise sources using sound pressure – engineering methods for an essentially free field over a reflecting plane. 2010.

[3] Y. I. Bobrovnitskii and G. Pavić. Modelling and characterization of airborne noise sources. *Journal of Sound and Vibration*, 261(3):527–555, 2003.

[4] W. Desmet. Mid-frequency vibro-acoustic modelling: challenges and potential solutions. In *Proceedings of the International Conference on Noise and Vibration Engineering (ISMA 2002)*, pages 835–862, Leuven Belgium, Sept 16-18 2002.

[5] J. D. Maynard, E. G. Williams, and Y. Lee. Nearfield acoustic holography: I. theory of generalized holography and the development of NAH. *The Journal of the Acoustical Society of America*, 78(4):1395–1413, 1985.

[6] E. G. Williams. *Fourier acoustics: sound radiation and nearfield acoustical holography*. Academic press, 1999.

[7] E. G. Williams, H. D. Dardy, and K. B. Washburn. Generalized nearfield acoustical holography for cylindrical geometry: Theory and experiment. *The Journal of the Acoustical Society of America*, 81(2):389–407, 1987.

[8] E. G. Williams. The nearfield acoustical holography (NAH) experimental method applied to vibration and radiation in light and heavy fluids. *Computers & structures*, 65(3):323–335, 1997.

[9] T. Loyau, J.-C. Pascal, and P. Gaillard. Broadband acoustic holography reconstruction from acoustic intensity measurements. I: Principle of the method. *The Journal of the Acoustical Society of America*, 84(5):1744–1750, 1988.

[10] A. Sarkissian. Near-field acoustic holography for an axisymmetric geometry: A new formulation. *The Journal of the Acoustical Society of America*, 88(2):961–966, 1990.

[11] M. Villot, G. Chaveriat, and J. Roland. Phonoscopy: An acoustical holography technique for plane structures radiating in enclosed spaces. *The Journal of the Acoustical Society of America*, 91(1):187–195, 1992.

[12] E. G. Williams, B. H. Houston, and P. C. Herdic. Fast Fourier transform and singular value decomposition formulations for patch nearfield acoustical holography. *The Journal of the Acoustical Society of America*, 114(3):1322–1333, 2003.

[13] R. Steiner and J. Hald. Near-field acoustical holography without the errors and limitations caused by the use of spatial DFT. *International Journal of Acoustics and Vibration*, 6(2):83–89, 2001.

[14] S. F. Wu. Methods for reconstructing acoustic quantities based on acoustic pressure measurements. *The Journal of the Acoustical Society of America*, 124(5):2680–2697, 2008.

[15] B. K. Gardner and R. J. Bernhard. A noise source identification technique using an inverse Helmholtz integral equation method. *Journal of Vibration and Acoustics*, 110(1):84–90, 1988.

[16] W. A. Veronesi and J. D. Maynard. Digital holographic reconstruction of sources with arbitrarily shaped surfaces. *The Journal of the Acoustical Society of America*, 85(2):588–598, 1989.

[17] M. R. Bai. Application of BEM (boundary element method)-based acoustic holography to radiation analysis of sound sources with arbitrarily shaped geometries. *The Journal of the Acoustical Society of America*, 92(1):533–549, 1992.

[18] A. F. Seybert, B. Soenarko, F. J. Rizzo, and D. J. Shippy. An advanced computational method for radiation and scattering of acoustic waves in three dimensions. *The Journal of the Acoustical Society of America*, 77(2):362–368, 1985.

[19] M. Costabel. Principles of boundary element methods. *Computer Physics Reports*, 6(1):243–274, 1987.

[20] B.-K. Kim and J.-G. Ih. On the reconstruction of the vibro-acoustic field over the surface enclosing an interior space using the boundary element method. *The Journal of the Acoustical Society of America*, 100(5):3003–3016, 1996.

[21] C. Langrenne, M. Melon, and A. Garcia. Boundary element method for the acoustic characterization of a machine in bounded noisy environment. *The Journal of the Acoustical Society of America*, 121(5):2750–2757, 2007.

[22] C. Langrenne, M. Melon, and A. Garcia. Measurement of confined acoustic sources using near-field acoustic holography. *The Journal of the Acoustical Society of America*, 126(3):1250–1256, 2009.

[23] C. Langrenne and A. Garcia. Data completion method for the characterization of sound sources. *The Journal of the Acoustical Society of America*, 130(4):2016–2023, 2011.

[24] A. Schuhmacher, J. Hald, K. B. Rasmussen, and P. C. Hansen. Sound source reconstruction using inverse boundary element calculations. *The Journal of the Acoustical Society of America*, 113(1):114–127, 2003.

[25] N. Valdivia and E. G. Williams. Implicit methods of solution to integral formulations in boundary element method based nearfield acoustic holography. *The Journal of the Acoustical Society of America*, 116(3):1559–1572, 2004.

[26] V. Arsénine and A. Tikhonov. *Méthodes de résolution de problémes mal posés*. Editions Mir, Moscou, 1976.

[27] A. Pereira. *Acoustic imaging in enclosed spaces*. PhD thesis, INSA de Lyon, 2013.

[28] F. Presezniak, P. A. G. Zavala, G. Steenackers, K. Janssens, J. R. F. Arruda, W. Desmet, and P. Guillaume. Acoustic source identification using a generalized weighted inverse beamforming technique. *Mechanical Systems and Signal Processing*, 32:349–358, 2012.

[29] A. Lindberg and G. Pavić. Characterisation of air-borne noise by a dummy-source approach. In *Proceedings of Noise and Vibration - Emerging Technologies (NOVEM)*, April 2015.

[30] A. Lindberg. *Airborne noise characterisation of a complex machine using a dummy source approach*. PhD thesis, INSA de Lyon, 2015.

[31] A. Lindberg and G. Pavić. Computation of sound radiation by a driver in a cabinet using a substitute source approach. *The Journal of the Acoustical Society of America*, 138(2):1132–1142, 2015.

[32] F. Holste. An equivalent source method for calculation of the sound radiated from aircraft engines. *Journal of Sound and Vibration*, 203(4):667–695, 1997.

[33] M. Ochmann. The complex equivalent source method for sound propagation over an impedance plane. *The Journal of the Acoustical Society of America*, 116(6):3304–3311, 2004.

[34] L. Feng and P.O. Berglund. Acoustic models of axial and centrifugal fans for NST technology. Nalpes, 2003. Proc. Euronoise2003.

[35] M. Ochmann. Synthesis of multipole radiators – an effective method for calculation of sound radiation of vibrating structures of arbitrary surfaces (in german). *Acta Acustica united with Acustica*, 72(4):233–246, 1990.

[36] L. H. Chen and D. G. Schweikert. Sound radiation from an arbitrary body. *The Journal of the Acoustical Society of America*, 35(10):1626–1632, 1963.

[37] Y. I. Bobrovnitskii, K. I. Mal'tsev, N. M. Ostapishin, and S. N. Panov. Acoustical model of a machine. *Soviet physics. Acoustics*, 37(6):570–574, 1991.

[38] G. H. Koopmann, L. Song, and J. B. Fahnline. A method for computing acoustic fields based on the principle of wave superposition. *The Journal of the Acoustical Society of America*, 86(6):2433–2438, 1989.

[39] R. Jeans and I. C. Mathews. The wave superposition method as a robust technique for computing acoustic fields. *The Journal of the Acoustical Society of America*, 92(2):1156–1166, 1992.

[40] G. Pavić. An engineering technique for the computation of sound radiation by vibrating bodies using substitute sources. *Acta Acustica united with Acustica*, 91(1):1–16, 2005.

[41] G. Pavić. A technique for the computation of sound radiation by vibrating bodies using multipole substitute sources. *Acta Acustica united with Acustica*, 92(1):112–126, 2006.

[42] M. Ochmann. The source simulation technique for acoustic radiation problems. *Acta Acustica united with Acustica*, 81(6):512–527, 1995.

[43] Z. Wang and S. F. Wu. Helmholtz equation-least-squares method for reconstructing the acoustic pressure field. *The Journal of the Acoustical Society of America*, 102(4):2020–2032, 1997.

[44] S. F. Wu and J. Yu. Reconstructing interior acoustic pressure fields via Helmholtz equation least-squares method. *The Journal of the Acoustical Society of America*, 104(4):2054–2060, 1998.

[45] N. Rayess and S. F. Wu. Experimental validations of the HELS method for reconstructing acoustic radiation from a complex vibrating structure. *The Journal of the Acoustical Society of America*, 107(6):2955–2964, 2000.

[46] M. Ochmann. The full-field equations for acoustic radiation and scattering. *The Journal of the Acoustical Society of America*, 105(5):2574–2584, 1999.

[47] N. Atalla, G. Winckelmans, and F. Sgard. A multiple multipole expansion approach for predicting the sound power of vibrating structures. *Acta Acustica united with Acustica*, 85(1):47–53, 1999.

[48] M. Ochmann and R. Piscoya. The source simulation technique with complex source points for computing acoustic radiation problems. In *Proceedings of the 13th International Congress on Sound and Vibration (ICSV13)*, 2006.

[49] M. E. Johnson, S. J. Elliott, K. H. Baek, and J. Garcia-Bonito. An equivalent source technique for calculating the sound field inside an enclosure containing scattering objects. *The Journal of the Acoustical Society of America*, 104(3):1221–1231, 1998.

[50] A. T. Moorhouse and G. Seiffert. Characterisation of an airborne sound source for use in a virtual acoustic prototype. *Journal of Sound and Vibration*, 296(1):334–352, 2006.

[51] T. M. Tomilina, Y. I. Bobrovnitskii, V. B. Yashkin, and A. A. Kochkin. Power output of noise sources operating near elastic scatterers of finite dimensions. *Journal of Sound and Vibration*, 226(2):285–304, 1999.

[52] M. B. S. Magalhaes and R. A. Tenenbaum. Sound sources reconstruction techniques: A review of their evolution and new trends. *Acta Acustica united with Acustica*, 90(2):199–220, 2004.

[53] G. J. O'Hara. Mechanical impedance and mobility concepts. *The Journal of the Acoustical Society of America*, 41(5):1180–1184, 1967.

[54] G. Pavić and A. S. Elliott. Structure-borne sound characterization of coupled structures – part I: Simple demonstrator model. *Journal of Vibration and Acoustics*, 132(4):041008, 2010.

[55] G. Pavić and A. S. Elliott. Structure-borne sound characterization of coupled structures – part II: Feasibility study. *Journal of Vibration and Acoustics*, 132(4):041009, 2010.

[56] A. Elliott and A. T. Moorhouse. Characterisation of structure borne sound sources from measurement in-situ. *The Journal of the Acoustical Society of America*, 123(5):3176, 2008.

[57] A. T. Moorhouse, A. S. Elliott, and T. A. Evans. In situ measurement of the blocked force of structure-borne sound sources. *Journal of Sound and Vibration*, 325(4):679–685, 2009.

[58] A. S. Elliott, A. T. Moorhouse, and G. Pavić. Moment excitation and the measurement of moment mobilities. *Journal of Sound and Vibration*, 331(11):2499–2519, 2012.

[59] D. Lennström, M. Olsson, F. Wullens, and A. Nykänen. Validation of the blocked force method for various boundary conditions for automotive source characterization. *Applied Acoustics*, 102:108–119, 2016.

[60] J. M. Mondot and B. Petersson. Characterization of structure-borne sound sources: the source descriptor and the coupling function. *Journal of Sound and Vibration*, 114(3):507–518, 1987.

[61] B. A. T. Petersson and B. M. Gibbs. Use of the source descriptor concept in studies of multi-point and multi-directional vibrational sources. *Journal of Sound and Vibration*, 168(1):157–176, 1993.

[62] B. Petersson and J. Plunt. On effective mobilities in the prediction of structure-borne sound transmission between a source structure and a receiving structure, part I: theoretical background and basic experimental studies. *Journal of Sound and Vibration*, 82(4):517–529, 1982.

[63] B. Petersson and J. Plunt. On effective mobilities in the prediction of structure-borne sound transmission between a source structure and a receiving structure, part II: procedures for the estimation of mobilities. *Journal of Sound and Vibration*, 82(4):531–540, 1982.

[64] M. H. A. Janssens and J. W. Verheij. A pseudo-forces methodology to be used in characterization of structure-borne sound sources. *Applied Acoustics*, 61(3):285–308, 2000.

[65] B. M. Gibbs, R. Cookson, and N. Qi. Vibration activity and mobility of structure-borne sound sources by a reception plate method. *The Journal of the Acoustical Society of America*, 123(6):4199–4209, 2008.

[66] M. M. Späh and B. M. Gibbs. Reception plate method for characterisation of structure-borne sound sources in buildings: Assumptions and application. *Applied Acoustics*, 70(2):361–368, 2009.

[67] A. D. Jones. Modelling the exhaust noise radiated from reciprocating internal combustion engines – A literature review. *Noise Control Engineering Journal*, 23:12–31, 1984.

[68] L. J. Eriksson and P. T. Thawani. Theory and practice in exhaust system design. Technical report, SAE Technical Paper, 1985.

[69] H. Bodén and F. Albertson. Linearity tests for in-duct acoustic one-port sources. *Journal of Sound and Vibration*, 237(1):45–65, 2000.

[70] M. G. Prasad and M. J. Crocker. Acoustical source characterization studies on a multi-cylinder engine exhaust system. *Journal of Sound and Vibration*, 90(4):479–490, 1983.

[71] D.F. Ross and M.J. Crocker. Measurement of the acoustic internal source impedance of an internal combustion engine. *The Journal of the Acoustical Society of America*, 74(1):18–27, 1983.

[72] M. L. Kathuriya and M. L. Munjal. Experimental evaluation of the aeroacoustic characteristics of a source of pulsating gas flow. *The Journal of the Acoustical Society of America*, 65(1):240–248, 1979.

[73] H. S. Alves and A. G. Doige. A three-load method for noise source characterization in ducts. In *Proceedings of NOISE-CON 87*, pages 329–334, 1987.

[74] A. F. Seybert and D. F. Ross. Experimental determination of acoustic properties using a two-microphone random-excitation technique. *The Journal of the Acoustical Society of America*, 61(5):1362–1370, 1977.

[75] H. Bodén. The multiple load method for measuring the source characteristics of time-variant sources. *Journal of Sound and Vibration*, 148(3):437–453, 1991.

[76] M.G. Prasad. A four load method for evaluation of acoustical source impedance in a duct. *Journal of Sound and Vibration*, 114(2):347–356, 1987.

[77] H. Rämmal and H. Bodén. Modified multi-load method for nonlinear source characterisation. *Journal of Sound and Vibration*, 299(4):1094–1113, 2007.

[78] G. Pavić. Air-borne sound source characterization by patch impedance coupling approach. *Journal of Sound and Vibration*, 329(23):4907–4921, 2010.

[79] L. Du and G. Pavić. Acoustical source-receiver intrefacing uisng the patch impedance approach. In *Proceedings of Conference Français d'Acoustique (CFA 2014)*, pages 1407–1413, Potiers, April 22-25 2014.

[80] G. Pavić. Air-borne sound source characterisation by plane surface harmonics. In *Proceedings of Inter-Noise 2012*, New York, August 19-22 2012.

[81] W. Desmet. A wave based prediction technique for coupled vibro-acoustic analysis. *These, Katholieke Universiteit Leuven, Belgique*, 1998.

[82] B. V. Genechten, D. Vandepitte, and W. Desmet. On the coupling of Wave Bsed models with modally reduced Finite Element models for 3D interior acousitc analysis. In *Proceedings of the International Conference on Noise and Vibration Engineering (ISMA 2008)*, pages 1631–1652, 2008.

[83] H. Kuttruff. *Room acoustics*. CRC Press, 2009.

[84] K. Shin and J.K. Hammond. *Fundamentals of singal processing for sound and vibration engineers*. Wiley, 2007.

[85] A. Lindberg and G. Pavić. Measurement of volume velocity of a small sound source. *Applied Acoustics*, 91:25–32, 2015.

[86] P. M. Morse and K. U. Ingard. *Theoretical acoustics*. Princeton University Press, 1968.

Appendix A

List of Symbols

Table A.1 Main symbols

Symbol	Meaning	units
ρ_0	Density of the fluid	kg/m^3
c	Sound speed	m/s
ε	Damping coefficient	–
ω	Angular frequency	$rads^{-1}$
ω_n	Natural angular frequency	$rads^{-1}$
j	Imaginary unit ($j = \sqrt{-1}$)	–
k	Wave number	–
λ	Wavelength	m
f	Frequency	Hz
P	Complex Pressure amplitude	Pa
V	Complex velocity amplitude	m/s
U	Volume of the cavity	m^3
Z	Surface impedance	$kg \cdot m^{-2} \cdot s^{-1}$
Π	Pressure amplitude corresponding to surface harmonics	Pa
Γ	Velocity amplitude corresponding to surface harmonics	m/s
Ω	Harmonic impedance	Pa$\cdot s/m$
Q	Complex volume velocity amplitude	m^3/s
Z^q	Surface impedance	$kg \cdot m^{-4} \cdot s^{-1}$
D_d	Dipole strength	m^4/s
ΔS	Patch area	m^2
G	Auto or cross spectrum	
$[\cdot]^t$	matrix transpose	
$[\cdot]^*$	conjugate transpose	

Appendix B

Identification of Source and Receiver Impedances using Two-microphones Method

We define the x-axis starting from the interface surface S and pointing to the two microphones in Fig. B.1. The distance between the two microphones is s and the distance between the interface surface S and the closer microphone is l. The pressure response at the microphone closer to the interface surface S is denoted by p_o while that at the other microphone is $p_\times$. The state, represented by sound pressure P and particle velocity V, can be idealized as the sum of the incident and reflected plane waves in the tube [86]:

$$P(x) = P_+ e^{-jkx} + P_- e^{jkx} \tag{B.1a}$$

$$V(x) = \frac{1}{\rho_0 c}(P_+ e^{-jkx} - P_- e^{jkx}) \tag{B.1b}$$

where k is the wave number, P_+ and P_- are the pressure amplitudes of the incident and reflected waves. Let $H = \frac{P_o}{P_\times}$ denote the transfer function of the two microphones. By substituting P_o and $P_\times$ into Eq. (B.1), we have

$$\frac{P_+}{P_-} = \frac{H - e^{-jks}}{e^{jks} - H} e^{j2k(l+s)} \tag{B.2}$$

The impedance of the interface surface S is then computed by

$$Z = \frac{P}{V}|_{x=0} = \frac{\frac{P_+}{P_-} + 1}{\frac{1}{\rho_0 c}(\frac{P_+}{P_-} - 1)} \tag{B.3}$$

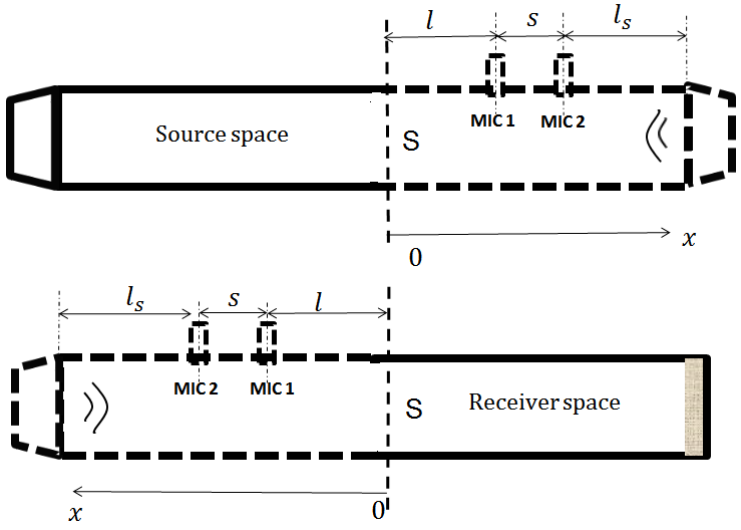

Fig. B.1 Measurement of source impedance (top) and receiver impedance (bottom) using the two-microphones method.

Appendix C

Formula Derivation

C.1 Abbreviations for analytical modelling of Harmonic technique

$$B_{l,n} = \int_{y_0}^{y_0+b_0} cos(\frac{l_y\pi}{b_0}(y_e - y_0))cos(\frac{n_y\pi}{b}y_e)dy_e \int_{z_0}^{z_0+h_0} sin(\frac{l_z\pi}{h_0}(z_e - z_0))cos(\frac{n_z\pi}{h}z_e)dz_e \tag{C.1}$$

Let $y = y_e - y_0, z = z_e - z_0$,

$$\begin{aligned} B_{l,n} &= \int_0^{b_0} cos(\frac{l_y\pi}{b_0}y)cos(\frac{n_y\pi}{b}(y+y_0))dy \int_0^{h_0} sin(\frac{l_z\pi}{h_0}z)cos(\frac{n_z\pi}{h}(z+z_0))dz \\ &= \Big[cos(\frac{n_y\pi}{b}y_0)\int_0^{b_0} cos(\frac{l_y\pi}{b_0}y)cos(\frac{n_y\pi}{b}y)dy - sin(\frac{n_y\pi}{b}y_0)\int_0^{b_0} cos(\frac{l_y\pi}{b_0}y)sin(\frac{n_y\pi}{b}y)dy\Big] \\ &\Big[cos(\frac{n_z\pi}{h}z_0)\int_0^{h_0} sin(\frac{l_z\pi}{h_0}z)cos(\frac{n_z\pi}{h}z)dz - sin(\frac{n_z\pi}{h}z_0)\int_0^{h_0} sin(\frac{l_z\pi}{h_0}z)sin(\frac{n_z\pi}{h}z)dz\Big] \end{aligned} \tag{C.2}$$

Let $\frac{n_y}{b} = \frac{n_y^\gamma}{b_0}, \frac{n_z}{h} = \frac{n_z^\gamma}{h_0}$, e.g. $n_y^\gamma = n_y b_0/b, n_z^\gamma = n_z h_0/h$. n_y^γ and n_z^γ are not necessarily integers. Thus,

$$\begin{aligned} B_{l,n} = &\Big[cos(\frac{n_y\pi}{b}y_0)\int_0^{b_0} cos(\frac{l_y\pi}{b_0}y)cos(\frac{n_y^\gamma}{b_0}y)dy - sin(\frac{n_y\pi}{b}y_0)\int_0^{b_0} cos(\frac{l_y\pi}{b_0}y)sin(\frac{n_y^\gamma}{b_0}y)dy\Big] \\ &\Big[cos(\frac{n_z\pi}{h}z_0)\int_0^{h_0} sin(\frac{l_z\pi}{h_0}z)cos(\frac{n_z^\gamma}{h_0}z)dz - sin(\frac{n_z\pi}{h}z_0)\int_0^{h_0} sin(\frac{l_z\pi}{h_0}z)sin(\frac{n_z^\gamma}{h_0}z)dz\Big] \end{aligned} \tag{C.3}$$

Four integrations in the brackets can be computed by following equations.

- If l, n are integers

$$\int_0^a cos(\frac{l\pi x}{a})cos(\frac{n\pi x}{a})dx \text{ or } \int_0^a sin(\frac{l\pi x}{a})sin(\frac{n\pi x}{a})dx = \begin{cases} \frac{a}{2}, & \text{for } l = n \\ 0, & \text{for } l \neq n \end{cases} \tag{C.4}$$

$$\int_0^a sin(\frac{l\pi x}{a})cos(\frac{n\pi x}{a})dx = \begin{cases} 0, & \text{for } l-n = \text{even number} \\ \frac{2la}{\pi(l+n)(l-n)}, & \text{for } l-n = \text{odd number} \end{cases} \tag{C.5}$$

- If l is an integer and n is a fraction

$$\int_0^a cos(\frac{l\pi x}{a})cos(\frac{n\pi x}{a})dx = \frac{(-1)^{l+1}ansin(n\pi)}{\pi(l+n)(l-n)} \tag{C.6}$$

$$\int_0^a sin(\frac{l\pi x}{a})sin(\frac{n\pi x}{a})dx = \frac{(-1)^{l+1}alsin(n\pi)}{\pi(l+n)(l-n)} \tag{C.7}$$

$$\int_0^a sin(\frac{l\pi x}{a})cos(\frac{n\pi x}{a})dx = \frac{al[(-1)^{l+1}cos(n\pi)+1]}{(l+n)(l-n)\pi} \tag{C.8}$$

C.2 Sound radiation of dipole source in rectangular room

The pressure response P at a point $\mathbf{r} = (x, y, z)$ due to a point source of strength Q_e at a point $\mathbf{r}_e = (x_e, y_e, z_e)$ in a rectangular room of size $a \times b \times h$ is

$$P(\mathbf{r}) = j\frac{\omega\rho_0 c^2}{U}Q_e(\mathbf{r}_e)\sum_n^N \frac{\phi_n(\mathbf{r}_e)\phi_n(\mathbf{r})}{\omega_n^2 - \omega^2 + 2j\varepsilon\omega} \tag{C.9a}$$

$$\phi_n(x,y,z) = \zeta(n)cos(\frac{n_x\pi x}{a})cos(\frac{n_y\pi y}{b})cos(\frac{n_z\pi z}{h}) \tag{C.9b}$$

$$\zeta(n) = \sqrt{2^{sgn(n_x+n_y+n_z)}} \tag{C.9c}$$

where ω_n are the natural frequency, ε is an equivalent damping coefficient, U is the volume of the room. The integers n_x, n_y, n_z are mode indices in x, y, z directions.

A dipole at $\mathbf{r}_e$ consists of two point sources with strength Q_e opposite in phase and separated by an infinitesimal distance d. The pressure response at the point $\mathbf{r}$ due to the

dipole is

$$P(\mathbf{r}) = \lim_{d\to 0}[P_+(\mathbf{r}) - P_-(\mathbf{r})] \tag{C.10}$$

The dipole strength is $D_d = Q_e d$. If the dipole with strength D_d is in a direction shown in Fig. 5.13. The strength in x, y, z directions is

$$\begin{aligned} D_{dx} &= D_d sin\psi cos\theta \\ D_{dy} &= D_d sin\psi sin\theta \\ D_{dz} &= D_d cos\psi \end{aligned} \tag{C.11}$$

Then the pressure response $P(\mathbf{r})$ can be decomposed to the sum of three components,

$$P(\mathbf{r}) = P(\mathbf{r})|_x + P(\mathbf{r})|_y + P(\mathbf{r})|_z \tag{C.12}$$

where $P|_x$ presents the pressure response due to the dipole strength D_{dx} in x direction, and so on. Substituting Eq. (C.9) to Eq. (C.10), we have

$$\begin{aligned} P(\mathbf{r})|_x &= \lim_{d\to 0}[P_+(\mathbf{r}) - P_-(\mathbf{r})]|_x \\ &= \left\{ \lim_{d\to 0}\{jQ_e \frac{\omega\rho_0 c^2}{U} \sum_n^N \frac{[\phi_n(\mathbf{r}_{e+}) - \phi_n(\mathbf{r}_{e-})]\phi_n(\mathbf{r})}{\omega_n^2 - \omega^2 + 2j\varepsilon\omega}\} \right\} \Bigg|_x \\ &= \left\{ jQ_e d \frac{\omega\rho_0 c^2}{U} \sum_n^N \frac{\phi_n(\mathbf{r})}{\omega_n^2 - \omega^2 + 2j\varepsilon\omega} \left[\lim_{d\to 0} \frac{\phi_n(\mathbf{r}_{e+}) - \phi_n(\mathbf{r}_{e-})}{d} \right] \right\} \Bigg|_x \\ &= jD_{dx} \frac{\omega\rho_0 c^2}{U} \sum_n^N \frac{\phi_n(\mathbf{r})}{\omega_n^2 - \omega^2 + 2j\varepsilon\omega} \left[\lim_{d\to 0} \frac{\phi_n(\mathbf{r}_{e+}) - \phi_n(\mathbf{r}_{e-})}{d} \right] \Bigg|_x \\ &= jD_{dx} \frac{\omega\rho_0 c^2}{U} \sum_n^N \frac{\phi_n(\mathbf{r})}{\omega_n^2 - \omega^2 + 2j\varepsilon\omega} \left[\frac{\partial\phi_n(\mathbf{r}_e)}{\partial x_e} \right] \end{aligned} \tag{C.13}$$

Similarly,

$$P(\mathbf{r})|_y = jD_{dy} \frac{\omega\rho_0 c^2}{U} \sum_n^N \frac{\phi_n(\mathbf{r})}{\omega_n^2 - \omega^2 + 2j\varepsilon\omega} \left[\frac{\partial\phi_n(\mathbf{r}_e)}{\partial y_e} \right] \tag{C.14}$$

$$P(\mathbf{r})|_z = jD_{dz} \frac{\omega\rho_0 c^2}{U} \sum_n^N \frac{\phi_n(\mathbf{r})}{\omega_n^2 - \omega^2 + 2j\varepsilon\omega} \left[\frac{\partial\phi_n(\mathbf{r}_e)}{\partial z_e} \right] \tag{C.15}$$

with

$$\frac{\partial \phi_n(\mathbf{r})}{\partial x} = \zeta(n)\frac{n_x\pi}{a}sin(\frac{n_x\pi x}{a})cos(\frac{n_y\pi y}{b})cos(\frac{n_z\pi z}{h}) \tag{C.16}$$

$$\frac{\partial \phi_n(\mathbf{r})}{\partial y} = \zeta(n)\frac{n_y\pi}{b}cos(\frac{n_x\pi x}{a})sin(\frac{n_y\pi y}{b})cos(\frac{n_z\pi z}{h}) \tag{C.17}$$

$$\frac{\partial \phi_n(\mathbf{r})}{\partial x} = \zeta(n)\frac{n_z\pi}{h}cos(\frac{n_x\pi x}{a})cos(\frac{n_y\pi y}{b})sin(\frac{n_z\pi z}{h}) \tag{C.18}$$

The pressure averaged across the patch of area ΔS centered at $\mathbf{r} = (x,y,z)$ due to the dipole source is

$$< P(\mathbf{r}) >_{\Delta S} = \frac{1}{\Delta S}\int_{\Delta S} P(\mathbf{r})dS = \frac{1}{\Delta S}\int_{\Delta S}[P(\mathbf{r})|_x + P(\mathbf{r})|_y + P(\mathbf{r})|_z]dS \tag{C.19}$$

with

$$\frac{1}{\Delta S}\int_{\Delta S} P(\mathbf{r})|_x dS = jD_{dx}\frac{\omega\rho_0 c^2}{U}\sum_n^N \frac{\frac{1}{\Delta S}\int_{\Delta S}\phi_n(\mathbf{r})dS}{\omega_n^2 - \omega^2 + 2j\varepsilon\omega}\left[\frac{\partial \phi_n(\mathbf{r}_e)}{\partial x_e}\right] \tag{C.20}$$

$$\frac{1}{\Delta S}\int_{\Delta S} P(\mathbf{r})|_y dS = jD_{dy}\frac{\omega\rho_0 c^2}{U}\sum_n^N \frac{\frac{1}{\Delta S}\int_{\Delta S}\phi_n(\mathbf{r})dS}{\omega_n^2 - \omega^2 + 2j\varepsilon\omega}\left[\frac{\partial \phi_n(\mathbf{r}_e)}{\partial y_e}\right] \tag{C.21}$$

$$\frac{1}{\Delta S}\int_{\Delta S} P(\mathbf{r})|_z dS = jD_{dz}\frac{\omega\rho_0 c^2}{U}\sum_n^N \frac{\frac{1}{\Delta S}\int_{\Delta S}\phi_n(\mathbf{r})dS}{\omega_n^2 - \omega^2 + 2j\varepsilon\omega}\left[\frac{\partial \phi_n(\mathbf{r}_e)}{\partial z_e}\right] \tag{C.22}$$

Here if the patch centered is on $y-z$ plane and of size $\Delta y \times \Delta z$,

$$\frac{1}{\Delta S}\int_{\Delta S}\phi_n(\mathbf{r})dS = \phi_n(x,y,z)sinc(\frac{n_y\Delta y}{2b})sinc(\frac{n_z\Delta z}{2h}) \tag{C.23}$$

If the patch is on $x-y$ plane and of size $\Delta x \times \Delta y$ or the patch is on $x-z$ plane and of size $\Delta x \times \Delta z$,

$$\frac{1}{\Delta S}\int_{\Delta S}\phi_n(\mathbf{r})dS = \phi_n(x,y,z)sinc(\frac{n_x\Delta x}{2a})sinc(\frac{n_y\Delta y}{2b}) \tag{C.24}$$

$$\frac{1}{\Delta S}\int_{\Delta S}\phi_n(\mathbf{r})dS = \phi_n(x,y,z)sinc(\frac{n_x\Delta x}{2a})sinc(\frac{n_z\Delta z}{2h}) \tag{C.25}$$

Appendix D

Identification of Source Function of Driving Patch using Blocked Pipe Method

This section will introduce the measurement of source function of driving patch using blocked pipe method. With the identified source function, the coupling impedance between the driving and receiving surfaces in a circular tube is predicted.

The driving patch is as shown in Fig. D.1, the rectangular back cavity is of $0.753m \times 0.58m \times 0.0054m$, as the compression chamber shown in Fig. 6.7(b). Mount the driving patch at one end of a circular tube of diameter $a = 0.1m$ and fix a microphone at the other rigid end, as the configuration shown in Fig. D.2. The coupling impedance between the driving patch and the pressure response at $\mathbf{r}$ is $Z^q = \Psi^q \Xi^q$ with source function of driving patch $\Psi^q = \frac{P(\mathbf{i})}{Q(\mathbf{r}_s)}$ and space function $\Xi^q = \frac{P(\mathbf{r})}{P(\mathbf{i})}$. Based on the blocked pipe method, the source function $\hat{\Psi}^q_{n-0.5}$ at the half-order frequency $f_{n-0.5}$ is

$$\hat{\Psi}^q_{n-0.5} = -j(-1)^{-n+1} \frac{\rho_0 c}{\pi a^2} \frac{\hat{P}(\mathbf{i})}{\hat{P}_{bp}}, n \geq 2 \tag{D.1}$$

where $\hat{P}(\mathbf{i})$ and $\hat{P}_{bp}$ are the measured pressure responses by the microphones at the back cavity and the rigid end of the tube. Since the source function fitted to the following polynomial,

$$j\omega\Psi^q = \psi_0 + j\omega\psi_1 - \omega^2\psi_2 + \cdots \tag{D.2}$$

by substituting Eq.(D.1) into Eq.(D.2) at half-order frequency $f_{n-0.5}$, we have

$$\begin{bmatrix} j\omega_{2-0.5}\hat{\Psi}_{2-0.5} \\ j\omega_{3-0.5}\hat{\Psi}_{3-0.5} \\ \vdots \\ j\omega_{n-0.5}\hat{\Psi}_{n-0.5} \end{bmatrix} = \begin{bmatrix} 1 & j\omega_{2-0.5} & -\omega_{2-0.5}^2 \\ 1 & j\omega_{3-0.5} & -\omega_{3-0.5}^2 \\ & \vdots & \\ 1 & j\omega_{n-0.5} & -\omega_{n-0.5}^2 \end{bmatrix} \begin{bmatrix} \psi_0 \\ \psi_1 \\ \psi_2 \end{bmatrix} \tag{D.3}$$

With the measured source function $\hat{\Psi}^q_{n-0.5}$, we can get the coefficients ψ_0, ψ_1, ψ_2. By substituting computed coefficients ψ_0, ψ_1, ψ_2 into Eq. (D.2), we could estimate source function at all the frequencies. The source function is shown in Fig. D.3. The dashed line corresponds to the source function obtained by the adiabatic law, the solid line is the measured source function at the half-order frequencies. From the figure, we can see that the estimated the source function matches well the reference.

The coupling impedance in the tube can be computed by Eq. (D.4),

$$Z^q = -j\frac{\rho_0 c}{\pi a^2}\frac{cos(kx)}{sin(kl)} \tag{D.4}$$

where l is the length of tube, it is $1.02m$, x is the distance between the receiving point and the rigid end, it is $0.301m$. The computed impedance is as the dashed line shown in Fig. D.4. With the measured space function, we compute the coupling impedance Z^q, as the solid line shown in Fig. D.4. The good agreement of measured and computed results proves that the piezoceramic speaker and the back cavity together can be able to act as a driving patch.

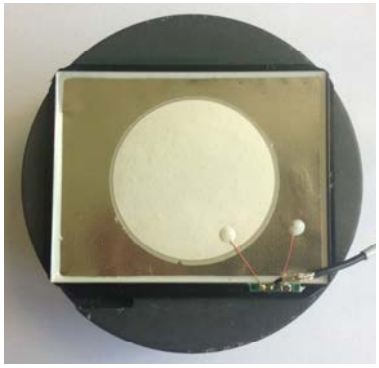

Fig. D.1 Driving patch

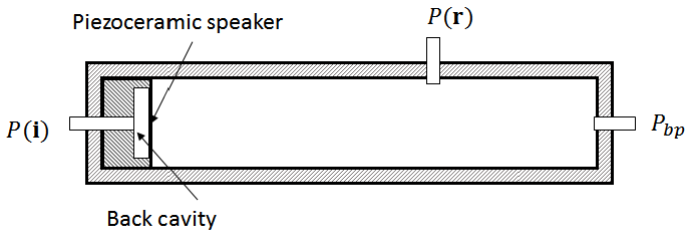

Fig. D.2 Schematic view

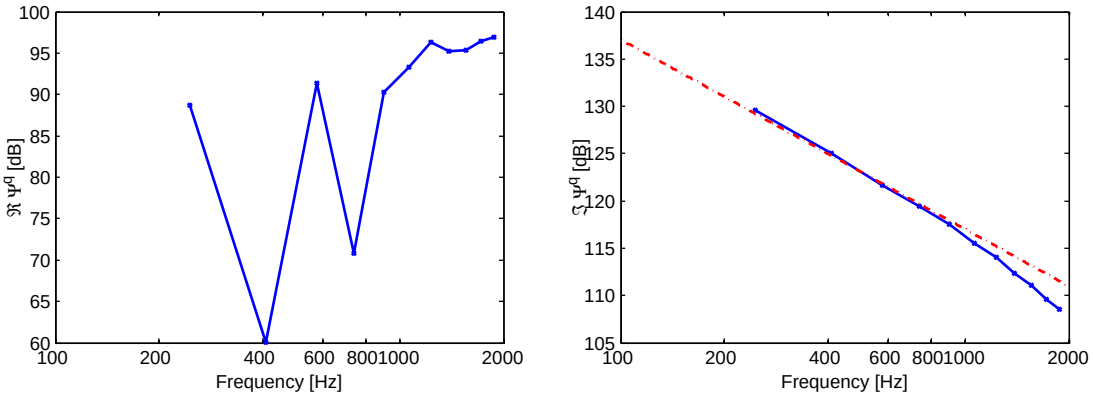

Fig. D.3 Source function Ψ^q. Left: real part, right: imaginary part

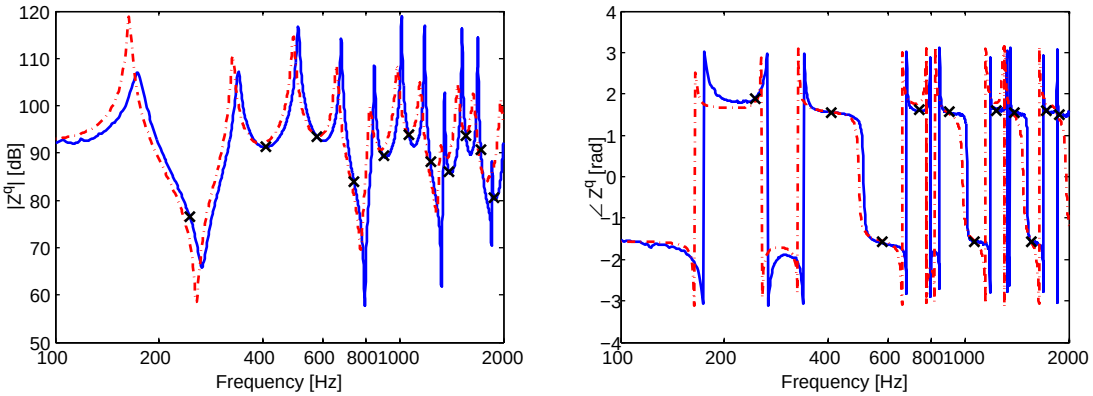

Fig. D.4 Transfer impedance Z^q. $\times$: measured impedance at half-order frequencies, solid line: estimated impedance, dashed line: computed impedance. Left: amplitude (ref $1kg \cdot m^{-4}/s$), right: phase.